Characterizing Recharge to Fractured Bedrock in a Temperate Climate

by

Ryan Oliver Burgess

B.Sc., Canterbury University, 2010

Thesis Submitted in Partial Fulfillment of the
Requirements for the Degree of
Master of Science

in the
Department of Earth Sciences
Faculty of Science

SIMON FRASER UNIVERSITY

Summer 2017

Approval

Name:	**Ryan Oliver Burgess**
Degree:	**Master of Science (Earth Science)**
Title:	***Characterizing Recharge to Fractured Bedrock in a Temperate Climate***
Examining Committee:	**Chair:** Andrew Calvert Professor

Dr. Diana Allen
Senior Supervisor
Professor

Dr. Dirk Kirste
Supervisor
Associate Professor

Pat Lapcevic
External Examiner
Section Head, Water Protection BC
Ministry of Forests, Lands and Natural Resources Operations

Date Defended/Approved: May 16, 2017

Abstract

Fractured bedrock aquifers can have large seasonal water table fluctuations due to their low storage capacity. This study uses a land surface – subsurface model, MIKE SHE, to investigate the spatial and seasonal rainfall-runoff-recharge dynamics on Gabriola Island, in a temperate region of British Columbia, Canada. The model results suggest that recharge averages 20% of the annual precipitation, occurring dominantly over 70% of the island, typically at higher elevation. Perennial seepage areas are simulated over 4% of the island, and are generally confined to breaks in slope in low topography areas. The high water table in late fall to early spring causes both seepage and saturated overland flow to contribute to more runoff. Increases in precipitation due to climate change leads to increased runoff (+36% to +40%) and recharge (+8% to +10%) relative to today. Recharge changes are most significant in winter (+13% to +16%), compared to summer (-3% to -4%).

Keywords: MIKE SHE; groundwater recharge, fractured rock, integrated model, temperate climate, climate change

Acknowledgements

First and foremost, I would like to thank my senior supervisor, Dr. Diana Allen, for her guidance, support, and expertise. I also wish to thank my committee member Dr. Dirk Kirste, and the external examiner Pat Lapcevic for their useful insights. Thank you to my lab mates, it was a pleasure to work with you all. Also, thank you to the rest of the students and staff of the Earth Sciences Department, especially Rodney, Matt, Lorena and Glenda.

This research was supported by a grant to Simon Fraser University by the Regional District of Nanaimo and the Gabriola Island Local Trust Committee of the Islands Trust. Additional funding was provided by Simon Fraser University and a Natural Sciences and Engineering Research Council Discovery Grant to Diana Allen.

Finally, this thesis would not have been possible without the support of my loving partner, Nicola. I am forever grateful for her support and encouragements.

Table of Contents

List of Tables

List of Figures

Chapter 1.

Introduction

Groundwater is an important water resource that is subject to increasing stressors globally, including over abstraction, urbanization and climate change (Green et al., 2011; Taylor et al., 2012). These stressors have the potential to negatively impact both the quantity and quality of this resource (Sophocleous, 2004; Warner, 2007; Bates et al., 2008; Ali et al., 2012; Rivard et al., 2014, Wada et al., 2014). Groundwater characterization studies, focusing in particular on groundwater recharge, are an effective means to evaluate the sustainability of groundwater resources under historic and future stressors (Toews and Allen, 2009; Currell et al., 2010; Mays, 2013; Metcalf and Robbins, 2014, Beigi and Tsai, 2015; Shamir et al., 2015; Meixner et al., 2016).

However, groundwater recharge can be one of the most difficult components to quantify and is often approximated (Crosbie et al., 2010; Healy and Scanlon, 2010; Singh, 2011; Niazi et al., 2017). Accurately quantifying the amount of recharge to a groundwater system is critical for assessing the sustainability of the resource. In some settings, such as islands, groundwater can be the main fresh water source available (Tribble, 2008; Holding et al., 2016), increasing the importance placed upon adequately assessing the sustainability of the resource. The amount of recharge in island settings also influences the position of the saltwater wedge, which may respond by moving inland under reduced recharge conditions, thereby leading to increased potential for salinization of groundwater (Barlow and Reichard, 2010; Ferguson and Gleesn, 2012; Wener et al. 2013; Luoma and Okkenen, 2014). Moreover, recharge is of upmost importance in the sustainability of aquifers with a lesser ability to store water, such as fractured bedrock (Rutqvist et al., 1998). In fractured systems, the low storage potential along with seasonality of the climate strongly influences the recharge dynamics. Hence, the accurate estimation of recharge to fractured bedrock is essential for ensuring the sustainability of the resource.

1.1. Background

1.1.1. Recharge Processes

Recharge is an important component of a groundwater system, representing the replenishment of the groundwater resource. Groundwater recharge is characterized by the downward movement of water that reaches the saturated zone, and is dependent upon such factors as the amount of rainfall, surface runoff, vegetative interception, evapotranspiration, root zone depth, and permeability of the subsurface (Scanlon et al., 2002). Recharge (R) can be approximated knowing the various components of the water budget equation:

$$R = P + Q_{in} + GW_{in} - ET + Q_{out} + GW_{out} \pm \Delta S_{GW} + \Delta S_{SW} \quad (1.1)$$

where, R is the annual groundwater recharge, P is average annual precipitation, Q_{in} is the surface water inflow, GW_{in} is the groundwater inflow into the area, ET is evapotranspiration, Q_{out} is the surface water outflow, GW_{out} is the groundwater outflow from the area, ΔS_{GW} is the change in storage in groundwater, and ΔS_{SW} is the change in storage in surface water.

Climate has a significant influence on recharge. The climate controls the amount of precipitation, but also the ET rate which is influenced by air temperature, solar radiation, humidity, wind speed, etc. In temperate regions, the seasonality of precipitation and temperature control when in the year recharge occurs (Allen et al., 2010).

Differences in geomorphology, reflected by the topography, vegetation, and soil type, influence recharge. Groundwater flow as long been linked to topography (Tóth, 1963), with recharge generally conceptualized to occur at topographic highs, and discharge at topographic lows. Steep slopes tend to have higher overland flow rates and, consequently, lower recharge, while more gentle slopes result in less overland flow and more recharge (Lu and Godt, 2013). Recharge is generally much greater in non-vegetated than in vegetated regions (Gee et al., 1994) and is greater in areas of annual crops and grasses than in areas of trees and shrubs (Prych, 1998). Recharge is often limited by the ability of the aquifer to store and transmit water, processes that are strongly affected by subsurface geology (Scanlon et al., 2002). The infiltration capacity of low permeability soils, such as those with a fine-grained texture

or the presence of clay, is generally lower than of coarser materials. In most cases, more permeable subsurface materials are able to receive more recharge than less permeable ones, and respond relatively rapidly to rainfall events.

Surface water features can also provide sources of recharge to groundwater systems (Sophocleous, 2002). Streams, rivers, and lakes are often in hydraulic connection with groundwater, providing a conduit for water transfer. The transfer can be in either direction, with the flux varying both spatially (e.g. along a stream reach) and seasonally. This type of recharge is termed focused recharge. Diffuse recharge, on the other hand, is defined as the amount of recharge directly from precipitation.

Groundwater discharge is characterized by the movement, or removal, of water from a groundwater system (Freeze and Cherry, 1977). Groundwater discharge occurs primarily as springs and as fluxes to water bodies (i.e. discharge to rivers, lakes, and into the ocean). Other forms of discharge include groundwater abstractions and evapotranspiration.

As part of the groundwater system, recharge and discharge are linked. This linkage can be expressed as a mass balance equation:

$$\Delta\, Storage = Recharge - Discharge \tag{1.2}$$

Over the long term this water balance is dynamically stable (ΔStorage=0), with variations in storage occurring over smaller time scales. The water budget becomes non-zero when water is added to or taken out of storage over different time periods. Seasonally, this results in the water table going up and down, while over the long term, climate change and abstractions can result in imbalance. The amount of water that can be added to or removed from storage in the aquifer is related to its storativity, S. In an unconfined aquifer, this storage parameter is the specific yield, Sy. Aquifers with low Sy values (e.g. fractured bedrock, as discussed below) display large amplitude variations in groundwater level in response to stressors. Consequently, they can respond rapidly to imbalances and so are at risk from stressors such as climate change and abstraction. Additionally, the seasonal variability in climate often results in recharge not occurring uniformly over the year. So, there is a strong dynamic of water moving in and out of storage, with the water table rising and falling accordingly. This

complicates recharge characterization and requires consideration of the transient behaviour of the system.

1.1.2. Recharge to Fractured Bedrock in a Temperate Climate

Recharge processes in fractured bedrock are complex (Heppner et al., 2007; Gleeson, 2009; Chesnaux, 2013; Rivard et al., 2014; Rohde et al., 2015). Compared with porous media, heterogeneities in the fracture orientation, extent and aperture make the investigation of fractured bedrock recharge more complicated (Salve et al., 2008). If surficial sediments are present, water will first pass through these sediments before entering the underlying fractured bedrock. When the bedrock is exposed, the recharge to the fractured bedrock is generally rapid, as fractures and joints are able to transmit water much faster than in porous aquifers (Gleeson, 2009). For the same reasons, the discharge from fractured bedrock is also generally rapid.

The recharge to bedrock is influenced by four factors: (1) relief of land and bedrock surface above groundwater discharge areas; (2) lateral trends in bulk-rock horizontal conductivity; (3) local topographic features; and (4) local surficial sediment stratigraphy (Harte and Winter, 1996). The storativity of bedrock is generally limited, and only a certain amount of recharge may be stored before the aquifer is 'full' (Rutqvist et al., 1998; Healy and Scanlon, 2010; Burbey et al., 2012). Once 'full', any further precipitation will typically occur as overland flow. This may have a significant control on recharge volumes. However, little research has focused on understanding how aquifers with low storativity influence rainfall-runoff-recharge processes. Further, this phenomenon of the aquifer reaching its storage capacity can be exacerbated in some cases where rainfall mainly occurs over one season of the year, such as in a temperate climate, as discussed below.

Recharge can show significant seasonal variability in temperate climates (Allen et al., 2010; Jasechko et al., 2014). Generally, recharge is minimal during summer when most precipitation is evapotranspired back to the atmosphere. In the fall and winter, recharge rates increase again when photosynthesis shuts down. This can be observed in the well hydrographs with peak groundwater levels present in mid to late winter, and a decline in levels in the summer and into the fall (Allen et al., 2010). In temperate climates, generally 5 to 25% of precipitation reaches the water table (Clark and Fritz, 1997). The rest is lost to runoff, evaporation from soils and transpiration by

vegetation (Healy and Scanlon, 2010). However, Jasechko et al. (2014) found that not all temperate climate aquifers are recharged predominately in the winter; the factors leading to this conclusion were unclear to those authors. It would seem further investigation into the controls on recharge in temperate climates is justifiable.

In temperate climates, recharge analysis has traditionally been focused on soil moisture budget parameters without developing a conceptual understanding of the influence of geology on recharge mechanisms and rates (Fitzsimons and Misstear, 2006). The recharge to fractured bedrock in temperate climates is therefore warranted, as previously little attention has been given to how the rainfall-runoff-recharge processes are controlled in these low storativity and temporally variable precipitation settings.

1.1.3. Modelling Recharge

Over the past few decades, investigations into methods suitable to characterize recharge to fractured bedrock have been numerous (e.g. Cook et al., 1996; Abbott et al., 2000; Appaih-Adjei, 2006; Praamsma et al., 2009; Voeckler et al., 2012; Chesnaux, 2013; Foster, 2014; Rhode et al., 2015; Rathay, 2016). The methods applied previously include using groundwater ages (Cartwright and Morgenstern, 2012), stable isotopes (Gaye and Edmunds, 1996), numerical and analytical simulations (Sanford, 2011), and water table responses (Scibek et al., 2013); with a number of other methods summarized in the review by Scanlon et al. (2002).

Methods for estimating recharge are often grouped into the components of the hydrologic cycle that they represent: surface water methods, saturated zone methods, and unsaturated zone methods (Scanlon et al., 2002). In general, there are limitations to focusing the on one of these zones of the hydrological cycle. The extensive heterogeneity of fractures and joints in fractured bedrock limits the use of local estimates as proxies for regional scale studies. To minimize these limitations and uncertainties inherent to individual components of the hydrological cycle, a regional holistic approach is used. Fully integrated (or coupled) land surface - subsurface models (e.g. GSFLOW, HydroGeoSphere, MIKE SHE, etc.) model the water flow through the entire system. Using coupled codes provides an approach for estimating recharge that takes into account all three zones, thus reducing the limitations of focusing on one zone. Although relatively recent, coupled codes have proven to be

robust simulators of the land surface and subsurface components of the hydrological system (Smerdon et al., 2010; Foster, 2014; Voeckler et al., 2014).

Climate change has the potential to affect groundwater resources globally (Green et al., 2011), principally though changes in the climatic patterns of temperature and precipitation. Based on global climate model (GCM) simulations, the future atmospheric temperature, and the amount and intensity of precipitation are predicted to be altered. As discussed previously, temperature and precipitation, in part, directly control the amount of recharge an aquifer receives. An increase in temperature, for example, would increase evapotranspiration and potentially reduce the amount of recharge to groundwater from precipitation. Consequently, such changes to climate may have significant impacts on the sustainability of groundwater resources in the future.

This study aims to characterize recharge to fractured bedrock in a temperate climate, specifically identifying key factors that control recharge and how recharge is influenced by climate both seasonally and under future climate conditions. The coupled land surface – subsurface code, MIKE SHE, is used.

1.2. Study Area Context

Gabriola Island, British Columbia, Canada has been chosen as the study location for this proposed research. Gabriola Island represents a fractured bedrock system in a temperate climate, with a groundwater supply that is coming under increasing pressure from residential development, and potentially climate change. Thus, estimating the recharge on the island is vital for maintaining the sustainability of the groundwater resource. The selection of Gabriola Island as a study location for investigating recharge processes and controls is appropriate in a number of ways. Firstly, an island represents a relatively isolated hydrological system, where inputs and outputs of water from the system other than from/to the land surface and ocean are not present (such as deep regional groundwater). Secondly, the study location is a mountainous terrain, allowing the examination of rainfall-runoff-recharge processes over a variety of topographical conditions. Lastly, Gabriola Island already has a significant amount of data necessary (discussed in Chapter 2) to develop a coupled land surface and subsurface model.

1.3. Research Objectives

The goal of this research is to improve understanding of groundwater recharge in fractured bedrock in a temperate climate. To achieve this goal, the following objectives will be met:

- Characterize the physical parameters, in particular topography, which influence the spatial distribution of recharge and discharge in a fractured bedrock;
- Determine the rainfall-runoff-recharge relationships that control seasonal groundwater level variability in fractured bedrock; and
- Estimate how climate change may influence recharge in a temperate climate setting.

1.4. Scope of Work

The scope of work for this study included the following tasks:

- To meet objectives 1 and 2:
  - Install lysimeters in different vegetation settings on the island, and use these to estimate ET (short term record) for comparison with the modeled estimates of ET.
  - Infer groundwater age from tritium and hydrochemistry data. These data will help constrain the conceptual model and provide field observations for model calibration.
  - Develop a coupled land surface - subsurface numerical flow model of Gabriola Island using the MIKE SHE code. The model will be calibrated to the available groundwater elevation data and inferred groundwater ages using a trial and error approach.
  - Perform a sensitivity analysis to identify which parameters the model is most sensitive to, and thus influence recharge.
  - Explore the rainfall-runoff-recharge relationship to identify factors that control groundwater level variability temporally.
- To meet objective 3:
  - Use global climate change model forecasts to assess how variations in climate may affect the future recharge processes on Gabriola Island.

1.5. Thesis Organization

This thesis will be organized into five chapters:

- Chapter 1 focuses on the background, motivation and objectives of the research. It gives an overview of recharge and discharge processes in fractured bedrock and temperate climate setting, recharge estimation methods focusing on using numerical models to estimate recharge, and how recharge may be affected under future climate conditions.
- Chapter 2 focuses on the hydrogeology of Gabriola Island. It includes an analysis of all available climate, land surface, hydrometric, geological and hydrogeological datasets with the aim of defining a conceptual model for Gabriola Island that can use used to develop the numerical model.
- Chapter 3 describes field studies carried out to obtain additional calibration data. It includes the tritium and geochemical data analysis and interpretation, and the ET measurements using lysimeters.
- Chapter 4 focuses on the development and calibration of the MIKE SHE model.
- Chapter 5 focuses on analysis and discussion of the MIKE SHE model results in the context of the research objectives of this thesis.
- Chapter 6 provides conclusions and recommendations of the thesis.

Chapter 2.

Study Area

2.1. Geography

The Gulf Islands are located in the Strait of Georgia, between the mainland of British Columbia (BC) and Vancouver Island (Figure 2.1). Gabriola Island, the study area for this research, is situated at the northern end of the archipelago, east of Nanaimo on Vancouver Island. It is bordered to the west by Vancouver Island, south by other Gulf Islands: Mudge, DeCourcy, and Valdes, and to the east by the Strait of Georgia. Gabriola is about 14 km long and 4.2 km wide, with a land area of 57.73 km^2 (Statistics Canada, 2015).

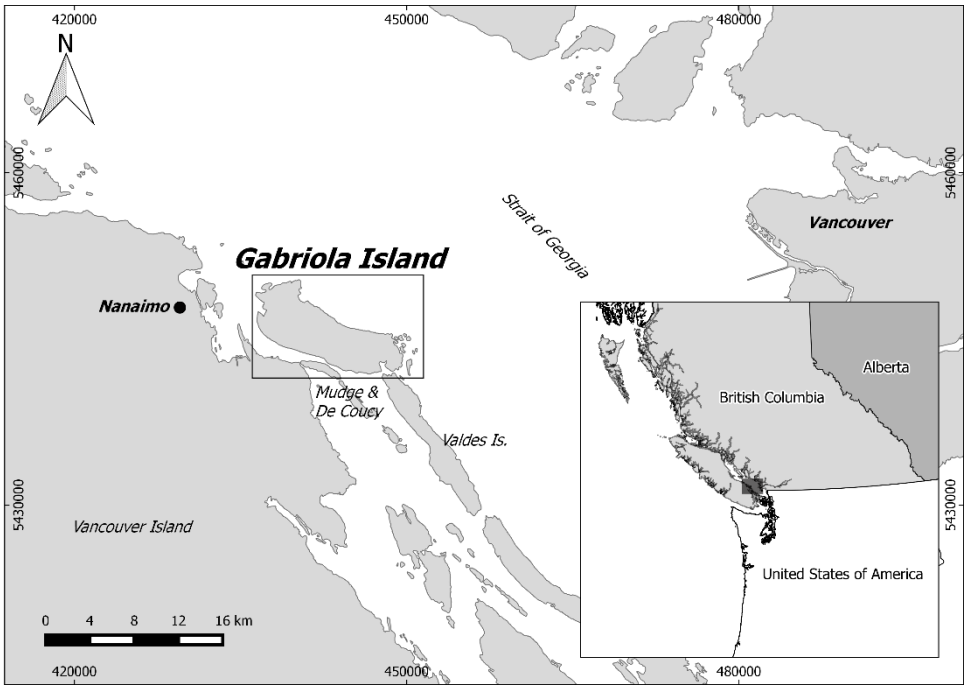

Figure 2.1 Location of Gabriola Island in Western British Columbia (inset map).

The topography of Gabriola Island, shown in Figure 2.2, is largely controlled by the underlying bedrock. The bedrock consists of alternating sandstone- and mudstone-dominant units. The less competent mudstone units have been preferentially weathered compared to the sandstone units, producing distinct sandstone ridges. Generally, the land surface is higher along the southwest of the island where a

prominent sandstone ridge rises to the highest point on the island to approximately 167 metres above sea level (masl). Towards the coast the elevation drops to sea level.

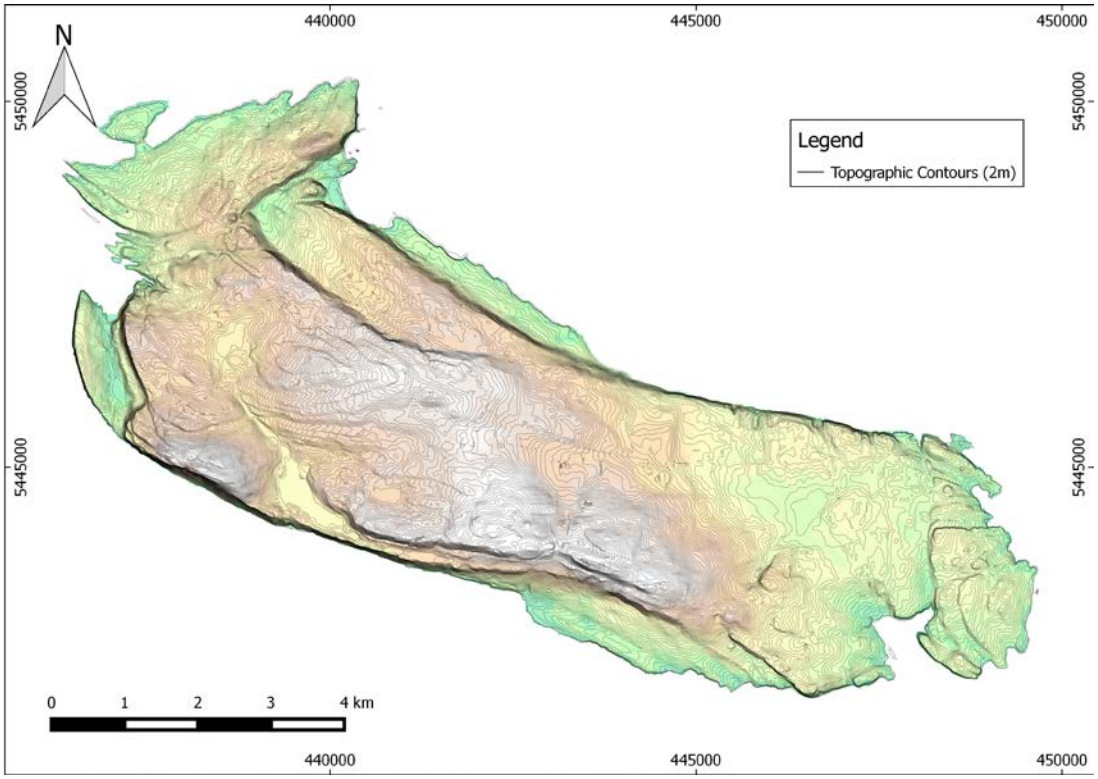

Figure 2.2 Topography of Gabriola Island.

2.2. Climate

Gabriola Island has a mild, temperate climate, with wet winters and dry summers, and lies in the rain-shadow zone of Vancouver Island. There is one active climate station on Gabriola (Climate ID: 1023042), with precipitation and temperature records dating back to March 1967. The mean daily temperature on Gabriola Island ranges from a low of 5.3°C in winter, to a high of 13.9°C in summer (Environment Canada, 2015). The mean annual precipitation (MAP) (1981-2010) is 958 mm (Environment Canada, 2015). The majority of the precipitation falls as rain, with only minor amounts falling as snow (Figure 2.3).

There is more than likely some spatial variation in both the temperature and precipitation across the island. However, due to the relatively low topography, it is unlikely that this spatial variation is significant (Scibek et al., 2013). Being a temperate climate, there is significant temporal variability in the amount of precipitation. Based on

the 1981 to 2010 monthly climate normals data (Environment Canada, 2015), 25% of the MAP falls over the drier summer period (April to September); <5% falls in the driest months of July and August (Figure 2.3). Approximately 75% of the MAP falls during the wetter months from October to March. During the wettest months (November to January), nearly 46% of the MAP falls.

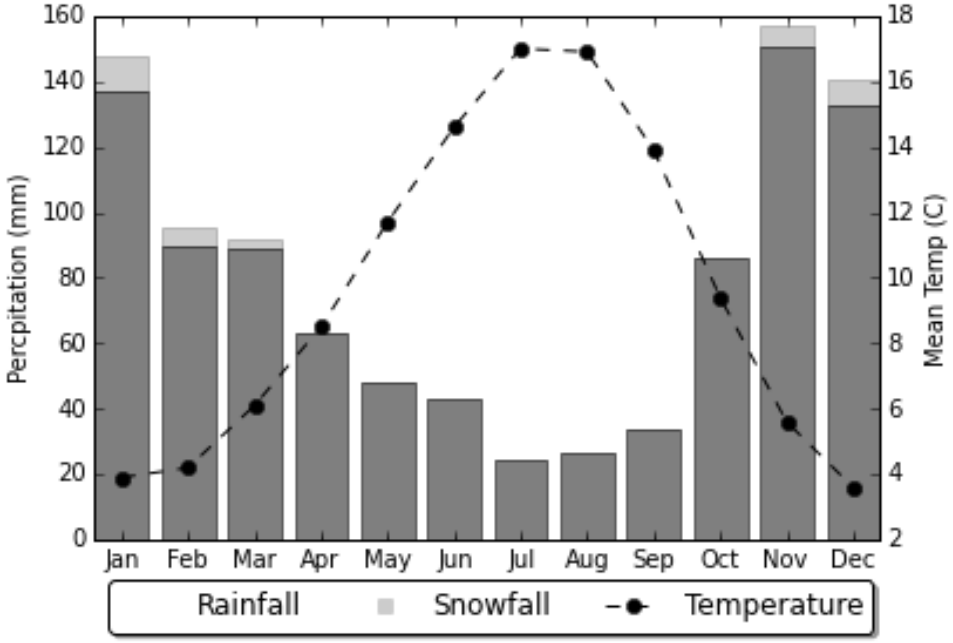

Figure 2.3 Gabriola Island climate normals (1980 – 2010). Blue bars represent average monthly precipitation, and the red line represents average monthly temperature for Gabriola Island climate station (Climate ID: 1023042).

There is also inter-annual variation in precipitation (Figure 2.4). Annual precipitation ranges from 800 to 1000 mm in most years. In the period of record, the mean annual rainfall on Gabriola varied between 405 mm in extremely dry years, and 1270 mm in very wet years. Temperature displays less inter-annual variation; however, there is a slight observable positive trend in median temperatures (Figure 2.4).

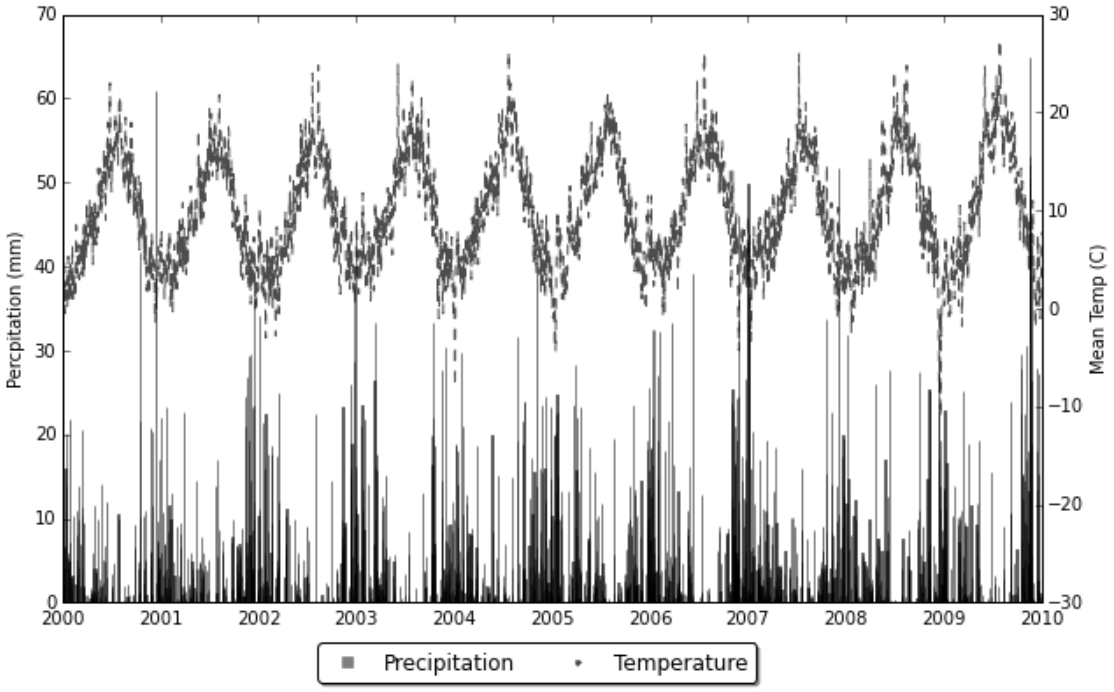

Figure 2.4 Gabriola Island climate variability. Black bars represent precipitation, and the points represent daily temperature for Gabriola Island climate station (Climate ID: 1023042).

2.3. Evapotranspiration

Evapotranspiration has long been one of the most difficult components of the hydrological cycle to estimate (Chiew and McMahon, 1991; Zhang et al., 2004). Evapotranspiration may be determined as potential (or reference) evapotranspiration (PET or RET) and actual evapotranspiration (AET). PET is the rate of evapotranspiration from a reference surface, often a hypothetical grass surface with specific characteristics, with an unlimited amount of water, or a measure of the moisture demand from a site (Penman, 1948). It is calculated from only climatic variables, and thus is independent of vegetation. AET is the net result of PET and ability of the reference surface to supply moisture. AET represents the actual amount of water evapotranspired, which is typically less than PET. Quantitative models often use PET to calculate AET.

In this study, PET was approximated following the Penman-Monteith (Monteith, 1981) method using the AWSET software (Cranfield University, 2002). The software calculates PET on a daily basis from temperature, humidity, wind speed, and solar radiation data. Only temperature data were available from the Gabriola climate station;

the humidity and wind speed data were obtained from the nearby Nanaimo Airport climate station (Climate ID: 1025370), while the solar radiation was approximated using the Solar Radiation Spatial Analyst tool in ArcGIS version 10.0 and linear interpolation. The relative humidity and wind speed data were averaged from hourly observations to a daily scale. The Solar Radiation tool provided approximations of solar radiation on specified days of a month (the 15th day of every month). Default parameters were used with an overcast sky setting. The daily values were then interpolated using the cubic spline method to provide a continuous daily estimate of solar radiation. The results of the calculated PET are presented in (Figure 2.5). The results show an annual variation in PET. As one would expect, high PET occurs during the summer months, when temperature and solar radiation are highest, and then drops to low values during the winter months. There appears to be only a small amount of inter-annual variation in the calculated PET results.

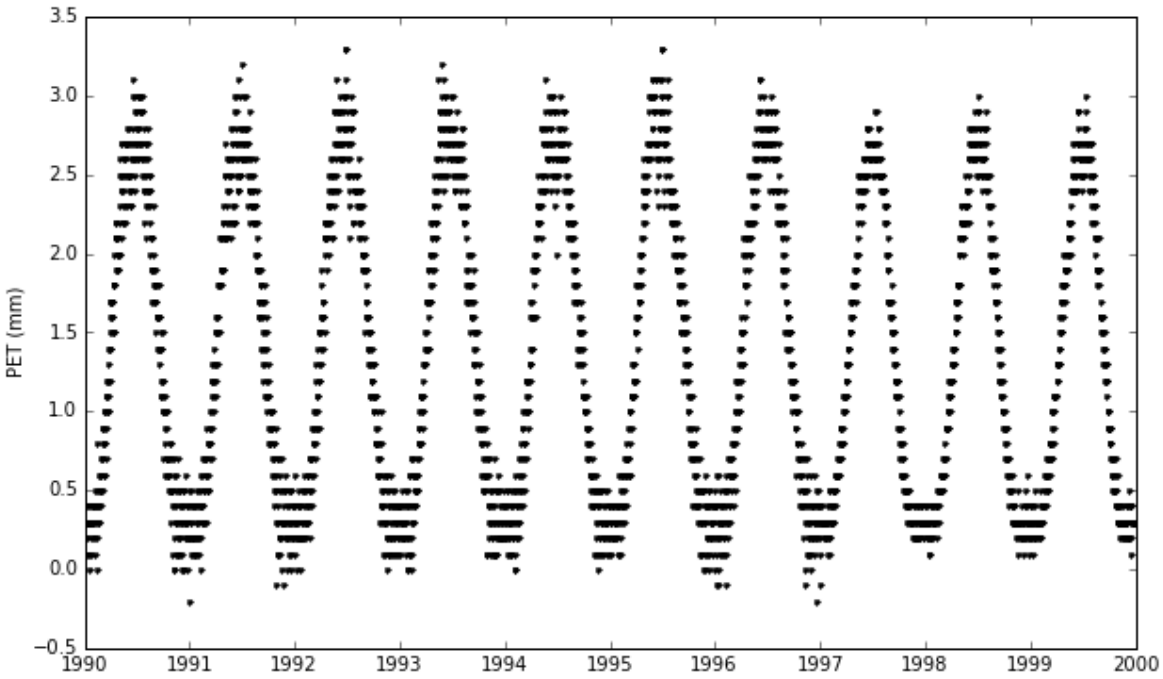

Figure 2.5 Calculated PET. PET was calculated using the AWSET software (Cranfield University, 2002).

No AET estimates have been made for Gabriola Island specifically; however, previous studies have estimated it for other Gulf Islands, other areas in BC, and for Canada as a whole. Liu et al. (2003) mapped the AET across Canada utilizing a remote sensing approach. Along the 49th parallel (the approximate location of Gabriola Island), the authors estimated AET to be between 250 to 350 mm/yr or approximately 26-36%

of MAP at Gabriola Island. Fernades et al. (2007) used a land surface model in a Canada wide study and estimated an annual AET flux of 385 mm (equating to approximately 40% of MAP on Gabriola Island) for the Pacific Coast region. Spittlehouse and Balck (1979) estimated the AET from a Douglas fir forest on the southwest coast of BC by using temperature and wind speed measurements in an energy balance method. For a period in July 1976, they calculated an average AET rate of approximately 5 mm per day, or over six times the average daily precipitation rate during July (~0.7 mm/day). Appiah-Adjei (2006) and Foster (2014) calculated estimates of AET from numerical models for other Gulf Islands and a watershed on Vancouver Island, respectively. Appiah-Adjei (2006) used a water balance based 1D code to simulate recharge for different combinations of soil and vadose zone properties, and water table depths. Foster (2014) used an integrated surface water-groundwater code (MIKE SHE) to simulate groundwater-surface water interactions along a river in a mountainous watershed. AET estimates ranged from 43-50% of MAP.

The spatial distribution of AET on Gabriola Island is uncertain. However, during a field visit in June, 2015, the southern side of the island was noticeably drier than northern side, indicating that AET is likely greater on this side of the island. As part of this study, AET on the island was investigated in the field using lysimeters (Chapter 3)

2.4. Vegetation and Land Cover

Land cover on the island consists predominantly of forested, agricultural, and residential areas. Figure 2.6 shows the land cover types across the island. Based on the spatial data from FLNRO (2011), young forest, described as forest less than 140 years old and greater than 6 m in height, makes up approximately 55% of the land cover; urban areas make up approximately 35% of the land cover; with agricultural land, water bodies, recently logged areas, and recreational areas making up the remainder. Although not so densely vegetated, trees over 6 m in height are largely ubiquitous throughout urban areas. Thus, the effective area of forest is likely upwards of 70% of the land surface area.

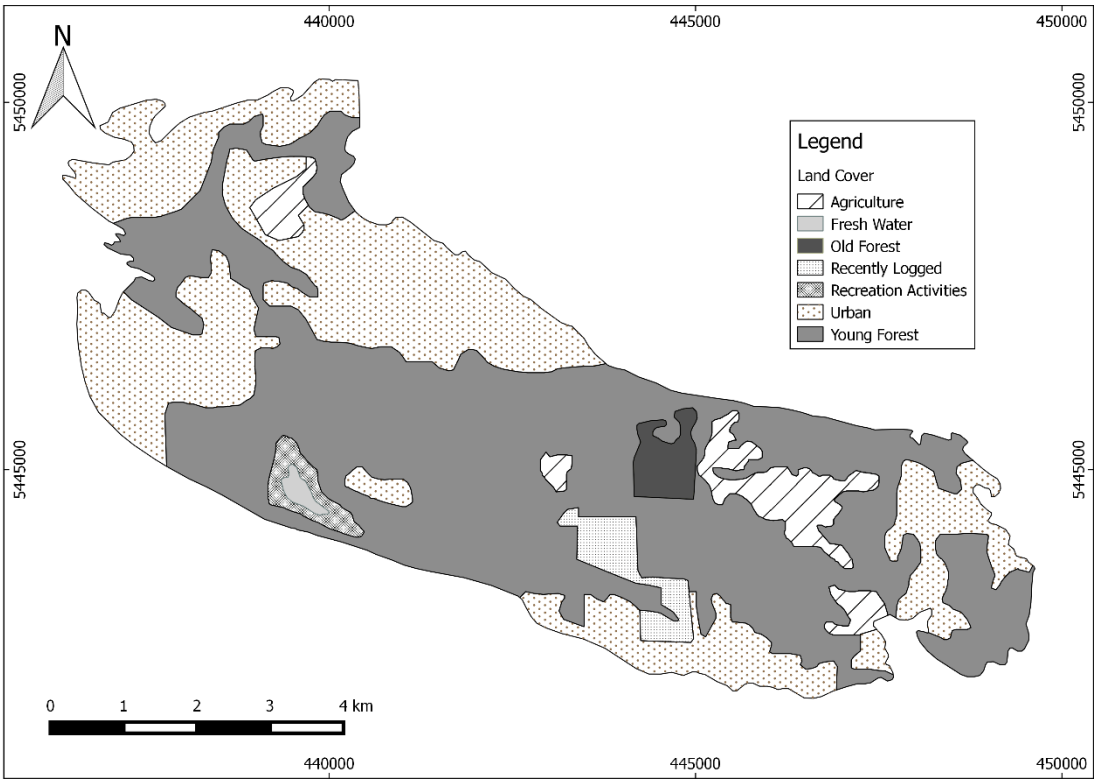

Figure 2.6 Gabriola Island land cover. Old Forrest represents forested areas older than 140 years; Young Forrest represents forested areas less than 140 years old; and Recently Logged represents areas logged in the last 20 years. Data from FLNRO (2011).

The vegetation of BC has been extensively mapped in the past by the BC Ministry of Forests (BCMoF). In 1991, the BCMoF produced a report that describes the terrestrial ecosystems of BC (Meidinger and Pojar, 1991). This report classified the terrestrial ecosystems into the biogeoclimatic ecosystem classification (BEC) system. This framework classifies the landscape into map units using, as the name suggests, a combination of climate and physiographic data, indicating areas that have the ability to support certain vegetation types or ecosystems. Gabriola Island sits within the Coastal Douglas-fir BEC zone. In this zone, the coastal variety of Douglas-fir is the most common (Nuszdorfer et al., 1991), with western red cedar, grand fir, arbutus, Gary oak, and red alder also present, depending on moisture levels and nutrient regimes. The understory of much of the forested areas of Gabriola Island consists of salal.

2.5. Surface Water

There are relatively few surface water bodies on Gabriola Island, with Lake Hoggan being the largest (Figure 2.7). The majority of the wetlands are seasonal; only a small number are present year round, such as Coats Marsh.

Ephemeral creeks on the island generally only flow for a week or two (Scibek et al., 2013), although there is a degree of variability in creek flow from year to year due to climate variability. During a field visit in June 2015, the majority of the creeks were dry, with only a few pools at certain locations along steam networks. This observation would indicate that while groundwater does discharge to the creeks through bedrock fractures, this discharge is insufficient to sustain the flow of the creeks during the drier summer months. None of the creeks are currently gauged. Between 1972 and 1978, the level of Hoggan Lake (station number 08HB046) and the outflow of the lake at Hoggan Creek (station number 08HB053) were measured by Water Survey of Canada. Scibek et al. (2013) estimated that approximately 60% of annual precipitation occurs as runoff. Welyk and Baldwin (1994) estimated the runoff annual volume from the stream catchments of Gabriola Island at approximately 318 mm per year or 32% of MAP. Accounting for this portion of the hydrological cycle is important when estimating recharge.

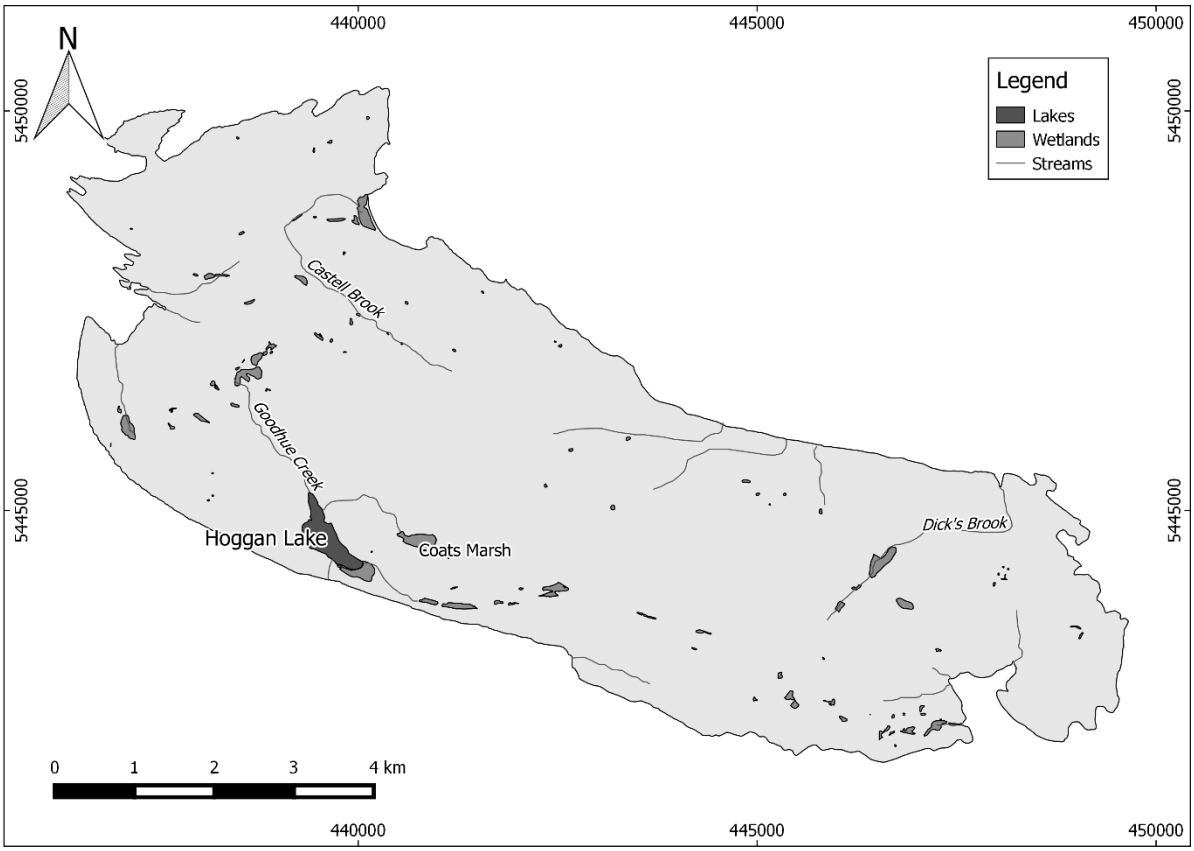

Figure 2.7 Gabriola Island surface water features.

2.6. Soils and Geology

The soil units of Gabriola Island (and other nearby Islands) were mapped in detail by the BC Ministry of Environment (Kenney et al., 1986). The mapping concluded that the majority of the soils (>70%) comprise sandy loam/loamy sand overlying bedrock. These soils are generally classed as imperfectly to well drained based on their inherent drainage ability (Figure 2.8). Occurrences of exposed sandstone bedrock are also present.

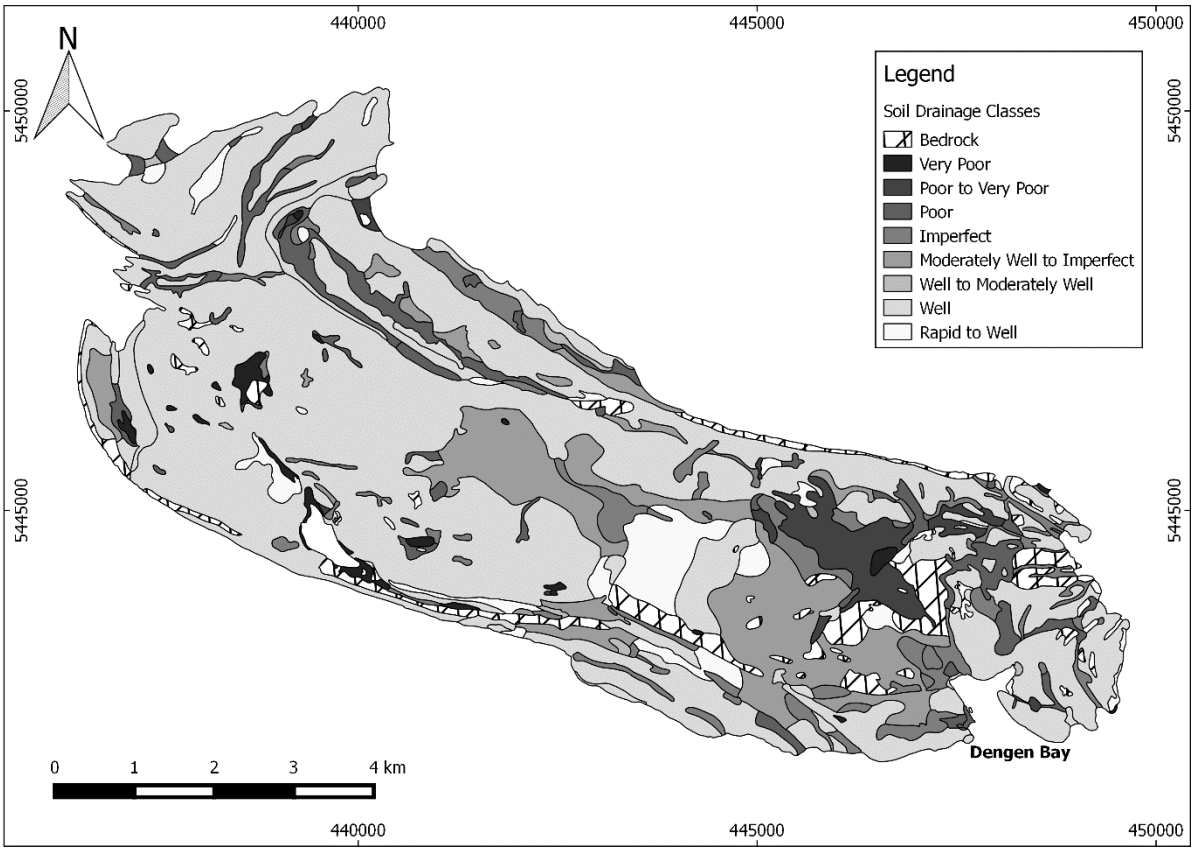

Figure 2.8 Gabriola Island soil drainability. Data from MoE (2015a).

Surficial deposits on Gabriola Island are predominantly glaciomarine sediments. Soils are sparse and thin (~2m), and are formed from bedrock weathering and from deposited glacial till and small pockets of glacial outwash (EBA, 2011). The thickest surficial deposits are in the southeast corner of Gabriola Island (up to 25 m of coarse gravel/boulder till deposits) west of Degnen Bay.

The bedrock geology of Gabriola consists of sedimentary formations of the Upper Cretaceous Nanaimo Group (Table 2.1). These formations are identified as successions of sandstone-conglomerate units interbedded with mudstone and fine-grained sandstone (Mustard, 1994). Four formations of the Nanaimo Group are recognized on Gabriola Island: the Gabriola, Spray, Geoffrey, and Northumberland. The Gabriola and Geoffrey Formations are mainly comprised of sandstone, while mudstone predominantly comprises the Spray and Northumberland Formations (Table 2.1).

Table 2.1 Stratigraphy of Gabriola Island. Modified from Mustard (1994).

Formation	Dominant Lithology	Period	Age
Gabriola	Sandstone	Cretaceous	
Spray	Mudstone		Maastrichtian
Geoffrey	Sandstone		
Northumberland	Mudstone		Campanian

The structural characteristics of the Upper Nanaimo Group are the result of two deformation events. First, ancient compression and extension deformation (Mustard, 1994), followed by more recent glacio-isostatic deformation (Clague, 1983). The bedrock throughout the Gulf Islands thus has been extensively folded and fractured (Journeay and Morrison, 1999). In addition to fractures, open bedding planes are common on the Gulf Islands; a result of the uplift and/or isostatic rebound after deglaciation (Mackie, 2002). On Gabriola Island, a fold called the Gabriola Syncline is the dominant structure (England, 1989); this syncline trends northwest to southeast along the length of the island (Figure 2.9).

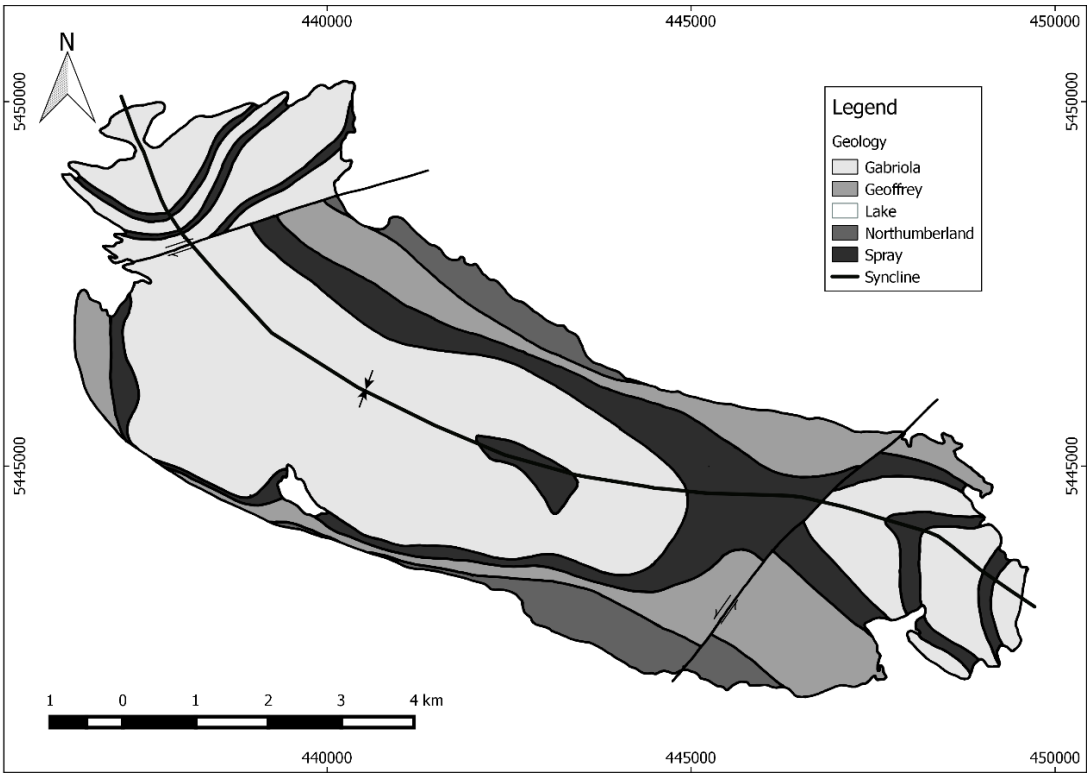

Figure 2.9 Geology of Gabriola Island. Modified from the B.C. Ministry of Energy and Mines (2005).

2.7. Hydrogeology

On Gabriola Island, the fractured bedrock represents the main aquifer material, with the surficial sediments not yielding significant amounts of groundwater (Hodge, 1977). The majority of the groundwater flows through the fractures and joints, bedding planes, and faults of the Nanaimo Group bedrock, with only a minor amount transmitted by the relatively low primary porosity (Dakin et al. 1983; England, 1989; Mackie, 2002). The fractures in the bedrock are considered moderately permeable, and are also easily drained and refilled (low storage ability).

The Nanaimo Group bedrock units have a range of hydraulic properties due to fracture heterogeneity (Surrette et al., 2008). Several Gulf Islands studies have attempted to characterize the hydraulic properties of the bedrock using various methods, ranging from pumping test analysis (e.g. Scibek et al., 2013; Larocque, 2014) to developing discrete fracture network models using measurements of fractures mapped throughout the Gulf Islands (e.g. Mackie, 2002; Surrette et al., 2008). Larocque (2014) summarized the hydraulic properties derived from pumping tests conducted throughout the Gulf Islands and found little difference between the transmissivity (T) values for sandstone dominated ($1.3x10^{-5}$ m/s) and mudstone ($9.5x10^{-6}$ m/s) dominated formations of the Nanaimo Group (Table 2.2). Allen et al. (2002) found the average storativity (S) for the sandstone-dominated formations on the Gulf Islands was $2.7x10^{-4}$. There were no S values available for the mudstone formations. The hydraulic property values are summarized in (Table 2.2).

Table 2.2 Summary of hydraulic properties (T values summarized from Larocque, 2014; S from Allen et al., 2002)

Rock Type	Transmissivity, T (m^2/s)			Storativity		
	Geometric Mean	Max Value	Min Value	Geometric Mean	Max Value	Min Value
Sandstone-dominant	$1.3x10^{-5}$	$5.4x10^{-2}$	$3.4x10^{-7}$	$2.7x10^{-4}$	$1.8x10^{1}$	$2.8x10^{-9}$
Mudstone-dominant	$9.5x10^{-6}$	$6.0x10^{-5}$	$7.6x10^{-7}$	N/A	N/A	N/A

Figure 2.10 shows the range of hydraulic conductivity values (K) for the different formations present on Gabriola Island. K values were calculated by dividing T calculated from the pumping test by the open hole length of the well (base of casing

to bottom of hole). There is significant variability in K despite the similar geometric mean values (Table 2.3).

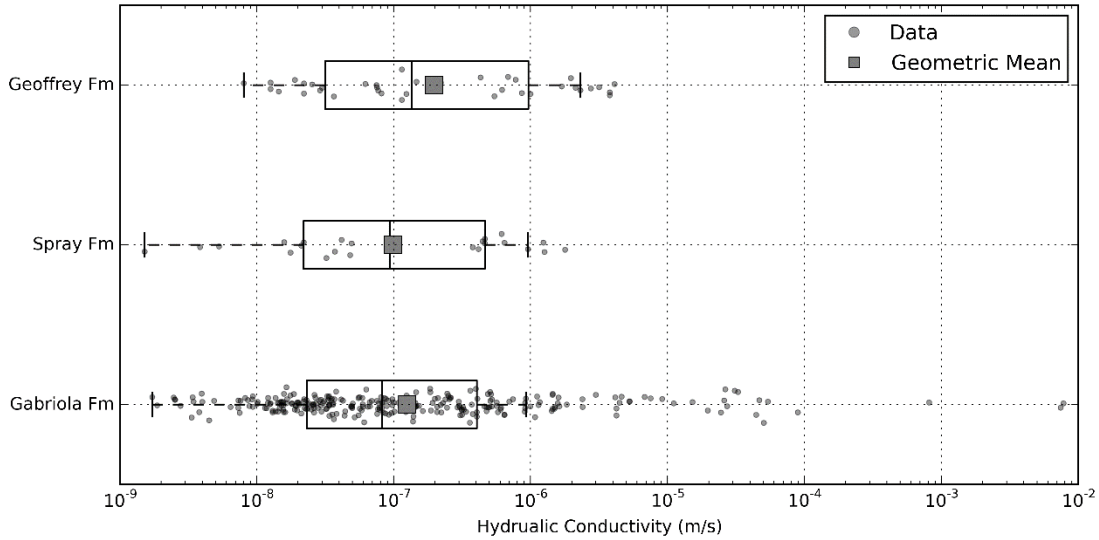

Figure 2.10 Hydraulic conductivity of Nanaimo Group bedrock. Hydraulic conductivity values originate from pumping test analysis results compiled by Allen et al. (2002). Note: the analysis did not include tests conducted in the Northumberland Formation.

Table 2.3 Average hydraulic conductivity of Nanaimo Group bedrock. (summarized from Larocque, 2014).

Rock Type	Hydraulic Conductivity, K (m/s)
Sandstone-dominant	2.5×10^{-7}
Mudstone-dominant	4.7×10^{-7}

Primary porosity of the Nanaimo Group is estimated to be <5% (reported by Mustard, 1994), leading to the general consensus that the primary permeability is likely very low and that the fractures provide the dominant permeability. Using a discrete fracture network modelling approach, secondary porosity values for the fracture network have been estimated to range from 0.005% to 0.13% (Surrette et al., 2008; Chesnaux et al., 2009). While the secondary porosity is very low, the openness of the fractures results in relatively higher permeability. Groundwater flow modelling studies to date, have only employed an equivalent porous medium (EPM) approach to represent the fractured bedrock (Liteanu, 2003; Trapp, 2011; Larocque, 2014). These

studies used similar K values to those reported above, with porosity values ranging from 1 to 10%. Clearly porosity remains highly uncertain.

Given the similar hydraulic properties of the Nanaimo Group units across the Gulf Islands, albeit without data from the Northumberland Formation, the formations on Gabriola Island can be conceptualized as a single hydrogeological unit for the purpose of this study, which focuses on recharge estimation and characterization. Moreover, because there are no overlying low permeability layers, the aquifer is likely unconfined. Scibek et al. (2013) suggested that the base of the aquifer coincides with the bottom of the Northumberland Formation, but given that the Northumberland is underlain by the de Courcy formation (sandstone-dominant) there is no geological reason for this to be the case. Rather, the base of the aquifer is more likely related to the depth (or zone) at which the fractures cease to transmit significant flow. Fracture aperture and connectivity often decrease with increasing depth (Snow, 1968; Carlsson et al., 1983). Thus, the hydraulic conductivity of the fractured bedrock aquifer on Gabriola Island likely decreases with depth. Previous studies in fractured bedrock have assumed that flow becomes minimal at a depth of 150-200 m (e.g. Liteanu, 2003; Welch and Allen, 2012; Foster, 2014; Larocque, 2014; Voeckler et al. 2014).

Although the rate of decrease is unknown, simple equations have been derived to estimate the decrease in hydraulic conductivity in fractured rock with depth (e.g. Oda, 1986; Wei et al., 1995; Jiang et al., 2010). Wei et al. (1995) used a hyperbolic equation to describe this decrease in permeability for a fractured rock mass as follows:

$$\frac{k}{k_0} = \left[1 - \frac{z}{A + Bz}\right]^3 \tag{2.1}$$

where z is the depth from ground surface to the point of calculation; k and k_0 represent the hydraulic conductivity at surface and at depth, z, respectively; and A and B are two constants. A and B are defined as:

$$A = \frac{z_c}{1 - \left({b_r}/{b_0}\right)}, \quad B = \frac{1}{1 - \left({b_r}/{b_0}\right)} \tag{2.2) \& (2.3}$$

where $\boldsymbol{b_r}$ is the residual aperture as depth, $\boldsymbol{b_0}$ is the effective fracture aperture at depth, and $\boldsymbol{z_c}$ is a reference depth. Wei et al. (1995) estimated values that indicate $\boldsymbol{b_r}$ is approximately 2.0% of $\boldsymbol{b_0}$ and $\boldsymbol{z_c}$ is 56.86 m. These values were deemed constant for any fractured rock mass (Wei et al., 1995). By applying the combined average hydraulic conductivity value of 3.6×10^{-7} m/s, from the sandstone- and mudstone-dominated units (Table 2.3), as k_0, to Eq. (2.1), the estimated hydraulic conductivity (k_0), at 200 m depth below sea level (z), for the fractured bedrock on Gabriola Island is approximately 3.6×10^{-9} m/s.

2.8. Recharge

Recharge to the Gulf Islands aquifers is dominantly by infiltration of precipitation (Allen and Suchy, 2001). Recharge is thought to occur rapidly through the expansive thin, well-drained soils before localized recharge is transmitted through fractures and joints of the fractured bedrock aquifers (Scibek et al., 2013). Rathay (2016) observed a groundwater discharge zone along a bedding plane on Gabriola Island (seep) respond to a heavy precipitation event in less than 24 hours. The dissipation rate was also rapid. 46 hours after the heavy rain event the seepage area had decreased by approximately 85%. This would indicate that, at least at locally, recharge can occur rapidly though the fractures and joints present in the bedrock.

The dynamics of recharge are recorded in the groundwater level hydrographs. Groundwater levels on Gabriola Island have been recorded by British Columbia's provincial government since the 1970s. Currently, there are four active monitoring wells that continuously measure the depth to the water table. Table 2.4 provides a summary of the monitoring wells (active and deactivated) and the period of record of each well. The groundwater level on Gabriola Island varies seasonally, with low levels in the dry summer, and high levels in the winter wet season. The hydrographs show that the groundwater level reaches a peak relatively quickly, with no further increase during the continuation of the wet season (Figure 2.11). This phenomenon is due to the combination of two things: the low storage ability of the aquifer, and the temperate climate; this is discussed further in below.

Another observation from Figure 2.11 is the fact that the depth to groundwater below the ground surface varies at different locations on Gabriola Island. Although the

hydraulic properties of the bedrock units are, on average, very similar, the heterogeneous nature of the fractures of the bedrock cause the hydraulic properties to vary significantly at a local scale. Thus, the depth to groundwater varies. For example, in Figure 2.11, observation wells OW316 and OW196 have a fairly similar depth to groundwater, whereas the groundwater level at OW197 is approximately 4 m lower. Alternatively, the deference in depth to groundwater could be a result of the location of the well along a groundwater flowpath. In discharge zones, the groundwater level is at a shallower depth. Conversely, the groundwater level tends to be deeper in recharge zones.

Table 2.4 Observation wells on Gabriola Island.

Obs. Well No.	Well Tag No.	Status	Period of Record	
			From	To
OW196	26709	Active	Oct 1, 1973	Present
OW197	37811	Active	Aug 1, 1973	Present
OW385	102208	Active	Jul 9, 2010	Present
OW316	7895	Active	Sep 2, 1992	Present
OW194	26710	Deactivated	Aug 1, 1973	2007
OW317	26350	Deactivated	Sep 2, 1992	2006

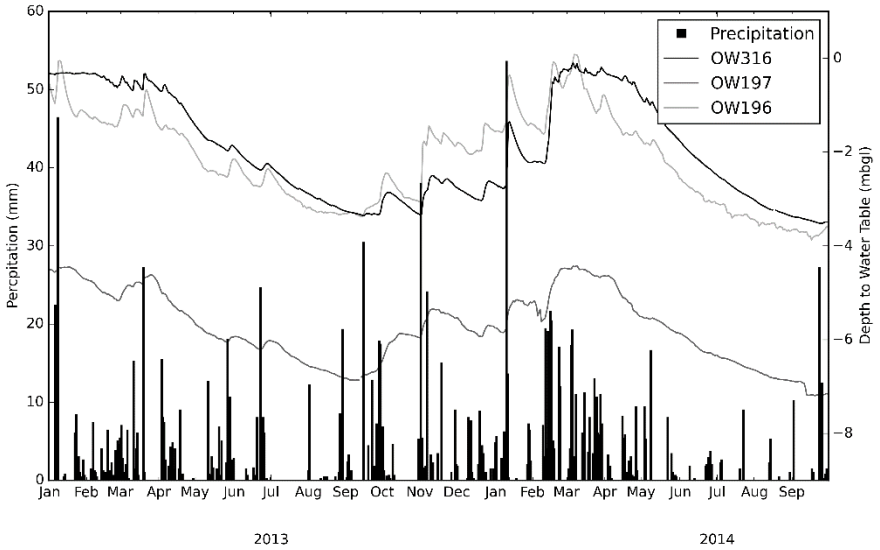

Figure 2.11 Seasonal groundwater level variation. Shown for three provincial observation wells, along with precipitation.

Groundwater recharge is thus seasonally variable. As previously discussed (Section 2.2), due to Gabriola Island's temperate climate, 75% of the precipitation occurs in the wet season (October to March). Given the low ET during this period (see Figure 2.5), it is likely that majority of recharge occurs over this period too. The temporal variability of recharge over an average water year can be broken down into three distinct phases, which are evident in the groundwater level hydrographs. With the onset of the wet season, the low storage causes the volumetric capacity of the fractures in the aquifer to be filled, via recharge, relatively quickly (September to January), causing the water table to rise. Then once filled, the recharge rate slows to the rate of discharge (January to April). Over this period, the water table level remains relatively constant. Once the rainfall rate wanes at the end of the wet season, the recharge rate reduces to less than the discharge rate, and the water table lowers over the summer (April to September), until the wet season begins again.

The spatial distribution of recharge is controlled by many factors, such as the type vegetation, amount of AET, changes in topography, soil type, and hydraulic properties of aquifers. At a regional scale, the hydraulic properties of the aquifers vary little, meaning that all likelihood, this does not control recharge spatially. However, the degree of localized fracturing likely plays an important role in determining water levels at specific locations. While AET is anticipated to vary spatially to some degree, the rapid rate of recharge precludes this from being a significant control on recharge. This

leaves the vegetation type, soil type, and changes in topography as the likely controls on recharge. One of the main goals of this study will be to investigate how these three factors control recharge spatially.

Past studies have employed a range of techniques to estimate recharge to the Gulf Islands. The estimates produced from these studies vary widely, from 1% to 72% of MAP (Table 2.5). The techniques employed included: hydrograph analysis (Hodge, 1977, 1995), use of USEPA Hydrological Evaluation of Landfill Performance (HELP) model to simulate the percolation of precipitation though as soil column (Appiah-Adjei, 2006; Denny et al., 2007; Trapp, 2011; Larocque, 2014), calibration of 3-D numerical groundwater models (Liteanu, 2003), and using the water table fluctuation method (Scibek et al., 2013). The only study to investigate Gabriola specifically was Scibek et al. (2013). The study utilized the water table fluctuation method to estimate recharge values between 1 and 20% of mean annual precipitation. However, the authors noted that the likely recharge value lies some in the range of 10-45% of MAP; and that despite over 15 years of investigation using various techniques, the recharge rate to the Gulf Islands still remains uncertain.

Table 2.5 Recharge estimates of previous studies. nr: no record available.

Study	Study Area	Method	Recharge Estimate (%)	
			Mean	Range
Foweraker (1974)	Mayne Island	nr	3	nr
Hodge (1977 and 1995)	Salt Spring Island	Hydrograph	2.6	1 - 4.5
Appiah-Agjei (2006)	Gulf Islands	HELP	45	20 - 60
Denny et al. (2007)	Gulf Islands	HELP	36.5	12.1 - 62.7
Liteanu (2003)	Saturna Island	Numerical groundwater flow modelling	20	10 - 50
Trapp (2011)	Saturna Island	HELP	56	5 - 56
Scibek et al. (2013)	Gabriola Island	WTF method	10	1 - 20
Larocque (2014)	Salt Spring Island	Numerical groundwater flow modelling	20	3 - 45

2.9. Groundwater Flow and the Water Balance

The water table on Gabriola Island mimics topography with high elevation in the center of the island and low elevation towards the coast (Figure 2.12). As a result, the groundwater generally flows radially from the center of the island towards the coast.

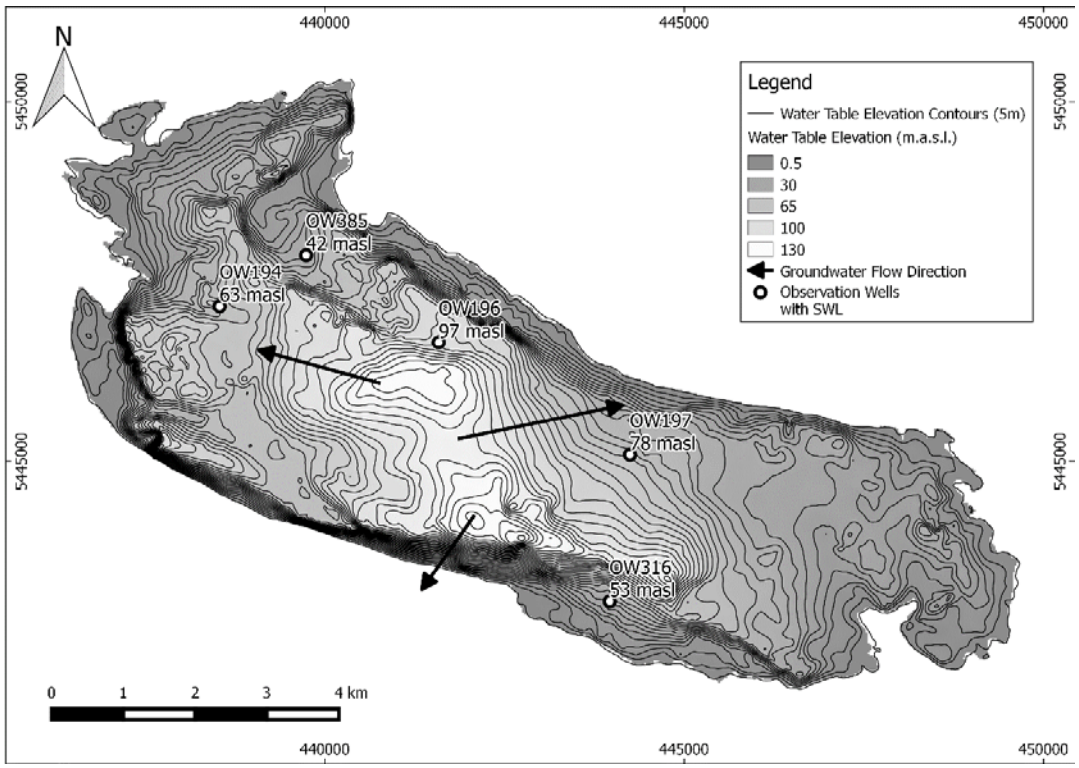

Figure 2.12 Water table elevation. Interpolation of water table elevation from groundwater levels observed following completion of private wells, modified after Scibek et al. (2013); SWL stands for static water level. The arrows show generalized groundwater flow directions.

A water balance helps to conceptualise the hydrological cycle. Scibek et al. (2013) developed a water balance, including recharge, discharge, and aquifer storage, for Gabriola Island. This work has been built upon based on the conclusions of previous studies detailed throughout this chapter (such as Table 4.5), to form an initial simple first-order approximation of the island water balance (Table 2.6).

Table 2.6 Estimated water balance. Values are show as a percentage of mean annual precipitation (% of MAP).

Water Balance Component	Range (% of MAP)	Initial Estimate (% of MAP)
Evaporation (AET)	26 to 50	45
Runoff	32 to 60	40
Recharge	1 to 62.7	15

2.10. Groundwater Geochemistry

The evolution of the groundwater in the Gulf Islands has been studied on a number of Gulf Islands. Based on groundwater samples collected on Saturna Island, Allen and Suchy (2001) proposed that Nanaimo Group groundwaters evolve from being relatively rich in Ca, Mg and HCO_3 near surface, to Na and HCO_3 rich at depth. Sodium enrichment is caused by cation exchange, and is largely ubiquitous given the interbedded nature of mudstones which host clay minerals that act as exchange sites. Salinization pathways are also evident as Na-HCO_3 to Na-Cl, or as Ca-HCO_3 to Na-Cl. This groundwater evolution is also observed in the sedimentary Nanaimo Group rocks on Hornby Island (Allen and Matsuo, 2001), Mayne Island (Allen and Kirste, 2012), and Salt Spring Island (Larocque, 2014).

Earle and Krogh (2004) investigated the groundwater of Gabriola Island, sampling 77 private domestic wells (Figure 2.13). All the wells had an open borehole construction. The authors concluded that the groundwater evolution on Gabriola Island is consistent with processes observed on other Gulf Islands. Figure 2.14 shows a Piper plot of the groundwater samples. The arrow indicates the direction of geochemical evolution from Ca-HCO_3 water type to Na-HCO_3 water type by cation exchange. Apart from two wells, there is no evidence of salinization in the groundwater sampled in that study.

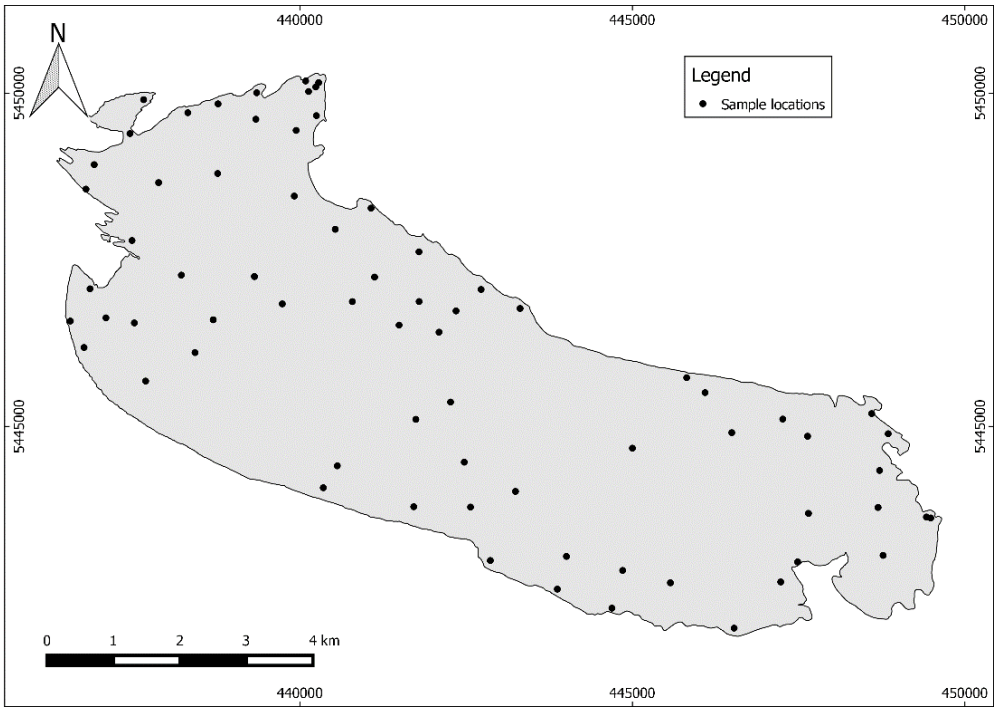

Figure 2.13 Groundwater sample locations. Locations of groundwater samples taken by Earle and Krogh (2004).

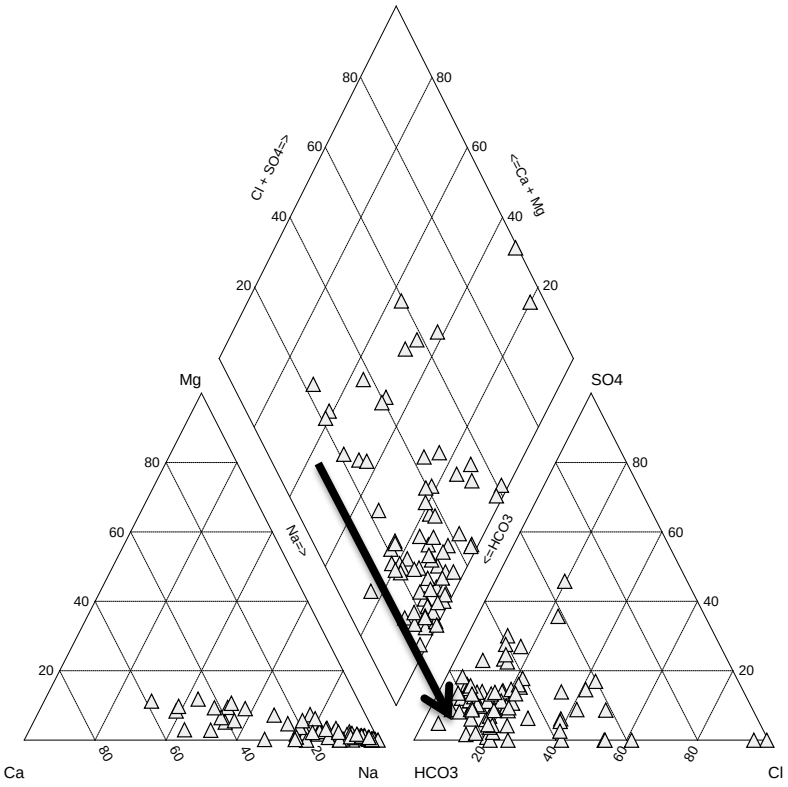

Figure 2.14 Groundwater geochemistry. Data sourced from Earle and Krogh (2004). All samples were taken from wells with an open borehole construction. The arrow indicates the process of cation exchange, where Ca is exchanged for Na from clay present in the aquifer.

2.11. Summary

Overall, there is assumed to be minimal variability in the climate of Gabriola Island such that precipitation, temperature and PET can all be considered spatially uniform. While there is variability in soil types, vegetation is considered to be relatively uniform (treed over 70% of the island). There are few surface water features and generally only ephemeral streams form during the rainy season. There is variability in the hydraulic properties of the fractured bedrock on Gabriola Island at a local scale, and in theory, with depth. However, on a regional scale the fractured bedrock is relatively homogenous in a horizontal direction. The decrease in hydraulic conductivity with depth can be approximated by a simple equation (Eq.2.1).

Chapter 3.

Field Investigation

This chapter focuses on the acquisition and analysis of data collected during a 10-day field study on Gabriola Island in June 2015. The main objectives of the field study were to estimate actual evapotranspiration, and to sample groundwater and surface water for geochemical and isotopic analysis.

3.1. Estimating Actual Evapotranspiration

3.1.1. Background

Actual evapotranspiration (AET) is an important process of water transfer in the recharge process. AET typically varies spatially (Section 2.3), and can be difficult to measure (Xu and Singh, 2005; Gao et al., 2011; Rwasoka et al., 2011), but field observations of AET can be compared with AET simulated in a numerical hydrological model in order to validate model outcomes. For this research, field measurements of AET were made using inexpensive microlysimeters (MLs). These were deployed at a variety of locations, with the aim of quantifying AET variability on Gabriola Island.

Lysimeters have been used globally to measure AET, predominantly for the agricultural industry (e.g. Klocke et al., 1985; Todd et al., 1991; Kinama et al., 2005). A lysimeter is a container placed in the field and filled with soil, in which vegetation can be maintained. The container can either be fully closed (to measure AET) or have a gauged opening to measure the volume of water percolated downward (a direct measurement of recharge). The container is weighed (or percolation flow measured) over an appropriate timescale, with precipitation accounted for. A reduction in mass indicates a loss in water mass, or AET.

The dimensions of lysimeters vary, with traditional lysimeters ranging in size from 3-10 m^3 (Parisi et al., 2009). However, micro-lysimeters (MLs), characterized by a smaller soil volume (less than 1 m^3), have been used to reduce installation and management costs (e.g. Allen, 1989; Daamen et al., 1993; Plauborg, 1994). The

reduced installation cost and effort make MLs an attractive option to studies requiring AET measurements in a number of geomorphic settings.

3.1.2. Methodology

Field Experiments

Weighing MLs were used on Gabriola Island to estimate the actual evapotranspiration (AET) in different geomorphic settings. The field experiments were conducted over the course of seven days in June 2015. The MLs were installed at four locations, each with a different geomorphic setting, across the field site (Figure 3.1). The dominant soil type at all locations was sandy loam. The geomorphic settings of the four MLs locations can be described as: a moderately treed coastal area on the northern side of the island (Blue Whale) (Figure 3.2b), an open field of grass (Rolo Park) (Figure 3.2a), a moderately treed coastal area on the southern side of the island (Shaw Road) (Figure 3.2c), and a densely treed area (Middle Forrest) (Figure 3.2d). Five MLs were installed at each location to test for repeatability.

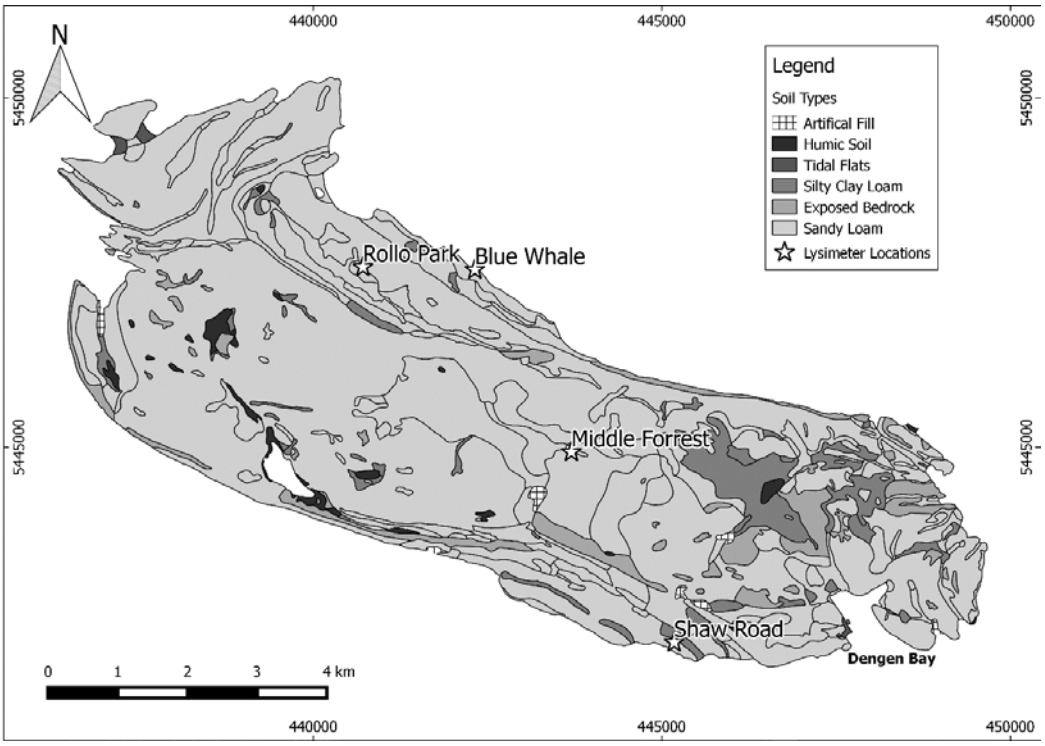

Figure 3.1 Locations of lysimeter experiments. Soil data from MoE (2015a).

Figure 3.2. Geomorphic settings of lysimeter locations. A) Blue Whale, B) Rollo Park, C) Shaw Road, D) Middle Forrest.

The MLs were constructed from aluminum cans, used for canned foods, and were 180 mm deep with an inside diameter of 150 mm. The aluminium cans were filled by pressing them into the soil by hand. The MLs were then excavated using a trowel and shovel and a small sheet of metal placed at the bottom of the soil block to retain the soil in the can. The bottom of the can was then wrapped in aluminium foil held in place by duct tape to prevent downward water leakage (Figure 3.3a). The MLs were placed back in the excavated holes and the excavated soil packed around the ML. The soil surfaces for the majority of the MLs were not flush with the surface due to the stone-rich ground proving difficult to push the MLs in by hand (Figure 3.3b).

Figure 3.3. Geomorphic settings of lysimeter locations. A) Example of ML construction at Rollo Park location, B) MLs in situ at Blue Whale location.

The MLs at Locations 1 and 2 were installed first, while the MLs at the remaining locations were installed one day later. Over the course of the experiment, the mass of the MLs was measured daily (except for Location 1 and 2, which were measured twice on June 14th) for a total of seven times for Locations 1 and 2, and six times for Locations 3 and 4. The measurements were taken throughout the day, although the majority of the measurements were taken before 12:00 pm. The mass of the each ML was measured using a standard kitchen scale accurate to 0.001 kg (equivalent to $\pm$ 0.06 mm of H_2O).

Two of the MLs at each location were tested under wet conditions. The soils were very dry when the MLs were deployed, so to gain some understanding of the daily AET from an initial damp state, some water was added. This was done by adding 50 g of water to the two 'wet' MLs (denoted with a 'w' suffix, i.e. GBL01w); this addition of water mass equates to approximately 2.8 mm of rainfall. The water was added to all the wet MLs before the first mass measurement was taken, except for Location 1, where water was added the day after installation.

The experiment assumed that there were no other external water inputs to the MLs other than the manual addition of water. Accordingly, no rain was recorded at the Nanaimo Airport climate station during the field study, except for a trace amount recorded on June 18th (at the time of writing there were no climate data available from the Gabriola Island climate station for June 2015). The climate normals (1981 to 2010) at the Gabriola climate station for the month of June show an average of 43.2 mm of

precipitation, and an average daily temperature of 14.6 °C. On average, in June, there are approximately 10, 3, and 1 day(s) with precipitation more than or equal to 0.2, 5, and 10 mm, respectively. During June 2015, the Nanaimo Airport climate station recorded only 7.6 mm of precipitation, meaning that conditions were much drier than average, and more similar to September (end of dry season). The weather was relatively constant over the experiment, with a mix of sun with some cloud, and moderate to low winds near the coast.

Data Analysis

The measurement of mass change of each ML was converted to a height equivalent daily flux in units of mm/day, representing AET. Since mass measurements were taken at different times of day, the mass change was normalized to a 24 hour period. The conversion from mass of water to height equivalent flux assumes a water density of 1.0 g/cm^3 and the radius of the MLs to be 75 mm.

3.1.3. Results

The average daily AET flux varied between each location (Figure 3.4). The average evapotranspiration (ET) flux ranged from a minimum of 0.11 ± 0.01 mm/day at the Shaw Road location, to a maximum of 0.30 ± 0.02 mm/day at the Rollo Park location. The Blue Whale and Middle Forrest locations had relatively similar average flux results of 0.163 ± 0.003 mm/day and 0.150 ± 0.004 mm/day, respectively. This data are summarized in Table 3.1. The higher ET flux at the Rollo Park location is attributed to the high exposure to direct sunlight of the open field setting. All the other sites were tree-covered to some degree, generally shading the MLs from direct sunlight.

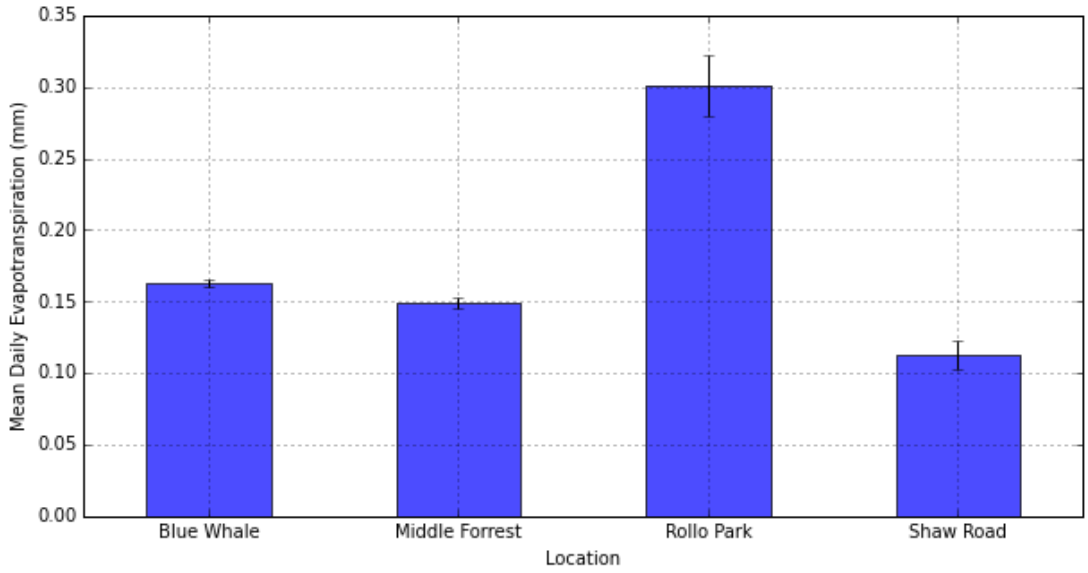

Figure 3.4 Mean daily AET from experiment locations.

Table 3.1 Mean daily AET results.

	Blue Whale	Middle Forrest	Rollo Park	Shaw Road
Mean Daily AET Flux (mm/day)	0.163 ± 0.003	0.150 ± 0.004	0.30 ± 0.02	0.11 ±0.01

Each day's results were averaged for each location, and then the daily results averaged over the whole experiment period.

The moisture content of a soil can limit the AET flux. To investigate this, the average AET flux from the dry and wet MLs were compared (Figure 3.5). The wet vs dry data are summarised in Table 3.2. On average, the 'wet' MLs lost more water mass to ET than the 'dry' MLs at all locations. The ET flux recorded from the Wet MLs was approximately double that recorded from the Dry MLs. From this observation, it would appear that low soil moisture content significantly limits evapotranspiration.

However, apart from the Shaw Road location, which produced erratic results (discussed below), an ET flux from the Dry MLs was measured at all locations. This suggests that there was sufficient soil moisture present at the time of measurement to result in a measurable ET flux.

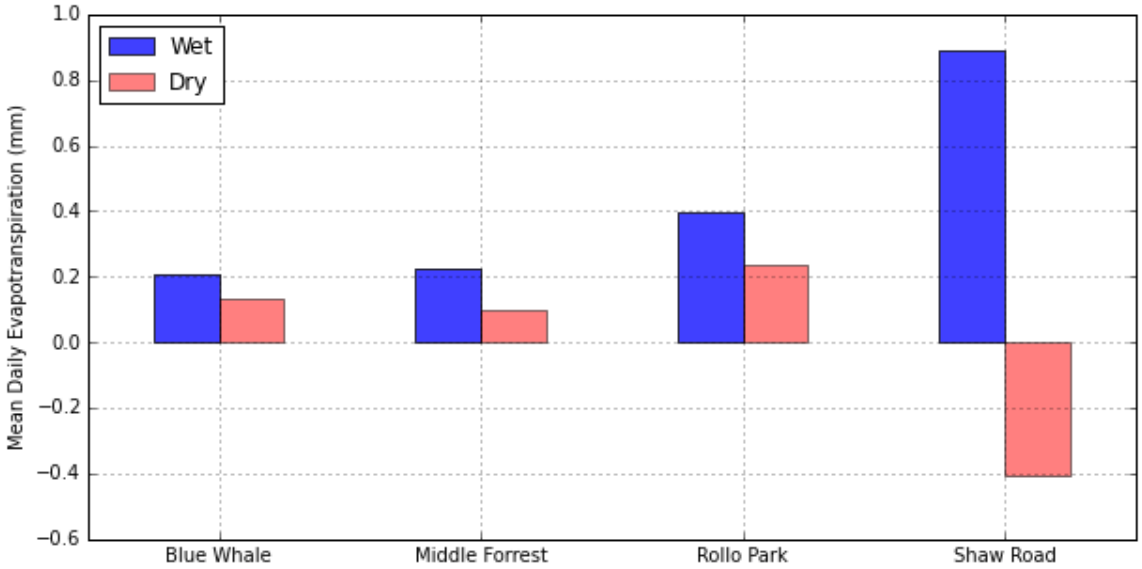

Figure 3.5 Mean daily AET from wet and dry lysimeters.

Table 3.2 Wet vs Dry AET results.

	Blue Whale		Middle Forrest		Rollo Park		Shaw Road	
	Wet	Dry	Wet	Dry	Wet	Dry	Wet	Dry
Mean Daily AET Flux (mm/day)	0.21	0.13	0.22	0.10	0.40	0.24	0.89	-0.41
Standard Deviation (mm/day)	0.16	0.16	0.61	0.44	0.82	0.77	1.65	1.82

Over the time period of the experiment, the average AET measured each day varied considerably (Figure 3.6). All the locations recorded both positive and negative AET flux measurements, or mass losses and gains. Since there was no rain recorded in the region, one would expect the AET flux to be only positive, representing water mass loss. This raises concern over the ability of the experiment to estimate AET accurately. For example, the results at the Shaw Road location show a negative AET flux three out of the five days. Furthermore, the days of higher and lower AET fluxes do not appear to correlate between locations. Excluding the Shaw Road location, the results from the other locations appear to be more consistent.

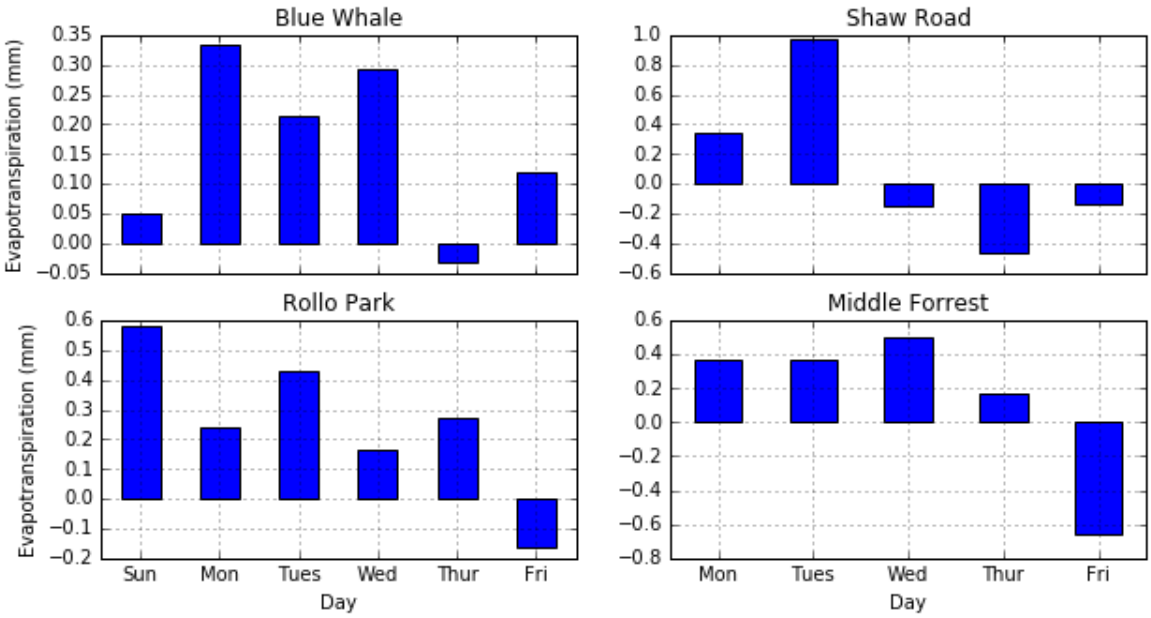

Figure 3.6 Temporal variation in measured AET.

There was a trace amount of rain recoded on June 18th (Thursday). However, it is unknown whether this affected the experiment results. The Rollo Park, Shaw Road, and Middle Forrest all show a negative AET flux the day after the trace amount of rain, but the Blue Whale location does not (Figure 3.6).

As previously mentioned, the measurements of the MLs at the Shaw Road location produced erratic results compared with the other locations. Figure 3.7 shows the statistical distribution of the all the results recorded across the week for individual MLs. The Shaw Road location had a much greater range of daily AET compared to the other locations. For example, the results from the dry MLs at this location indicated a negative ET flux overall (Figure 3.5), in other words a gaining of mass. Among other errors (discussed below in Section 3.1.4), one cause for this may be an unanticipated flux of water into the MLs. It was observed midway through the experiment that a nearby field was under irrigation for part of the day. It is possible that water from the irrigation may have been blown over to the Shaw Road experiment location. This possible addition of water may have caused the negative ET flux results measured at this location. However, the wet MLs recorded a water mass loss (higher AET flux) over two times as great as another location (Figure 3.5), appearing to not be affected by the proposed increase in water mass. It is unlikely that the irrigation only fell coincidently

on the dry MLs. It is more plausible that errors in the experiment were the cause of the erratic results. Because of this, the results from the Shaw Road experiment location are not included in the general interpretation of the results.

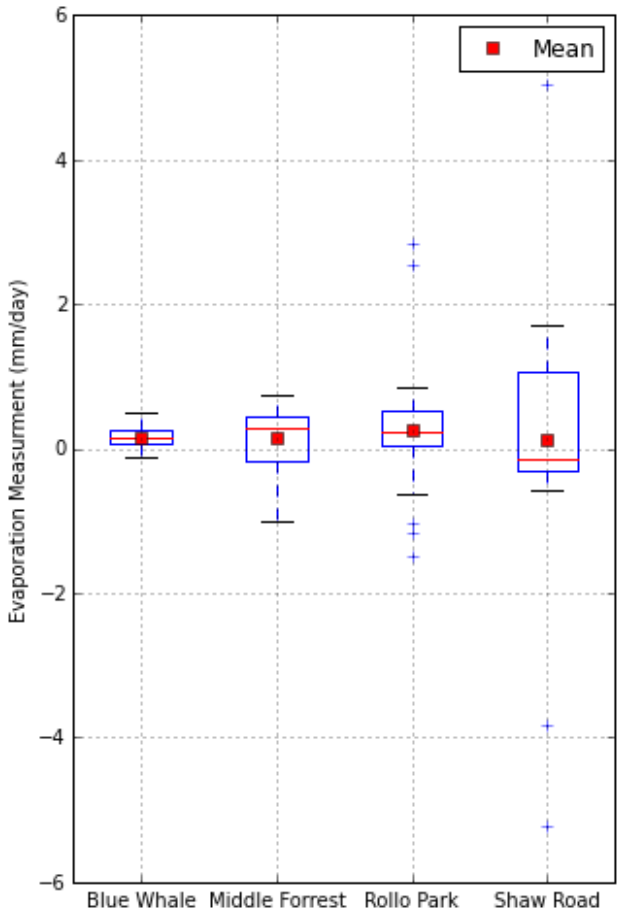

Figure 3.7 Boxplots of AET measurements. Mean represents the arithmetic mean.

3.1.4. Discussion

The location of the ML experiments impacted the AET estimates to some degree. As expected, the location most exposed to the sun (Rollo Park) had the highest AET estimate (0.3 mm/day). Whereas the locations covered by trees had lower AET estimates (between 0.163 and 0.150 mm/day), hinting at some spatial variability in AET.

Interestingly, the wind speed did not appear to significantly affect AET estimates. The experiments at the Blue Whale location, near the coast and subject to

moderate winds, and Middle Forrest location, densely vegetated area with little to no wind, produced comparable AET estimates, 0.163 and 0.150 mm/day, respectively. This observation is qualitative since the wind speed at each location was not measured.

The comparison of wet and dry MLs leads to the conclusion that the soil moisture content of the soil has a significant control on the rate of AET on Gabriola Island. During the relatively dry summer months, the low soil moisture content limits the amount of AET that occurs. Thus, in the summer month, there is a greater potential for AET to occur, but only when precipitation occurs is AET significant. As described in Section 3.1.2, the climate, and thus soil, was much drier than average when this field experiment was conducted. This may mean that in normal years, when more precipitation falls in June, the AET rate is less likely to be limited by the soil moisture content, leading to a higher AET rate than was observed.

One limitation of using MLs to estimate AET is that the approach does not take into account the AET from larger vegetation, such as trees and shrubs. Spittlehouse and Balck (1979) estimated that approximately 5 mm/day of water is evapotranspired from Douglas fir forests in the summer months, much higher than the AET rate estimated by this experiment. Since the majority of Gabriola Island is treed, coupled with the low soil moisture content of the soils during the summer, it would seem vegetation is the dominant contributor to AET. Thus, although there is some spatial variation in AET between open field land cover and densely vegetated areas, the island is mostly treed, so at a regional scale, AET rates will vary little spatially.

Although using MLs provides a way of relatively easily estimating AET, there are a number of sources of error in this experiment:

1. Although great care was taken when removing and returning the MLs to the holes for each measurement, it was possible that small amounts of soil/sticks/leaves were inadvertently added or removed from the ML. The median mass change measured was 0.004 kg, meaning that even the addition or removal of very small sticks/leaves/soil clumps could result in drastically different AET estimates.

2. The metal casing used to construct the MLs could have heated up, causing more soil moisture to evaporate than normal. However, this is only likely significant at the Rollo Park location since the other locations were not in direct sunlight.

3. During the installation of the MLs, the soil column was disturbed, potentially increasing the amount of air present. This increase in porosity may have led to an over estimate in AET compared to an in situ soil column.

The AET results most likely underestimate the amount of AET that occurs on Gabriola Island. Even the highest rate of 0.3 mm/day (Rollo Park) only equates to approximately 110 mm/year, which is approximately 11% of MAP (Mean Annual Precipitation) (958 mm). Previous studies report ranges in AET between 26 and 50% of MAP (see Section 2.3). Furthermore, as discussed in Section 2.3 there is almost certainly a seasonal trend in AET over a typical year, i.e. the highest rates of AET are during the summer months (June to September), and lowest during winter. Thus, the maximum rate of 0.3 mm/day during the summer months (e.g. June) would result in a lower total yearly rate than if the AET rate was considered constant over the year. Note, that this mean rate includes measurements from both wet and dry MLs. Since the experiment was conducted over an extremely dry period, and AET is dependent on soil moisture, the AET measurements from the dry MLs are most likely lower than if the experiment had been conducted during a 'normal' summer, when some rainfall occurs.

With the potential sources of error and limitations of this ML experiment notwithstanding, conclusions as to the how AET influences recharge dynamics can be drawn. AET is only significant when the soil is sufficiently moist, since the moisture content of the soil limits AET. This means that during the summer months, water potentially available for recharge likely only occurs during higher intensity rainfall when the precipitation rate exceeds the AET rate. During less intense events, the majority of the water is evapotranspired. In the winter months AET is most likely lower, and will have a reduced control on recharge. Thus, AET influences recharge temporally. The amount of AET varies by vegetation cover. Consequently, because much of the island is tree-covered, AET will not likely control the spatial variability of recharge

AET is only one factor that controls recharge. Other factors, such as the slope of the land surface, the soil moisture capacity, and storage potential of aquifers, can also play an important role.

3.2. Groundwater Geochemistry and Apparent Groundwater Age

Groundwater Evolution and Apparent Age

Analysis of groundwater geochemistry provides the ability to investigate groundwater evolution, and identify areas of recharge and discharge. Although important geochemical processes do occur in the soil and unsaturated zone, this study focuses on the water evolution along the groundwater flow path. Understanding the groundwater geochemical evolution can help inform, and constrain, the conceptual model of groundwater flow.

The groundwater geochemistry on Gabriola Island was described in Section 2.10. Ultimately, the groundwater geochemistry on Gabriola Island is similar to that of other Gulf Islands (e.g. Allen and Suchy, 2001). For the purposes of interpretation of the results of this study, groundwater evolution on the Gulf Islands is only briefly summarized here. Results specific to Gabriola are discussed later.

Groundwater evolution within the Nanaimo Group rocks of the Gulf Islands is controlled by three main stages. Firstly, as rainfall enriched in Na and Cl travels through the soil and unsaturated zone, the water becomes enriched in Ca and HCO_3 by the reaction of carbon dioxide (CO_2) and calcite ($CaCO_3$). This represents relatively young groundwater. Secondly, as groundwater moves along a flowpath, cation exchange, swapping Ca (in the water) for Na (on clay and mineral surfaces), results in a more mature Na-HCO_3 type water. The process of salinization, generally through mixing, to produce a Na-Cl type water is the final stage of the evolution. Direct salinization due to saltwater intrusion can also occur as evidenced by mixing between Ca-HCO_3 waters and seawater.

Although useful, analyzing the geochemical evolution of groundwater only provides qualitative information on the groundwater flow regime. For a numerical model, quantitative information is highly desirable. Tracer data, such as tritium content,

can augment the groundwater geochemical evolution analysis, and provide quantitative information, such as apparent groundwater age.

Tritium is the only radioactive isotope of hydrogen. It is a tracer with relatively low natural production through cosmic ray spallation in the atmosphere and neutron radiation of rocks on the surface (Clark and Fritz, 1997). Tritium is the only tracer that is incorporated as part of the water molecule. The tritium content of water in a sample is expressed in TU (tritium units), where one TU unit is equivalent to one molecule of $^{3}H^{1}HO$ in 10^{18} molecules of $^{1}H_2O$ (Solomon and Cook, 2000). When water becomes separated from the atmosphere through recharge into a groundwater system, the tritium source is isolated and the tritium concentration decreases over time due to radioactive decay. The half-life of the tritium isotope is approximately 12.32 years (Kazemi et al., 2006).

The concentration of ^{3}H in precipitation varies spatially and has been recorded through time at various locations around the world. Figure 3.8 shows ^{3}H levels in tritium units (TU) in the precipitation from the closest station with long-term data in Portland, Oregon (IAEA/WMO, 2015). The atmospheric tritium concentration has remained stable since approximately 1995, ranging between approximately 7 and 2 TU.

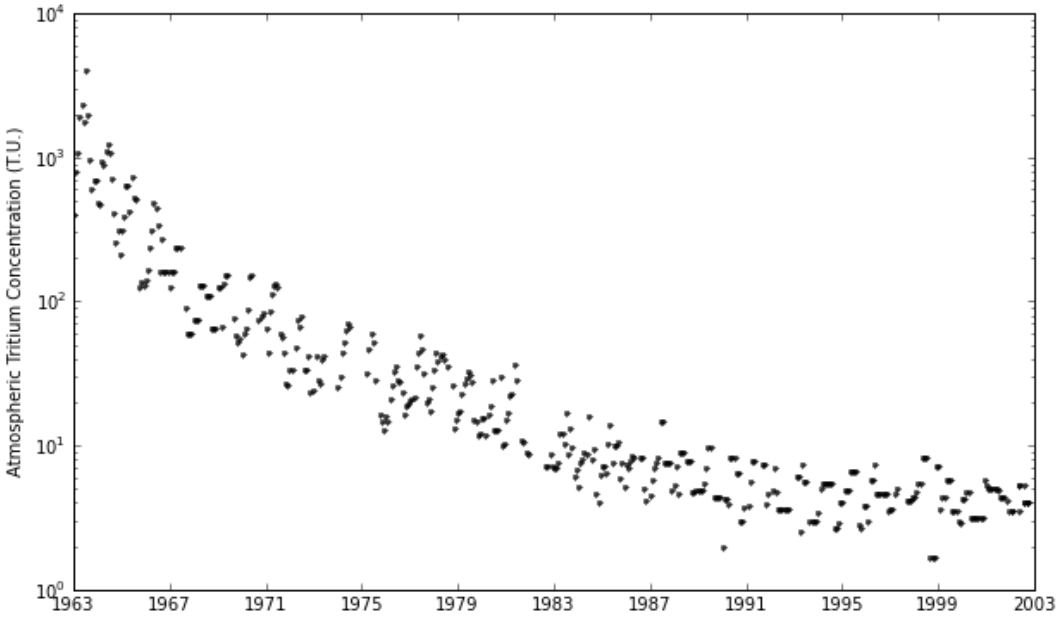

Figure 3.8 Atmospheric tritium concentration from Portland, WA. Data from IAEA/WMO (2015).

Atmospheric tritium production is relatively constant from incoming solar radiation (Clark and Fritz, 1997). Anthropogenic generation of tritium in the 1960s from atmospheric testing of nuclear bombs resulted in a large increase in the tritium levels in the atmosphere globally. A peak level was reached and is referred to as the 'bomb peak' (Clark and Fritz, 1997). ^{3}H in groundwater is derived from precipitation and thus the concentration of ^{3}H in groundwater reflects the atmospheric ^{3}H concentration at the time of recharge. Because ^{3}H is radioactive, groundwater that has lost contact with the atmosphere for a prolonged period of time (many decades or longer) exhibits low or non-detectable levels of ^{3}H (Kazemi, et al. 2006).

Traditionally, through a time series analysis of tritium content in groundwater, the movement of this bomb peak in aquifers was measured, allowing an apparent[1] age of groundwater to be estimated. Since this bomb peak was reached, the level of tritium has decreased due to decay and attenuation by oceans. The bomb peak is only preserved in very slow moving, stagnant groundwater. The usefulness of the bomb peak method for estimating the groundwater age has largely passed due to the loss of the signal in most groundwaters. Other methods are available however. One method involves the measurement of the abundance daughter product of tritium decay, helium-3 (^{3}He), and residual tritium to estimate a groundwater age (Clark and Fritz, 1997). However, the sampling of gaseous ^{3}He is non-trivial, and the cost of laboratory analysis is substantially greater than tritium alone.

In this study, a qualitative age of groundwater is estimated based on the presence of tritium in the groundwater. If tritium is present, then some part of the groundwater sample was recharged after the bomb peak, inferring a groundwater of <50 years. Conversely, if no tritium is present, then the groundwater was recharged prior to the bomb peak, giving an approximate age of >50 years since recharge. Surface waters (swamps and creeks) were also sampled for tritium analysis in order to interpret the potential contributions of groundwater.

3.2.1. Methodology

Ten groundwater and surface water samples were collected on Gabriola Island in June 2015. Of the ten samples, four were from creeks, two were from

[1] The term "apparent" is used because the tritium age represents a mixture of water with contributions from different flowpaths, and thus different ages.

wetlands/swamps, and four were from private domestic wells of open borehole construction. The locations of the collected waters samples are displayed in Figure 3.9, and details of the samples are summarised in Table 3.3. This time of year represented baseflow conditions for the creeks due to a relatively dry early summer period.

Table 3.3 Sample details.

Sample ID	Sample Type	Well Depth (mbgl)
HS1	Swamp	N/A
CM1	Swamp	N/A
CC1	Creek	N/A
CC2	Creek	N/A
GH1	Creek	N/A
DB1	Creek	N/A
GH2	Groundwater	43
CC3	Groundwater	61
CC4	Groundwater	84
CC5	Groundwater	61

Note: the well depth are anecdotal approximates from property owners.

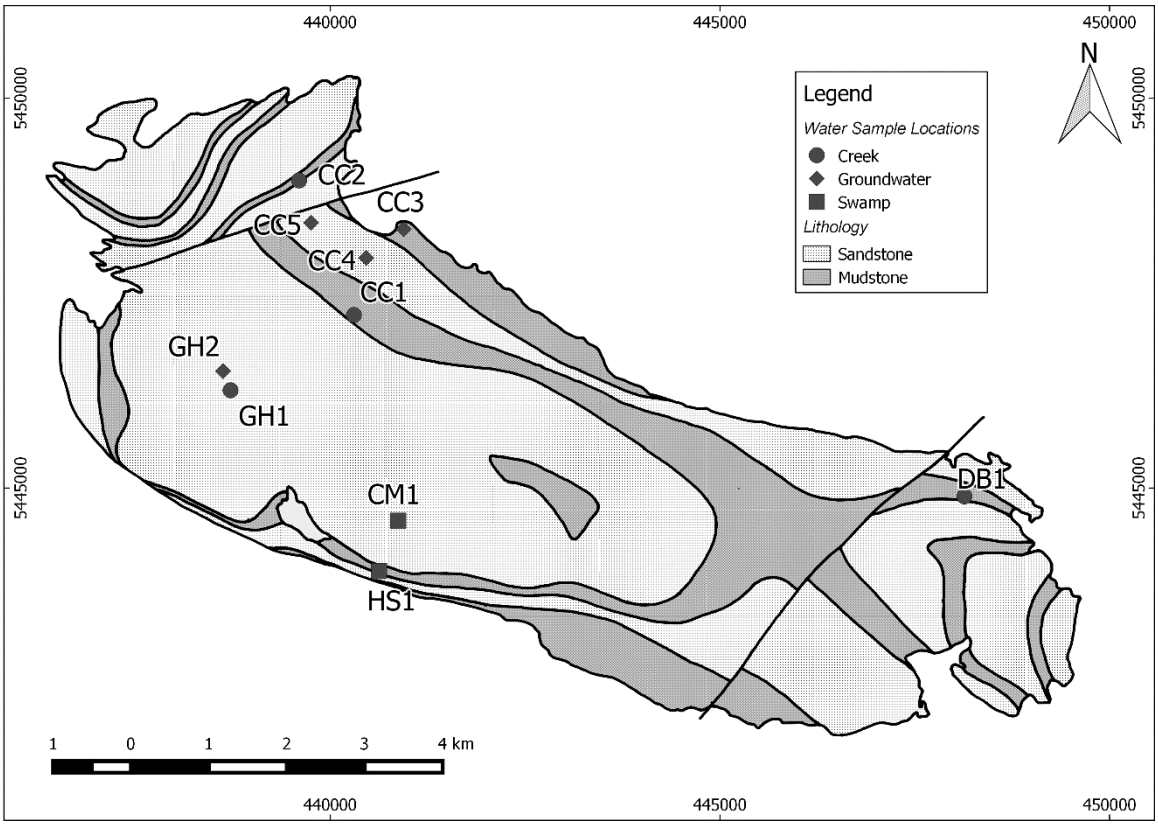

Figure 3.9 Locations of collected water samples. Sample locations are superimposed on lithology for comparison.

Field parameters, including pH, electrical conductivity (EC) and temperature, were recorded at the time of sample collection. Two samples were collected from each site; a one litre sample for tritium and anion analysis, and a smaller acidified 50 mL sample for cation analysis. All samples were 'grabbed' as a bulk sample. Samples were later analysed for metals and major anions, and tritium content in water. The cations and anions were analysed at the SFU Aqueous Geochemistry Lab using an Dionex ICS 3000 ion chromatography system to measure anions (F, Cl, Br, NO_3, PO_4, SO_4), and a Horiba Jobin Yvon Ultima 2 inductively coupled plasma atomic emission spectrometer to measure cations (K, Na, Ca, Mg, Al, Ba, B, Fe, Li, Mn, Si, Sr). Bicarbonate (HCO_3) was analysed by titration upon return from the field.

Tritium analysis was conducted at the Dissolved and Noble Gas Lab in the University of Utah, USA by the helium ingrowth method. Eight water samples: one swamp water sample; three creek water samples; and four groundwater samples were

analysed for tritium. The full water sample chemical analysis results are tabulated in the Appendix.

3.2.2. Results

Aqueous Geochemistry

The field parameters are summarised in Table 3.4, and the chemical results are presented on a Piper Diagram in Figure 3.10. The swamp water samples had the lowest TDS valued, followed by the creek water samples. The groundwater samples had the highest values of TDS measured. The water types range from Ca-HCO_3 (e.g. HS1) to Na-HCO_3 (e.g. CC3). Generally, the samples taken from swamps (HS1 and CM1) have a mixed Ca-Na-HCO_3 water type. The creek samples have a Na-Ca-HCO_3 type water, except for sample CC2, which displays a similar water type to the swamp water samples. The groundwater samples have a Na-HCO_3 water type.

Table 3.4 Field parameters.

Sample ID	Sample Type	EC (µS/cm)	TDS (ppm)	pH	Temp. (°C)
HS1	Swamp	142	90.9	6.40	14.2
CM1	Swamp	61	38.9	7.79	14.9
CC1	Creek	199	127	7.28	13.5
CC2	Creek	224	143	7.53	14.7
GH1	Creek	229	146	6.90	14.3
DB1	Creek	320	205	7.00	14.2
GH2	Groundwater	326	208	6.75	11.3
CC3	Groundwater	398	254	8.13	10.9
CC4	Groundwater	436	279	7.1	11.1
CC5	Groundwater	390	249	7.3	10.7

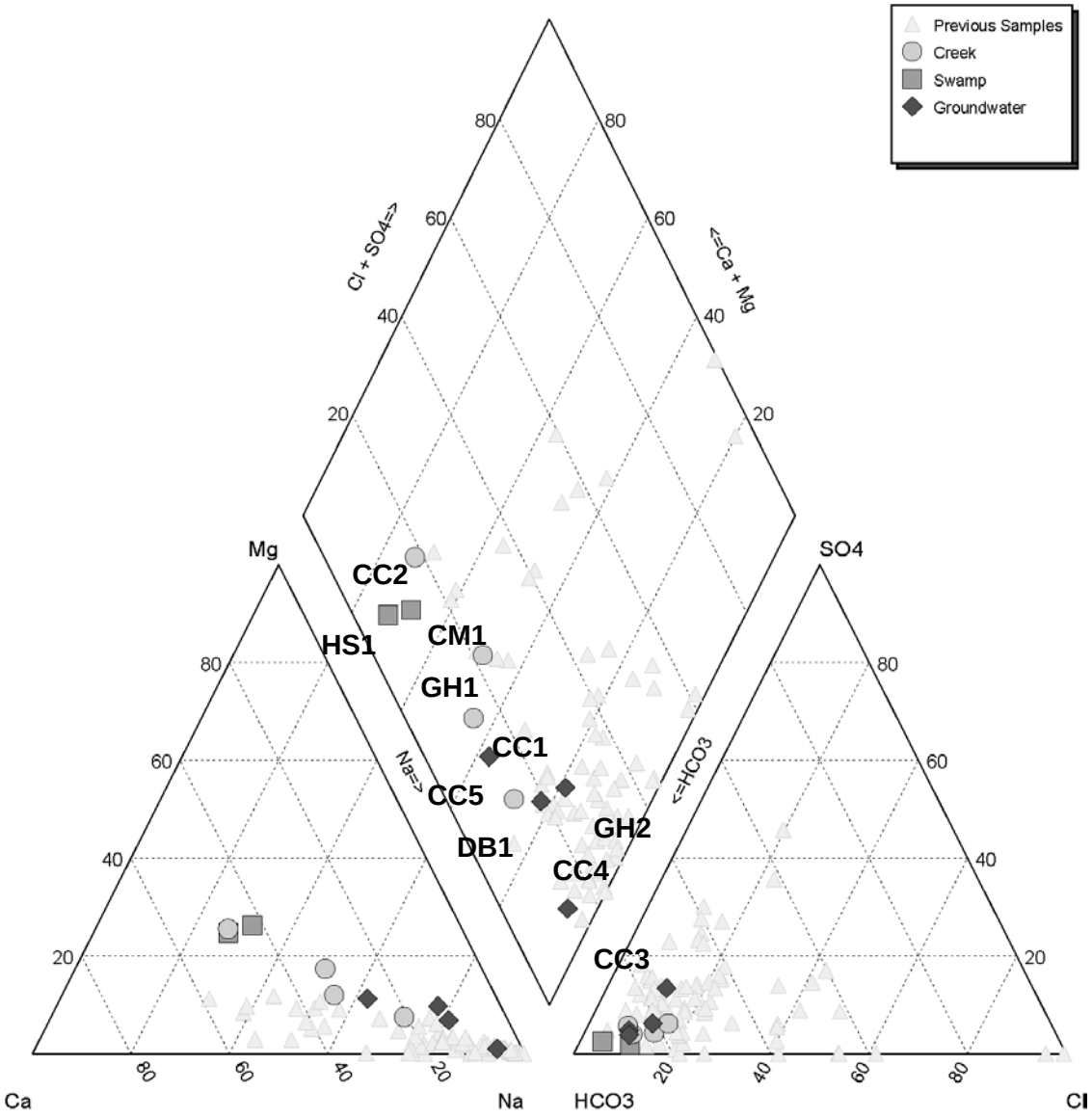

Figure 3.10 Piper diagram of water samples. The chemical composition of the 'Previous Samples' were sourced from Earl and Krogh (2004); all are groundwater samples.

As previously mentioned in Section 2.10, the geochemical evolution of groundwater hosted in Nanaimo Group bedrock follows a similar evolutionary pathway throughout the Gulf Islands, and indeed do so on Gabriola Island. The process of cation exchange dominates the groundwater evolution of this study, whereby the Ca in the young, Ca-HCO_3 water exchanges with Na ions hosted on the clay minerals in the bedrock to produce a more mature Na-HCO_3 type water. The term mature in this context is not related to the age of the water, rather, the extent to which the water has been evolved though the cation exchange process. Unlike the other Gulf Islands, there

is little evidence of mixing between Na-HCO_3 waters and Na-Cl waters (Figure 1.10). This does not mean that this process does not occur, rather few samples have been collected from this mixing line. No samples from this study or previous studies plot near the Na-Cl end member.

Tritium

The results of the tritium analysis are presented graphically in Figure 3.11, and a summary of the results is provided in Table 3.5. The tritium content of the water samples ranges from 1.45 to 3.14 tritium units (TU). The tritium content reflects the source of the water sampled (Figure 3.11). The surface water samples (Swamp and Creeks) have a high tritium content, and the groundwater samples have a lower content. The exception is the groundwater sample GH2, which has relatively high tritium content compared to the other groundwater samples. This well is somewhat shallower than the other wells (Table 3.3) suggesting that the residence time may be lower.

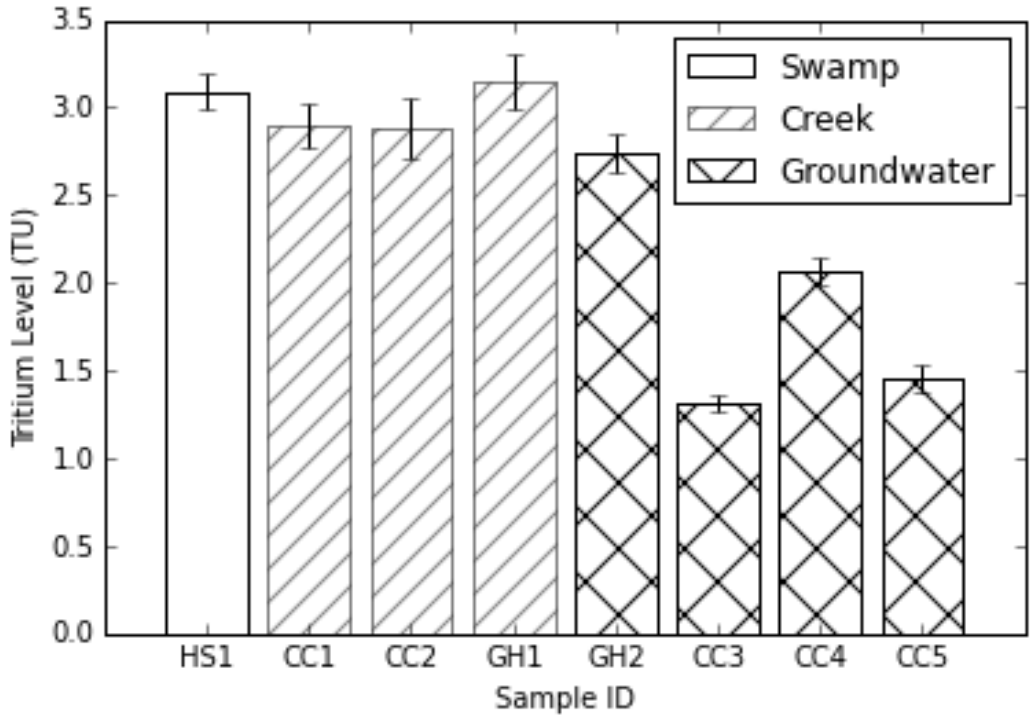

Figure 3.11 Tritium content of selected water samples.

Table 3.5 Tritium analysis results.

Sample ID	Tritium Level (TU)	Sample Type	Well Depth (mbgl)
HS1	3.09	Swamp	N/A
CC1	2.9	Creek	N/A
CC2	2.88	Creek	N/A
GH1	3.15	Creek	N/A
GH2	2.74	Groundwater	43
CC3	1.31	Groundwater	61
CC4	2.07	Groundwater	84
CC5	1.45	Groundwater	61

Note: the well depth are anecdotal approximates from property owners.

The presence of detectable tritium in all the wells sampled indicates that the apparent groundwater age is less than 50 years old.

3.2.3. Discussion

Both swamp samples, HS1 and CM1, have distinctly different chemical compositions than the creek and groundwater samples, except for CC2. The chemical signature of the swamp samples, Ca-HCO_3, is typical of soil water, indicating that the dominant source of water is likely surface runoff rather than groundwater discharge. The low TDS values measured further support this conclusion. The tritium level concentration similarity between the swamp and creek samples indicates similar mean residence times.

The creek samples have a wide range of chemical compositions (e.g. CC2 vs DB1), with DB1 having a chemical composition similar to several of the groundwater samples (e.g. CC4 and GH2). Furthermore, even creeks sampled that were in relatively close proximity to each other, CC1 and CC2, have distinctly different chemical signatures. This implies that proportion of groundwater discharging into the creeks varies over short distances. For example, given that CC2 has a Ca-HCO_3 water type, the dominant source of water is likely to be surface runoff or quick flow, with less influence of groundwater. In contrast, the CC1 and DB1 samples have a mixed to a more mature chemical signature, suggesting more mixing with groundwater. The presence of tritium in the creek samples suggests that any groundwater that does

discharge into the creeks is likely relatively young, deriving from a relatively shallow flow system, or that the proportion of deep groundwater (with no tritium) is very low.

In the groundwater samples, there appears to be little correlation between the chemical composition and tritium concentration. CC4 and GH2 have very similar chemical compositions, but only differ in tritium concentration by 0.7 TU, which equates to a difference in apparent age of approximately 5 years. Furthermore, CC5 had the least mature chemical signature, but a lower tritium concentration than either CC4 or GH2. CC3 has the most mature chemical signature, and the lowest tritium content, indicating a higher apparent age. The position of CC3 along a theoretical groundwater flow path, close to a discharge area (the ocean) where the groundwater is expected to be older is consistent with the lower tritium concentration. CC4 and CC5 are at intermediate positions along the flow path, which correspond to higher tritium concentration than CC3, but lower than the level of the creek and swamp samples. The high tritium content of GH2 may indicate it is located in an area of active recharge. In general, the chemical composition of groundwater varies, but there was detectible tritium in all samples. So either, the groundwater is relatively young, or there is a low proportion of deep groundwater contributing to the samples.

Overall, the chemical compositions of the samples varied, but the tritium concentrations were mostly consistent between within each sample group. The creek samples chemical composition likely varied due to differing proportions of groundwater discharge mixing with surface runoff. The presence of detectable tritium in all of the groundwater samples suggests that either the groundwater is generally relatively young, or that the proportion of deep, old, groundwater mixing is very low. Distinguishing between the two cases is difficult due to the limited amount of data available.

3.3. Summary

The spatial variability of AET, at four differing locations, on Gabriola Island was investigated using microlysimeters (MLs) over a 10-day field experiment in summer 2015. The different locations represented differing geomorphic settings. Soil moisture was found to be a limiting factor of AET on Gabriola Island. The MLs that had water added evapotranspired almost twice the amount of water than the dry MLs. During the

summer, a time of minimal rainfall, the AET from the soil is minor. Only when rainfall occurs is AET potentially significant. This may imply that the amount of AET is greater during Fall and Spring when rainfall is high, and soil moisture is higher.

The AET from this experiment only captures the AET occurring from the soil and grass, missing larger vegetation types such as trees or shrubs. The AET estimated from this field experiment is an order of magnitude lower than previous studies solely measuring AET from trees. Thus, the use of MLs may not be appropriate for measuring AET in densely vegetated areas. Since the majority of Gabriola Island is vegetated with trees and shrubs, it is unlikely that there is any significant spatial variation in AET at a regional scale. Thus, AET does not control spatial variation in recharge on the island.

Groundwater evolution and apparent groundwater age were investigated through geochemical and tritium analysis of water samples. A total of ten water samples from swamps (two), creek pools (four), and private groundwater wells (four) were obtained during a field visit in June 2015. All samples had the major ion chemistry and tritium concentration analysed. The groundwater samples had the highest TDS values, followed by the creek, and then swamp samples. The groundwater evolution is dominated by cation exchange, similar to previous studies in the Gulf Islands region. Specifically, Ca ions are exchanged with Na ions from the aquifer material, producing a water enriched in Na. In general, the swamps have geochemically immature composition characterized by a Ca-HCO_3 water type, the creeks have a transitional chemical composition spanning Ca-HCO_3 to Na-HCO_3 water types, and the groundwaters typically have a more a mature Na-HCO_3 composition. There was variation in this trend, particularly in the creek water samples.

All the water samples had tritium present, indicating that the mean residence time of all water samples is less than 50 years. In general, the swamp and creek pool water samples had higher tritium concentrations than the groundwater well samples, although local exceptions to this trend exist. The swamp samples had very similar tritium concentrations to the creek pool samples, suggesting similar mean residence times. The low TDS and relatively immature chemical composition indicates that the swamps are mostly sourced from surface runoff rather than groundwater discharge. The relatively high tritium concentrations and variable chemical signature of the creek pool samples points to differences in the proportion of groundwater mixing with surface

and shallow runoff derived water. Although mostly low, exceptions to the low tritium concentrations in the groundwater well samples did exist. At one location, the tritium concentration of a groundwater well was only slightly lower than an adjacent creek pool sample. This likely represents a local zone of rapid recharge. However, private wells constructed prior to 2004 may not have been constructed with surface seals (Lapcevic, personal communication), thus rapid recharge may be due to direct surface water leakage into the well.

Overall, the variable chemical composition and presence of tritium in all the samples suggests one of two things. Either, there is no deep, old, isolated groundwater reaching the swamps and creeks, and wells, or, the proportion of old groundwater mixing with younger water is very low. The limited amount of data makes it difficult to differentiate between these two possible flow regimes.

Chapter 4. Recharge Model Development

4.1. Introduction

A coupled land surface - subsurface model numerical model was developed to investigate recharge on Gabriola Island. This chapter documents the development and calibration of the model only. The development of the numerical model is based on the conceptual model outlined in Chapter 2. The analysis and discussion of the model solution with respect to the recharge dynamics, as outlined in the objectives of this thesis, are presented in the next following chapter, Chapter 5.

In this modelling study, there were three stages of simulation: a calibration stage, validation stage, and forecast stage. In the calibration stage, the input parameters are adjusted, within a reasonable range, to find the combination of parameters that produces model results that most closely match historic field observations. The calibrated model was then run in the validation stage using climate data from a separate time period to further demonstrate that the model was representing the system dynamics adequately. Finally, the simulation was run into the future, attempting to produce a forecast of the model results for future climate conditions.

4.2. Model Construction

MIKE SHE was developed by the Danish Hydraulic Institute (DHI), the British Institute of Hydrology, and the French consulting firm SOGREAH (Abbott et al., 1986). Early developments of the code, Système Hydrologique Européen (SHE), were based on the Freeze and Harlen (1969) blueprint. This code was further developed and extended by DHI from the mid-1980s. Today, MIKE SHE is a state-of-the-art, deterministic, fully-distributed and physically based modelling system that can simulate all of the major components of the land-based hydrological cycle (Jaber and Sukla, 2012). It employs a finite difference approach to solve partial differential equations of overland flow, unsaturated zone flow, and saturated zone flow (DHI, 2007). Evapotranspiration and interception are solved analytically or empirically. The finite difference method uses a network of grid squares to represent the spatial variability of the land surface. The vertical discretization of the model domain is completed through

the integration of unsaturated and saturated zone layers. A brief summary of the modules is discussed below (Jaber and Shukla, 2012):

- The interception and evaporation module computes the actual evapotranspiration (AET) from an area using the Kristensen and Jensen model and a user-defined potential evapotranspiration (PET). This model requires vegetation dependent parameters such as leaf area index (LAI) and root characteristics to calculate AET.
- The unsaturated flow in MIKE SHE is only calculated in 1-D, vertically. The van Genuchten parameters, along with the saturated hydraulic conductivity, are used to solve the Richards' equation for water flow in the unsaturated zone.
- The overland flow component simulates runoff when infiltration capacity of the soil is exceeded and when groundwater discharges to the surface. The finite difference method utilizes the diffusive wave approximation of the Saint-Venant equation to solve the overland flow water movement. The topographic slope, and the Manning's M coefficient control the direction and rate of runoff, respectively.
- The saturated zone flow component is solved in MIKE SHE using the 3-D groundwater flow equation. Boundary conditions such as: fixed head, zero flux, gradient, and specified flux are options which control the flow of groundwater within the model and attempt to mimic real world conditions. Subsurface conditions are modelled as layers and lenses, with representative hydraulic properties assigned.

4.2.1. Model Setup

The simulation period was from October 1st, 1990 to September 30th, 2015 (with September 30th, 2015 being the most recent date of available climate data for the study region). The simulation was broken up into two stages: firstly, an appropriate calibration period was simulated (15 years) beginning October 1st, 1990; and then a 10 year validation phase to check the performance of the calibrated model from January 1st, 2005 to September 30th, 2015.

Each component of the MIKE SHE model (i.e. unsaturated zone, saturated zone, etc.) can be set to a different time step. However, to aid in numerical stability there are specific requirements of the time step difference between each component. The time step of the Unsaturated Zone Module (UZ) must be an integer fraction of the Saturated Zone module (SZ), and the time step of the Overland Flow Module (OL) must be an integer fraction of the UZ (DHI, 2007). Since one of the objectives of the model is to investigate the temporal variability of recharge, a daily time step was required; hence a max time step of 24 hours was set for the SZ. To keep with the requirements, the UZ and OL max time steps were set to 4 hours and 1 hour, respectively.

4.2.2. Model Domain

A spatially uniform grid size of 150 m provided the best compromise between computation runtimes and model result resolution. This created a grid that was 90 grid cells (x) by 57 grid cells (y), with a total of 2594 finite difference grid cells. Initially, a finer grid (75 m by 75 m) was used; however, the computational effort to run such a refined grid caused a dramatic increase in computational time, which would limit the efficiency of calibration. Thus, a 150 m grid size was selected (the limitation of this is described in Section 4.3). The vertical discretization of the unsaturated and saturated zones are described in Sections 4.2.5 and 4.2.6, respectively.

As previously mentioned, the variation in topography plays a key role in the Rainfall-Recharge-Runoff process (Section 1.1); thus a high resolution topography dataset was desirable for this modelling investigation. The dataset assigned to the model domain was from a 25 m resolution digital elevation model (DEM); representing the finest resolution elevation data set available at the time of the study.

Since the groundwater and overland flow ultimately discharge to the ocean, the horizontal extent of the domain was specified along the coast of Gabriola Island. The model domain is shown in Figure 4.1.

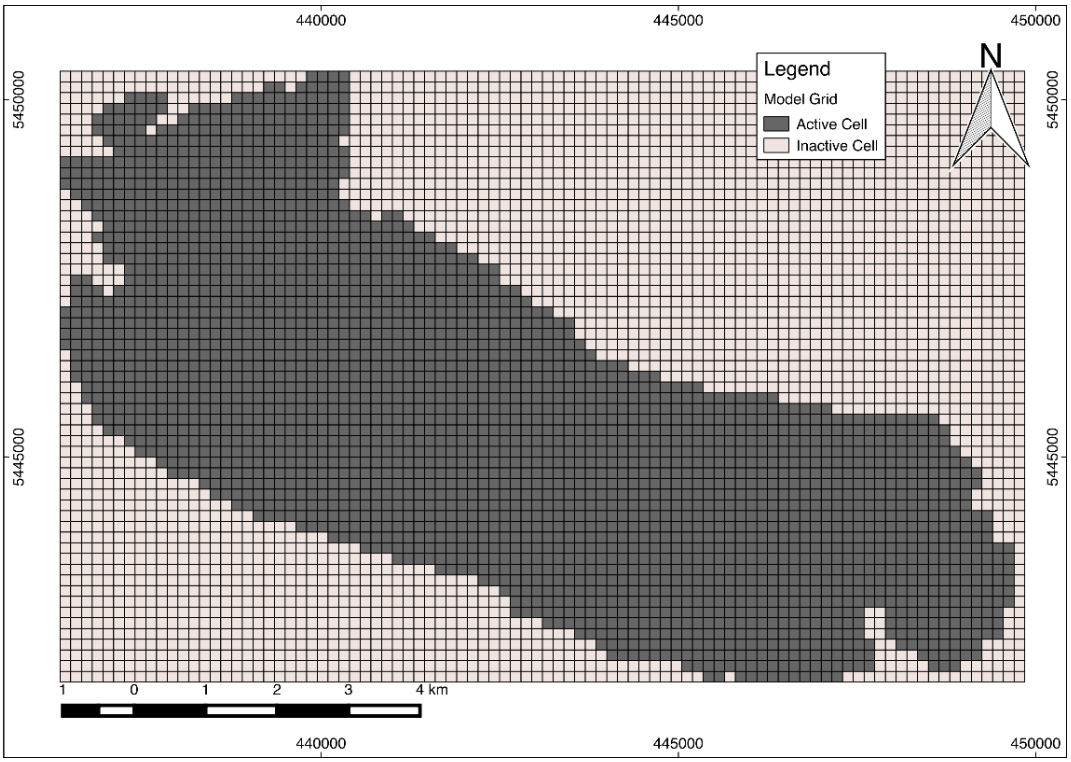

Figure 4.1 Model Domain. Active cells calculate water movement in the domain; inactive cells do not.

4.2.3. Climate Data

The climate data described in Section 2.2 were applied to the model, namely precipitation and reference evapotranspiration (RET). Since there is unlikely to be significant variation in precipitation or RET due to the relatively low relief of the island, the climate data were assigned as spatially uniform over the entire model domain. The temporal frequency of these datasets matched the simulation time step, i.e. daily.

4.2.4. Land Surface Data

To calculate actual evapotranspiration, MIKE SHE uses vegetation characteristics and RET. The two principal input components are Leaf Area Index (LAI), and Root Depth. LAI defines the area of leaves per area of ground surface, and the Root Depth is the depth below ground to which roots extend. As previously discussed in Section2.4, the vegetation on Gabriola Island is primarily Costal Douglas Fir (CDF). Although no studies investigating LAI and rooting depth have focused on Gabriola Island specifically, studies within the same BEC zone have focused on these vegetation characteristics of CDF; providing sufficient reference values. Trofymow et

al. (2007) investigated the LAI of CDF near Victoria on Vancouver Island. That study reported LAI values ranging between 7.1 and 10.3. A similar study on Douglas Fir in Washington State reported an average LAI of 8.6 (Thomas and Winner, 2000). Although LAI varies seasonally (highest in the summer when photosynthesis is most active), for this project, an initial value of 8.5 was determined to be a reasonable average over year. The rooting depth of Coastal Douglas Fir has also not been specifically investigated on Gabriola Island. However, on the eastern coast of Vancouver Island, in the same BEC zone, Black (1979) used rooting depths ranging between 650 and 850 mm to calculate AET. As such, a rooting depth of 750 mm was set. Since the vegetation is relatively uniform across the island (Section 2.4), the LAI and rooting depth were set as spatially uniform parameters. Similar to LAI, the rooting depth was also specified to be temporally uniform.

Overland flow is defined as the portion of runoff that occurs as sheet flow. If rainfall exceeds the infiltration capacity of the soil, water will move horizontally across the surface, being routed by surface topography, at a rate that is calculated in MIKE SHE using the diffusive wave approximation. The resistance to flow overland is controlled by the "roughness" of the land surface, which can be inferred from land use/cover maps. Within MIKE SHE, the Manning's M coefficient (reciprocal of Manning's n), which is equivalent to the Strickler roughness coefficient, controls the amount of friction and the velocity at which water can move horizontally. The value of M is typically in the range of 100 (smooth channels) to 10 (thickly vegetated channels) (DHI, 2007). USDA (1986) published Manning's n values for vegetated land surfaces ranging between 0.15 and 0.8 for short grass prairie and dense underbrush, respectively. These translate into Manning's M coefficient values of approximately 1 and 7 $m^{1/3}/s$, respectively. In a previous nearby study utilizing MIKE SHE, Foster (2014) used Manning's M coefficient of 2.5 $m^{1/3}/s$ to represent young forest, the dominant land cover on Gabriola Island. Since Gabriola Island is generally covered by relatively dense young forest, a uniformly distributed M of same value was used in this study.

Of the few surface water features present on Gabriola Island, only Lake Hoggan was included in this model. The remaining features, specifically the ephemeral streams, were not included, as they are not present year round (the lake is perennial).

4.2.5. UZ Data

Unsaturated flow within MIKE SHE is calculated only in the vertical direction. In this study, Richards' equation was used to model unsaturated flow. Precipitation that infiltrates the ground surface can either be evapotranspired or flow through the unsaturated zone to reach the saturated zone as recharge. The rate and amount of water that flows through the unsaturated zone generally depends on the initial soil saturation, precipitation intensity, and infiltration capacity of a soil. The infiltration capacity of the soil is governed by the saturated hydraulic conductivity and characteristic curve of a soil.

As outlined in the conceptual model (Section 2.6), the soils on Gabriola Island mainly consist of sandy loam with a thickness of approximately 1 m; below this is the fractured bedrock. These two units were specified as spatially uniform, and the UZ column was defined as vertically uniform in thickness (Figure 4.2). The sandy loam soil was assigned a depth of 1 m below ground level (mbgl), while the bedrock unit extended to below the base of the SZ (see the next section). Even though the UZ was relatively thin in comparison to the SZ, the UZ must overlap with the SZ in MIKE SHE in order to remain numerically stable. Within the UZ, the vertical profile must be discretized sufficiently for the Richards' equation to converge. The thickness of each cell in the UZ was set according to the MIKE SHE reference manual (DHI, 2007). The discretization used is tabulated in Table 4.1. A total of 51 cells were used.

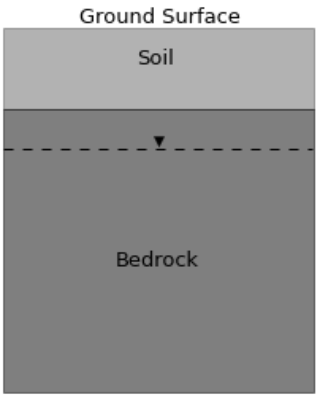

Figure 4.2 Conceptual UZ column.

Table 4.1 UZ vertical discretization.

From depth (mbgl)	To depth (mbgl)	Cell Thickness (m)	Number of Cells
0	0.3	0.1	3
0.3	0.6	0.15	2
0.6	1	0.2	2
1	5	0.5	8
5	10	1	5
10	20	2	5
20	50	5	6
50	250	10	20

To solve Richard's equation for unsaturated water flow, the saturated hydraulic conductivity (K_s) and soil characteristic curve of each unit, here, soil and bedrock, are required. In this study, these were specified from literature values; the van Genuchten model was used to approximate the soil characteristic curve. Table 4.2 summarises the unsaturated zone module input parameters.

Table 4.2 UZ property parameters.

Subsurface unit	K_s (m/sec)	Residual Moisture Content (θ_r)	Saturated Moisture Content (θ_s)	α (cm^{-1})	n	Bulk Density (kg/m^3)
Soil[1]	1.2e-05	0.065	0.41	0.075	0.189	1200
Bedrock[2]	3.0e-07	0.05	0.1	0.0036	0.08	2400

[1] Sourced from Leij et al. (1996); [2] Sourced from Voeckler et al. (2004), except for bedrock K_s which was approximated from Larocque (2014).

4.2.6. SZ Data

When modelling the groundwater flow through homogeneous fractured rock, an equivalent porous medium (EPM) approach can be used (Anderson et al., 2015). This approach assumes that groundwater effectively flows through the fractured material as it would in a porous medium (e.g. an alluvial sand aquifer), making no distinction between primary and secondary permeability, and treating the fractures and matrix as a continuum. This simplifying assumption has been used to model the groundwater flow in fractured bedrock on other Gulf Islands (e.g. Liteanu 2003; Larocque 2014). There are limitations to this approach, however. Although the EPM approach may simulate the behaviour of a regional flow system, heterogeneities of fractured rock at a small scale may result in the approach being unable to represent

local groundwater flow. This may result in local variations in hydraulic heads, for example, due to the presence or absence of localized fractures. However, for the purposes of this regional model, an EPM approach is a reasonable assumption.

The SZ module domain was represented as a single geological layer. This is reasoned on the assumption that the hydraulic properties of the Nanaimo Group bedrock are relatively homogenous at a regional scale (Section 2.7). In fractured bedrock, the depth at which groundwater flow becomes negligible is around 150 to 200 mbgl (Gleeson et al., 2011; Welch and Allen 2014). Further, the presence of tritium in groundwater samples suggest that the groundwater flow system is relatively shallow, thus simulating deeper groundwater flow paths is not required. Gabriola has a topographical high point of ~160 masl, thus the bottom of the model domain was set to a uniform value of -50 masl. This resulted in a maximum model domain depth of 210 m and a minimum depth (near the coast) of 50 m.

The SZ was discretized as a single computational layer. Therefore, groundwater flow in the SZ is assumed to be generally horizontal from areas of high hydraulic head to low hydraulic head (i.e. toward the coast).

The hydraulic properties of the fractured bedrock were described in detail the conceptual model (Section 2.7). In summary, the fractured bedrock on Gabriola Island is assumed homogenous and isotropic at a regional scale. Initial estimates of the hydraulic properties are summarised in Table 4.3.

Table 4.3 Hydraulic parameters.

Parameter	Initial Estimate	Range
Hydraulic Conductivity (m/s)	3.0×10^{-7}	5.0×10^{-8} to 5.0×10^{-6}
Specific Yield (-)	0.026[1]	0.01 to 0.1
Specific Storage (m^{-1})	2.0×10^{-6}	2.0×10^{-8} to 1.4×10^{-5}
Porosity (%)	8	1 to 10

[1]In MIKE SHE this value is automatically calculated from the UZ parameters used.

4.2.7. Boundary Conditions and Initial Conditions

In the model, the precipitation that falls onto the model domain is routed out of the model via three potential pathways: evaporation, overland flow reaching the ocean, and groundwater discharge to the ocean.

Two specified head boundary conditions were used in the SZ module of this model. To simulate the discharge of groundwater to the ocean, a specified head boundary condition was set around the edge of the model domain (coast of island). Although there are daily tidal fluctuations in sea level, they are not anticipated to have a significant influence at a regional scale. Thus, a temporally uniform value of 0 masl was set to this outer boundary condition. It is important to note that this coast boundary is actually a salt boundary. MIKE SHE cannot simulate density-dependent flow and solute transport; therefore, the specified head cells are placed to allow for a seepage face to develop at the coastline to allow the freshwater to discharge. The setup of this boundary condition implies that the seepage face of groundwater discharge to the ocean is approximately 50 m thick, since the base of the model is specified at 50 mbgl at the coast. The depth of the SZ, and thus seepage face thickness, was tested in the sensitivity analysis (Section 4.2.12). Further discussion of the limitation of this boundary condition can be found in Section 4.3. A single internal boundary condition was used to represent Hoggan Lake, the only lake of significant size present on the island. A value of 58 m.a.s.l. was extracted from the DEM of the island representing the average lake level. The distribution of the specified head cells is shown in Figure 4.3.

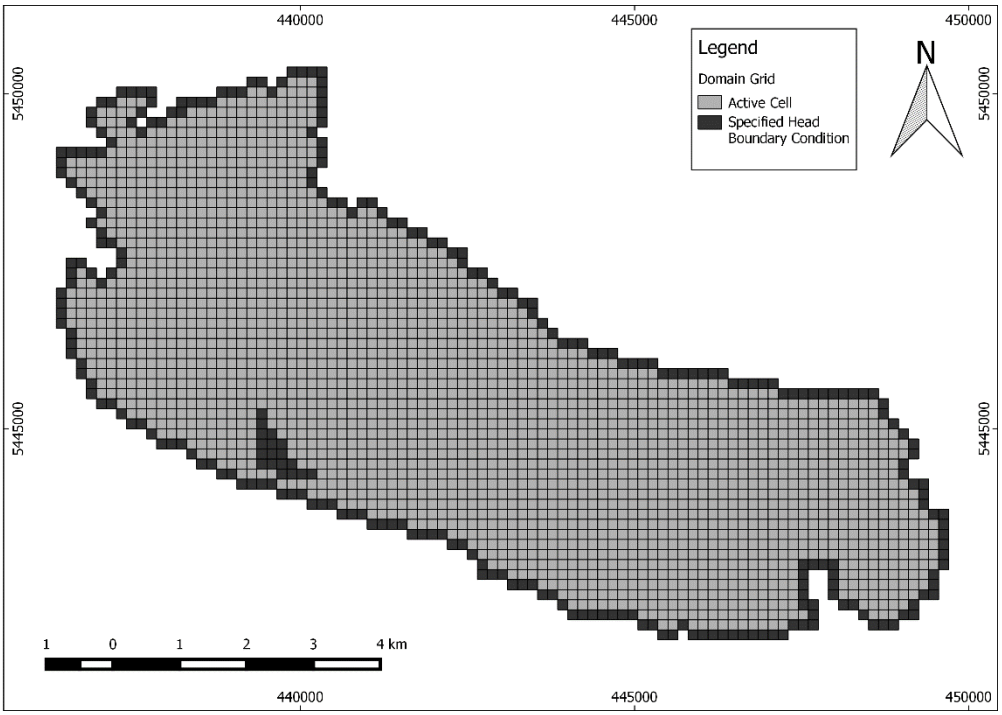

Figure 4.3 Location of specific head boundary conditions.

An initial head distribution is required to run MIKE SHE. The model spins up from this initial head distribution and gradually converges to a dynamic solution whereby the water level changes temporally, but reflects a stable overall head range. The initial head distribution was specified from a water table interpolated in a previous study (Scibek et al., 2013). Interpolation data were sourced from groundwater level measurements taken following the completion of well drilling. The surface is presented below in Figure 4.4.

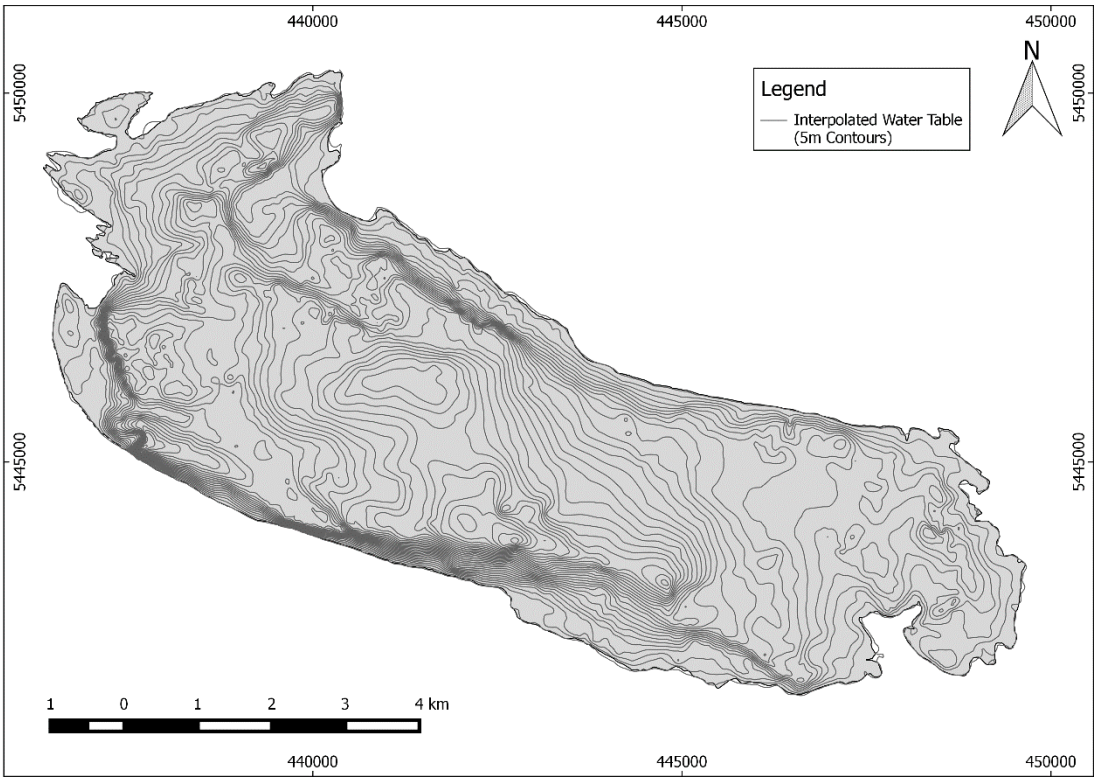

Figure 4.4 Initial hydraulic head based on interpolated water table elevation.

4.2.8. Particle Tracking

Particle tracking was utilized in MIKE SHE to compare simulated advective groundwater travel time to qualitative apparent groundwater age estimates from the tritium analysis results (samples CC3, CC4, CC5, and GH2 – see Chapter 3). The spatial extent of a 50 year well capture zone further helps to distinguish between old, tritium depleted groundwater, and a tritium-rich or highly mixed groundwater flow package. A small capture zone would suggest the latter (i.e. relatively young apparent ages). In MIKE SHE, particle tracking is achieved by releasing a defined number particles into every cell in the SZ module, and then simulating the advective transport these particles. In this study, five particles were released in each cell. While all the particle travel paths are simulated, only those particles that reach a sink (e.g. constant head boundary condition or pumping well) are registered. Since the samples for tritium analysis were collected from private domestic wells, with no pump usage available, very low flow pumping wells were specified at their location in the model; this enables particles entering the well cell to be registered while having a negligible effect on the water balance. A constant rate of 0.001 m^3/day was set as the pumping rate at each

of the four domestic wells. Since the SZ module of the model has only one layer, the depths of the wells were arbitrarily set to 30 mbgl.

Because all the groundwater samples contained measurable amounts of tritium, it is inferred that the mean groundwater residence time of that water sample is less than 50 years. As such, the particle tracking simulation was run for a 50 year period. Within MIKE SHE the groundwater flow solution used for particle tracking can be recycled. For this study, the 10 year validation period groundwater solution was used for particle tracking. This means that the 10 year flow solution was repeated five times for a particle tracking simulation of 50 years.

The originating locations of the registered particles was used to further elucidate groundwater flow dynamics.

4.2.9. Climate Change

Climate change has the potential to affect groundwater resources globally (Green et al., 2011), principally though changes in the climatic patterns of temperature and precipitation. Based on global climate model (GCM) simulations, the future atmospheric temperature, and the amount and intensity of precipitation are predicted to be altered. As discussed previously, temperature and precipitation, in part, directly control the amount of recharge an aquifer receives. An increase in temperature, for example, could potentially increase evapotranspiration (if there is water available) and reduce the amount of recharge to groundwater from precipitation. Consequently, such changes to climate may have significant impacts on the sustainability of groundwater resources in the future.

The GCMs take into consideration socioeconomic scenarios to make projections on how future greenhouse gas (GHG) emissions may change the global climate (Carter et al., 2001). Each model is run for a number of future climate emissions scenarios that include conservative through to optimistic GHG emissions. The GCMs forecast the future climate shifts for specific decades in the future, specifically: the 2020s, 2050s, and 2080s. The global climate change models are produced at a coarse regional scale and are often downscaled using various methods, such as TreeGen (Cannon, 2008). Previous studies (Appaih-Adjei, 2006; Foster, 2014; Larocque, 2014) used the forecasted change in climate (shifts) to assess how recharge on the Gulf

Islands and Vancouver Island may vary in the future. A similar approach has been employed in this study.

Recharge to Gabriola Island under future climate change conditions was assessed by applying the climate shifts (from GCM outputs) to the historic climate data input, specifically RET and precipitation. The future climate change predictions were limited to 2050s and 2080s since the 2020s are less than five years away. The GCM data were accessed utilizing the BC Regional Analysis Tool (Pacific Climate Impacts Consortium (PCIC) 2016). For this study, the 'SRES AR4 -PCIC TreeGen ensemble' was used. The ensemble consists of four downscaled CMIP3 GCMs: the CCCMA_CGCM3, CSIRO_MK30, GFDL_CM20, and MPI_ECHAM5. Various model runs are available for each GCM, and for different emissions scenarios, A1B, A2, and B1, which represent different degrees of forecasted climate change. The A2 scenario was utilized in this study since it represents the most serve impact on climate conditions. It is noted that historic trends in observed climate are consistent with the A2 scenario.

The climate shift data extracted from the GCMs focused on the climate properties required for estimation of RET and precipitation (inputs needed in MIKE SHE), namely: changes in mean, max and min temperature, incident solar radiation, relative humidity, and precipitation for the 2050s (2040 to 2069) and 2080s (2070 to 2099). The data were extracted from a clipped region around Gabriola Island. The shifts were applied to a daily historical climate data (2000 to 2010) to form climate datasets representative of the future periods. The GCM data are reported as monthly changes, thus to apply the shifts at a daily frequency the average monthly result of the A2 scenario from differing models (and their runs) were interpolated. This was done by assuming the GCMs results represent the middle of the month (15^{th} day of every month) and linearly interpolating to a daily scale. The type of shift differed between climate properties. Temperature and solar radiation shifts are as absolute changes, while precipitation and relative humidity shifts are as percent changes. The shifted temperature, solar radiation, and relative humidity were used, in the same way as the historical data, to estimate future RET using AWSET (see Section 2.3). Shifts in wind speed are not included in the GCMs results, and as such, the historical data were used to estimate RET; this assumes that average daily wind speed will not change significantly in the future.

The average monthly results of the shifts to RET and precipitation for the 2050s and 2080s are presented in Figure 4.5 and tabulated in Table 4.4.

Table 4.4 Changes to RET and precipitation under forecast future climate conditions.

	RET (% change)		Precipitation (% change)	
	2050s	2080s	2050s	2080s
January	5	8	10	11
February	7	10	9	13
March	5	8	9	11
April	3	5	16	21
May	4	6	12	19
June	6	9	2	6
July	11	16	-9	-13
August	13	18	-11	-10
September	9	13	8	10
October	5	8	15	17
November	4	7	12	15
December	5	8	7	11

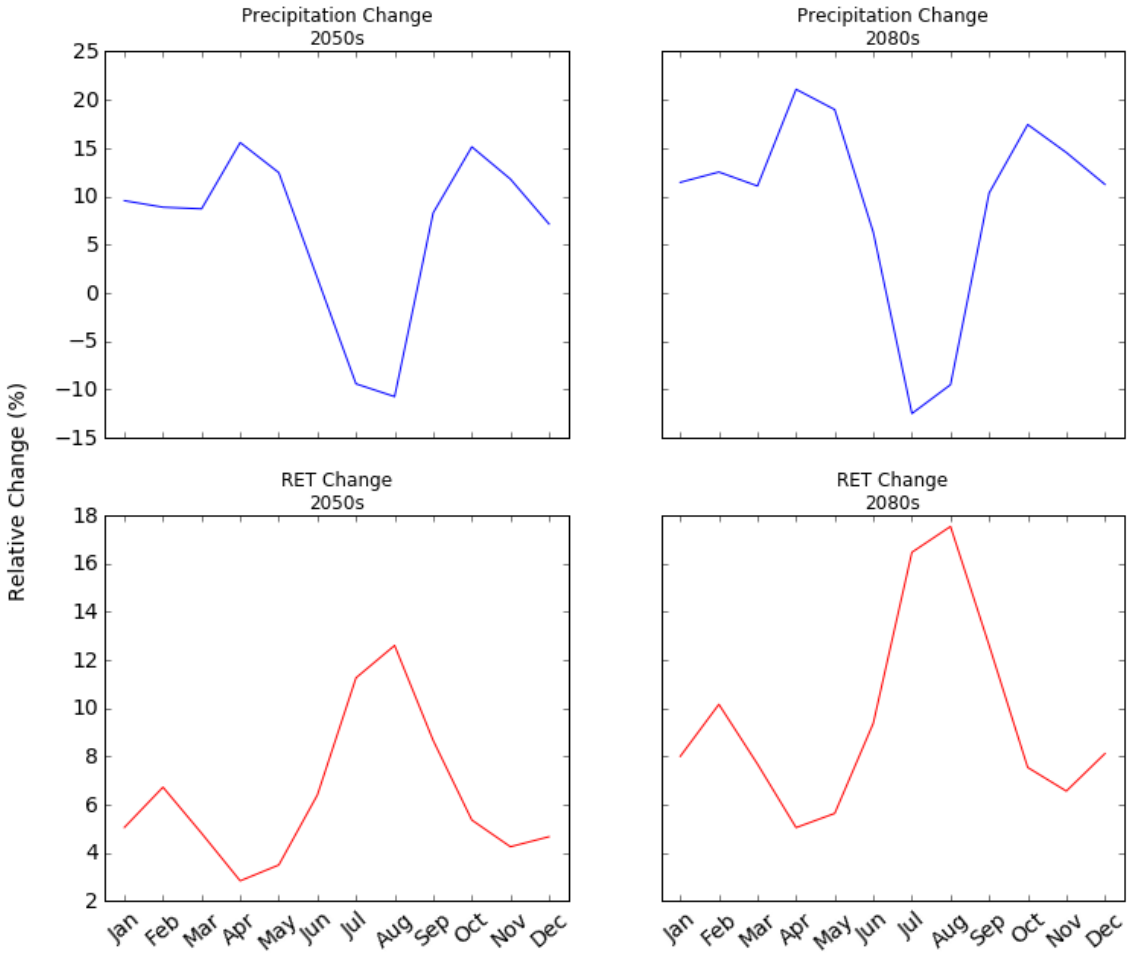

Figure 4.5 Monthly average future climate inputs. A2 scenario shifts were applied to precipitation and input data for RET calculation.

The biggest shifts in precipitation will be realised in the spring, summer and fall. In the spring and fall, precipitation is projected to increase by approximately 10 to 15% and 10 to 20% for the 2050s and 2080s, respectively. Conversely, the summer months will see a decrease in precipitation by approximately -5 to -10% for both the 2050s and 2080s. Precipitation in the winter months is projected to increase by a fairly consistent amount, approximately 10% in both periods. The calculated shifted RET indicates that the greatest changes will occur during the summer months, with a 10 to 12% and 14 to 18% increase in RET for the 2050s and 2080s, respectively. Lesser changes in RET are projected over the rest of the year, 2 to 6% and 6 to 10% increase for the 2050s and 2080s, respectively. Overall, the changes are greatest for both precipitation and RET in the 2080s. These shifts would seemingly accentuate the seasonality of a temperate climate.

Two MIKE SHE simulations (one representing the 2050s and one the 2080s) were run using the shifted precipitation and RET input datasets. The calibrated model groundwater level solution on September 1st 2005 (last time step of simulation) was used as the starting head condition, also known as a hot start. The results of these future projections are discussed in Chapter 5.

4.2.10. Observation Data

When modelling groundwater flow it is desirable to have stream flow and groundwater level observation data to constrain the calibration of the model. However, on Gabriola Island none of the streams are gauged. Thus, only groundwater level elevation observation data were available for this study; two datasets were used. First, six provincial observation wells with long term records were available to match the transient response of the model. Although heterogeneities in the hydraulic properties of the fractured bedrock at the local scale may preclude this dataset from being effective for calibration of this regional model, the observation time series is vital for insuring that the timing of the seasonal fluctuations in groundwater level are representative of the physical world. The locations of these observation wells are shown in Figure 4.6. As discussed in Section 2.8 (Table 2.4), only three of the six observation wells have measurement records that span both the calibration and validation periods (OW196, OW197, OW316). OW194 and OW317 were only used in the calibration period since they were deactivated in 2007 and 2006, respectively, whereas OW385 was only used in the validation since the period of record of this well only started in 2010.

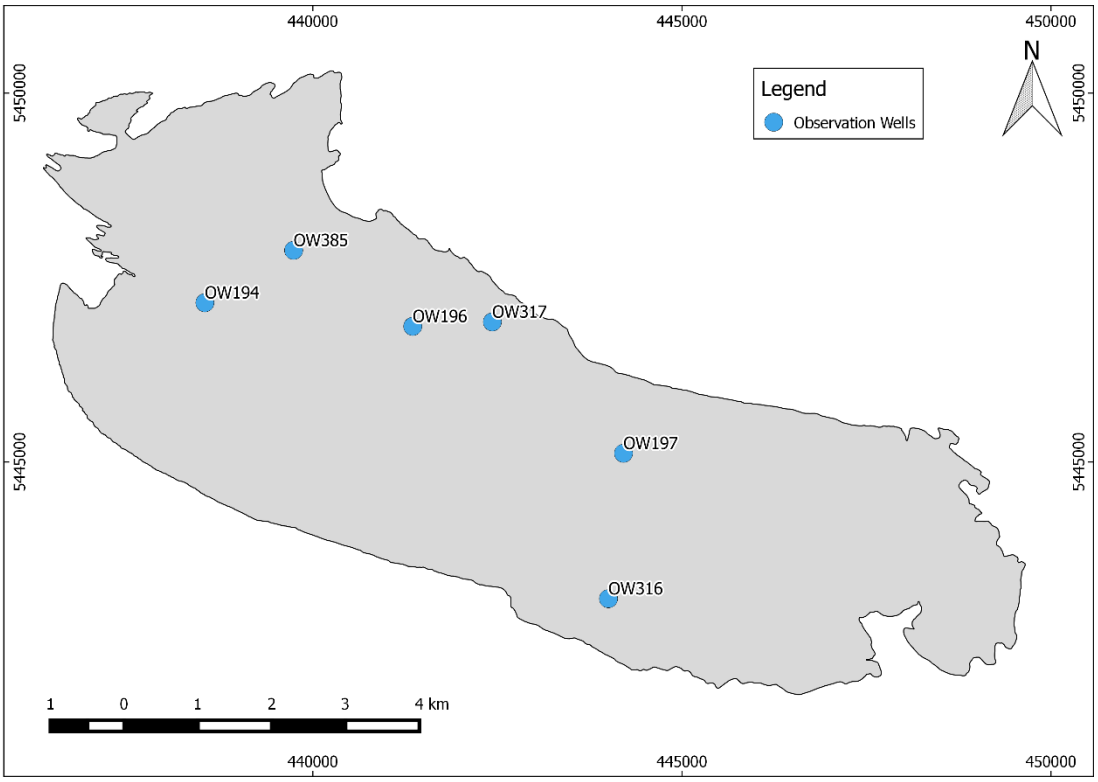

Figure 4.6 Location of provincial observation wells.

Second, available drilling records provide measurements of the groundwater elevation immediately following the completion of well drilling. These data are reported as static groundwater levels in the BC WELLS Database (MoE, 2015b). These 'average' groundwater levels can be compared to the average simulated transient groundwater level at the same point. The high number (2092 wells) and spatial distribution (Figure 2.2) of measurements help overcome the limitation of solely using the observation well time series as observation data, providing spatially distributed average groundwater level measurements. However, some caveats in using this second dataset exist, resulting in observation data that are somewhat biased. Firstly, immediately after drilling and completion of water wells the groundwater level will typically be lower than normal because the water level in the well has not fully recovered from drilling. Thus, these measurements can be expected to be lower than under natural conditions. Secondly, the private wells on the Gulf Islands are generally drilled in the summer. Since there is a pronounced seasonal variation in the groundwater levels on Gabriola Island (Section 2.8), the measurements can be expected to be lower than the annual average groundwater level. Despite the bias of lower groundwater levels from the WELLS database, previous studies have used these data to calibrate numerical models (e.g. Foster, 2014; Larocque, 2014).

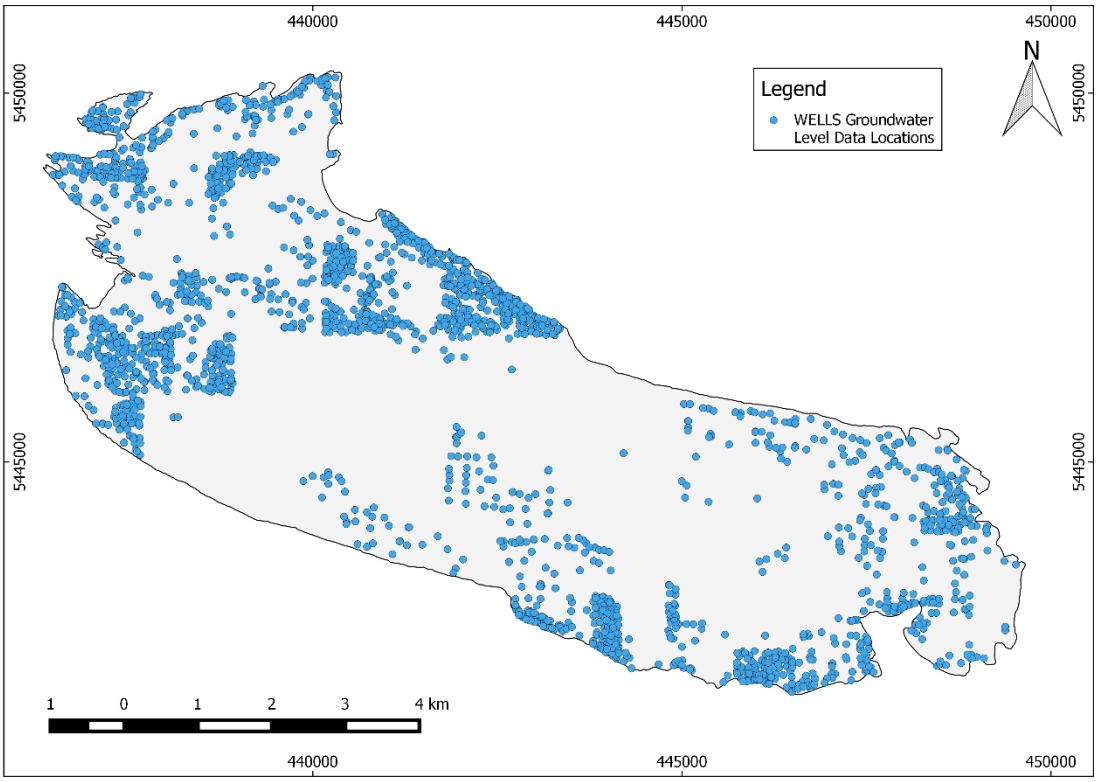

Figure 4.7 Location of water wells from the WELLS database used for model calibration.

4.2.11. Groundwater Abstraction

Groundwater abstraction on Gabriola Island mainly occurs through domestic and non-domestic (commercial and agricultural) wells. This abstraction was implemented in the model by including pumping wells in the SZ module of MIKE SHE. Data pertaining to the actual number of active wells and abstraction on Gabriola Island are scarce (Scibek et al., 2013); thus, and a number approximations were made regarding the location and abstraction rates. Firstly, domestic and non-domestic groundwater wells were not distinguished in the model – both were assigned the same abstraction rate. Second, the pumping wells were represented spatially based on locations in the BC WELLS Database (Figure 2.2). Third, two constant pumping regimes were assigned; a lower abstraction rate during the wetter times of the year (October to March), and a higher rate during the drier months (April to September). Due to the aforementioned scarcity of abstraction data, the island wide water demand estimated by Scibek et al. (2013) was used instead of actual abstraction data. For the two pumping regimes, this translated into a pumping rates of 0.50 and 1.62 m^3/day for the October to March, and April to September periods of each year, respectively.

These approximations assume that all the wells are in use every day, and that every well being used is in the database. In reality, neither of these assumptions hold true; however, they are deemed appropriate given the lack of data available. This pumping regime was also applied to future scenarios.

4.2.12. Model Calibration and Validation

The calibration of the model solely utilised the manual trial and error approach, as MIKE SHE does not have parameter estimation capabilities. The approach focused on varying the hydraulic conductivity of the bedrock within the range reported in Table 4.3 in an attempt to match simulated groundwater levels with observed groundwater levels. The specific storage of the fractured bedrock and saturated hydraulic conductivity of the soil were also varied initially; however, the model proved to not be sensitive to these input parameters. The van Genuchten parameters of the fractured bedrock were also altered in an attempt to force an increase in the specific yield in the SZ (the initial van Genuchten parameters resulted in a specific yield of the SZ that was too low). However, these changes made the model numerically unstable, and were thus abandoned.

The total model run time of 25 years was broken up into two phases. The initial calibration phase from 0 to 15 years, followed by a 10 year validation phase. The final calibrated hydraulic parameters are summarized in Table 4.5.

Table 4.5 Final calibrated hydraulic parameter values.

	Calibrated Value
Hydraulic Conductivity (m/s)	4×10^{-7}
Specific Yield (-)	0.0018
Specific Storage (1/m)	2.4×10^{-5}
Porosity (%)	8

The model was calibrated to two different types of groundwater level datasets: (1) the transient observed groundwater levels at observations wells, and (2) the static water levels reported in the WELLS database. Error statistics were used to measure the degree of model fit during the calibration process. These were: mean error (ME),

mean absolute error (MAE), root mean squared error (RMSE), Pearson coefficient (P_{cor}), and Nash-Sutcliffe coefficient (N-S).

The mean error is the mean difference of the residual errors (measured heads h_m minus simulated heads h_s):

$$ME = \frac{1}{n}\sum_{i=1}^{n}(h_m - h_s)_i \tag{4.1}$$

The ME provides a general representation of modal bias, but because both negative and positive residuals are included in the mean, errors can cancel each other, reducing the overall error reported. However, the sign of the reported ME can be used to assess whether overall the model is under (positive) or over predicting (negative).

The mean absolute error is the mean of the absolute value of the residual:

$$MAE = \frac{1}{n}\sum_{i=1}^{n}|h_m - h_s|_i \tag{4.2}$$

Taking the absolute values of the residuals ensures that positive and negative residuals do not cancel. However, large residuals (outliers) can influence the error reported.

The root mean squared error is the average of the squared residuals:

$$RMSE = \left[\frac{1}{n}\sum_{i=1}^{n}(h_m - h_s)_i^2\right]^{0.5} \tag{4.3}$$

The RMSE is less influenced by the effects of large outliers than the MAE.

The Pearson correlation measures the linear relationship between two datasets:

$$P_{cor} = \frac{n(\sum h_m h_s) - (\sum h_m)(\sum h_s)}{\{[\sum h_m - (\sum h_m)^2][n\sum {h_s}^2 - (\sum h_s)^2]\}^{0.5}} \tag{4.4}$$

Finally, the Nash-Sutcliffe efficiency is a normalized statistic that determines the relative magnitude of the residual variance compared to the measured data variance:

$$NS = 1 - \frac{\sum_{i=1}^{n}|(h_m - h_s)|_i^2}{\sum_{i=1}^{n}|(h_m - \overline{h_m})|_i^2} \tag{4.5}$$

where $h_m$is the mean of the observed head. It indicates how well the plot of observed verses simulated data fits the 1:1 line. NS ranges from $-\infty$ to 1, essentially the closer to 1, the more accurate the model is.

The ME, MAE, RMSE and P_{cor} error statistics were primarily used to assess the model calibration to the WELLS database observations. The NS was used to assess the dynamics of the simulated groundwater level in the transient calibration stage.

Transient Calibration

The transient phase of calibration aimed to calibrate the timing of the seasonal response of the model. The transient simulated groundwater levels were calibrated against five observation wells on Gabriola Island (Section 4.2.10). The initial value for hydraulic conductivity (see Table 4.3) was adjusted during calibration. Figure 4.8 and Table 4.6, present the groundwater water level results and error statistics for the five observation wells, respectively. In order to exclude results from the model spin-up period, the error statistics were calculated from October 1st 1992 until the end of the calibration period (September 30th 2005).

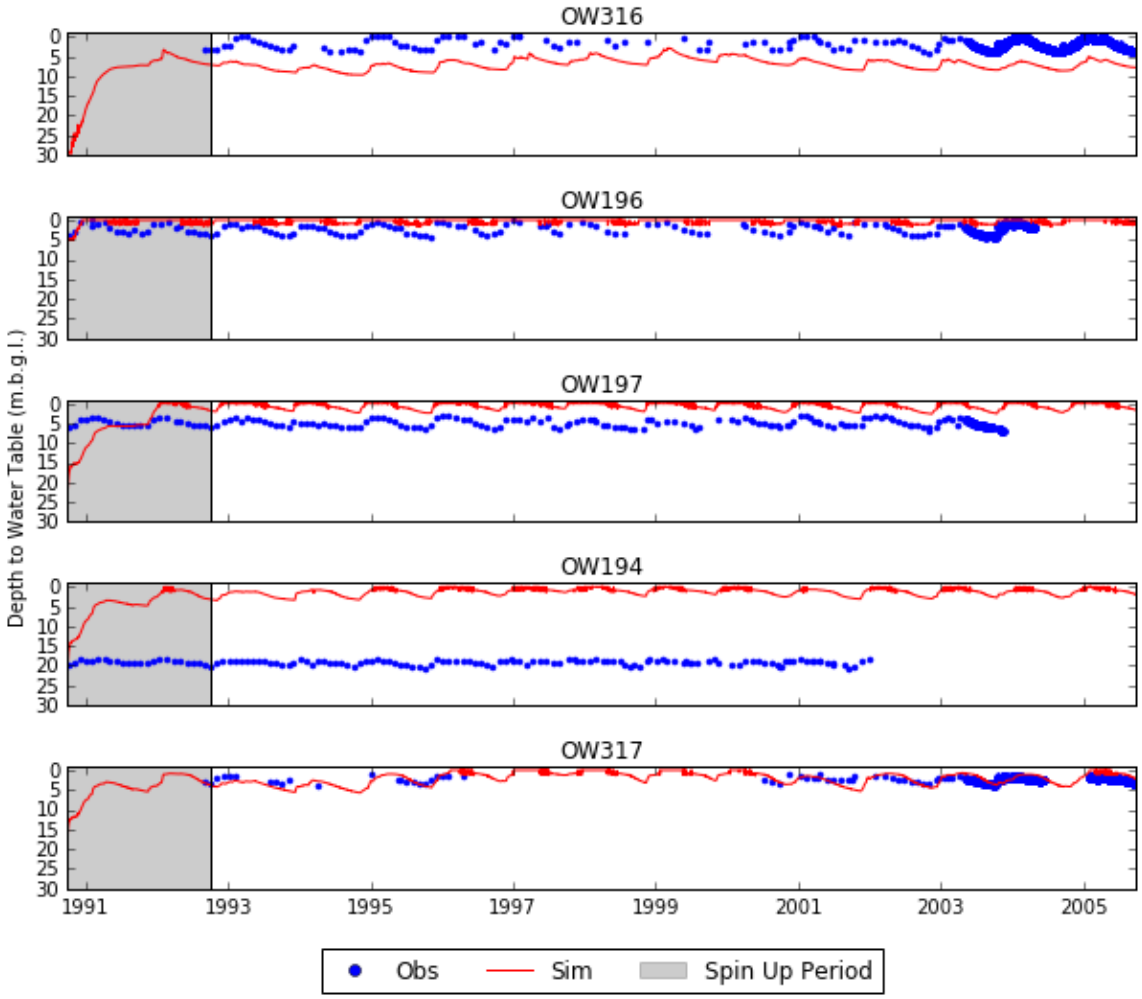

Figure 4.8 Simulated to observed fit of transient groundwater levels.

Table 4.6 Calibration observation well error statistics.

Error Statistic	OW316	OW196	OW197	OW194	OW317
ME (m)	3.8	-1.4	-4.4	-18.1	-1.3
RMSE (m)	3.8	1.5	4.4	18.2	1.5
P_{cor}	0.84	0.84	0.59	0.55	0.22
N-S	-9.7	-1.5	-27.8	-985.5	-9.37

The degree fit of the simulated groundwater levels to observed groundwater levels varies between the observation wells. The timing of the groundwater level rise and fall during the year is well represented in the model; this is most apparent in OW316. However, the average simulated groundwater level is consistently less than

the observed values at all observation points except OW316 (a negative mean error indicates an over prediction of groundwater levels).

The simulated depth to groundwater at OW196 and OW317 matched the observed values closest, with average RMSE of 1.5 m and 1.5 m, respectively. OW316 and OW197 had a moderate degree of fit to observed values, with calculated RMSE values of 3.8 m and 4.4 m, respectively. The largest error, observed both visually in Figure 4.8 and numerically in Table 4.6 was OW194, with a RMSE of 18.2 m. The Nash-Sutcliffe coefficient values indicate that all the simulated depths to groundwater are not that well matched to the observation data; the closer the coefficient is to 1, the more accurate the model is.

Overall, the groundwater levels at the observation wells are not well predicted by the model. The model generally over-predicts groundwater levels. In fact, the model is flooding near these observation wells as evidenced by the simulation results flattening in all observation wells except OW317. Numerous model calibration runs were undertaken in order to try and lower the heads in these wells. Efforts included varying the hydraulic conductivity and specific storage of the bedrock, altering the width of the seepage cells at the perimeter of the model domain. The cause for this lack of accuracy is likely due to local heterogeneities in the hydraulic properties in the fractured bedrock, which are not represented in the model due to its regional scale. Hydraulic conductivity can vary significantly at a local scale due to the presence of discrete fractures. The response of a well to stressors, such as seasonal changes in recharge, changes in tide, and pumping, are highly influenced by the occurrence of fractures, even though at a regional scale such features tend to impart so called equivalent hydraulic properties to the aquifer. Similar challenges with model calibration were met by Trapp (2011), Foster (2014) and Larocque (2014). Because of this, the average simulated depth to groundwater was compared to the WELLs database as a secondary calibration measure. Another possible cause of the elevated groundwater levels is that the model was set to a daily time-step. Heavy precipitation events occurring at a sub-daily time scale are accumulated over a day, decreasing the precipitation intensity simulated by the model. High intensity precipitation can exceed the infiltration capacity of soils, resulting in the occurrence overland flow and reduced recharge. Thus, reducing groundwater levels.

Average Groundwater Level Calibration

This phase of calibration aimed at calibrating the model spatially. The groundwater levels from the approximate end of the spin-up period (October 1st 1994) to the end of the calibration period (September 30th 2005) were averaged to produce a groundwater level dataset which was compared against the groundwater levels from the WELLS database. The results of the calibration are displayed in Figure 4.9, and the error statistics are reported in Table 4.7.

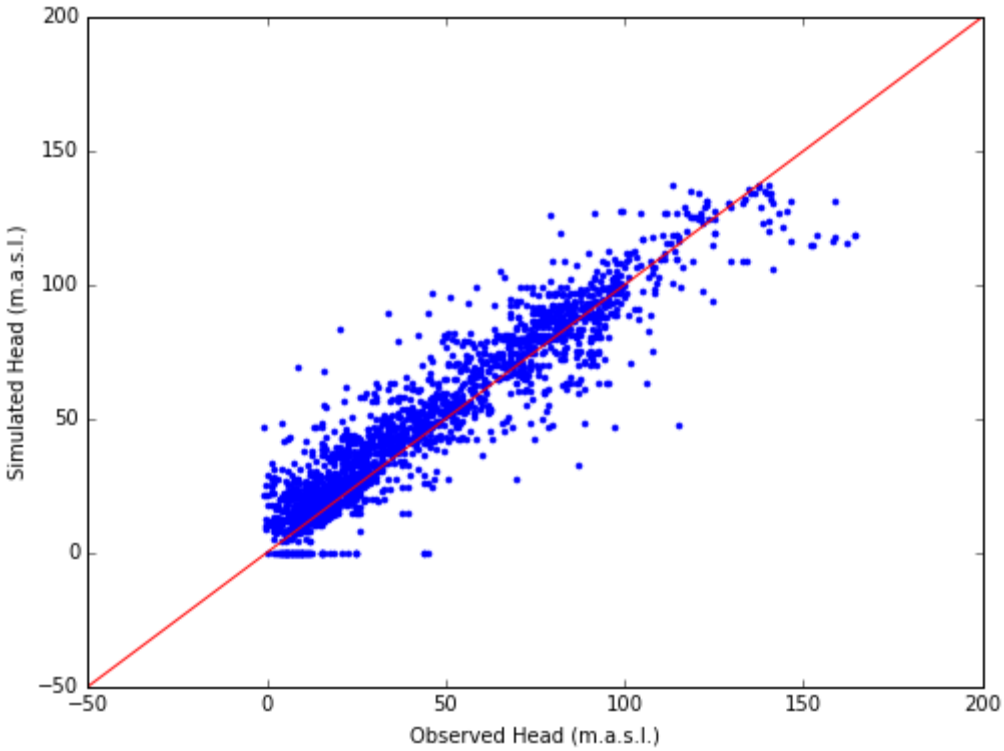

Figure 4.9 simulated to observed fit of groundwater levels.

Table 4.7 Calibration WELLS database error statistics.

Error Statistic	Value
ME (m)	-4.4
MAE (m)	9.0
RMSE (m)	12.5
P_{cor}	0.94

Overall there is a good match between the averaged simulated and observed WELLS database groundwater levels. In Figure 4.9, the majority of the simulated

values plot near the 1:1, and the P_{cor} value of 0.94 in Table 4.7, represents a reasonable fit to the observed data. The ME value of -4.4 m indicates that overall the simulated groundwater level results are higher than the observed values. However, since the majority of the observation data in the WELLS database are likely less than the yearly average groundwater level, this level of over prediction is acceptable.

A sufficiently calibrated model should also be unbiased, with the residual error randomly distributed both statistically and spatially. The statistical distribution of the residuals is displayed in Figure 4.10. The residual error is the difference between the observed groundwater level value and the simulated value. Figure 4.9 clearly shows an approximate Gaussian distribution, which indicates that the residual error is randomly distributed across the model, although the mean of the distribution indicates that the model is over-predicting the groundwater levels as indicated above. The spatial distribution of the residual error is also randomly distributed (Figure 4.11). In other words, there are no areas in the model domain that are biased towards over or under prediction of groundwater levels.

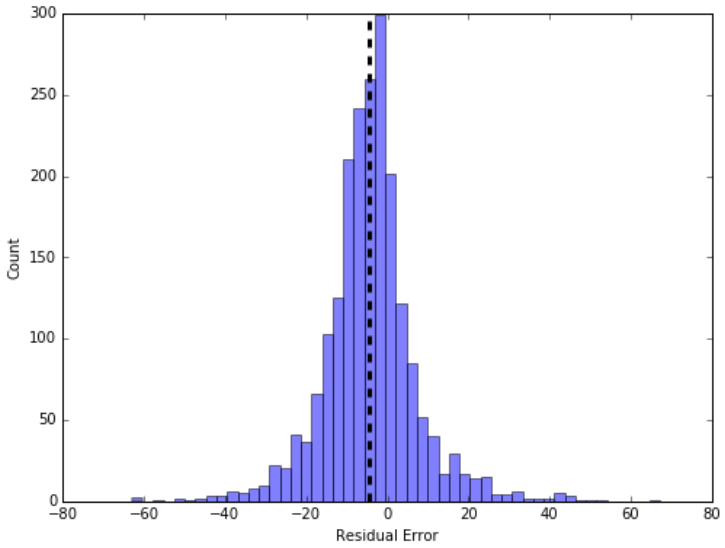

Figure 4.10 Statistical distribution of error. The mean residual error is represented by the dashed vertical line. The mean of the distribution suggests that the model is over-predicting the groundwater level.

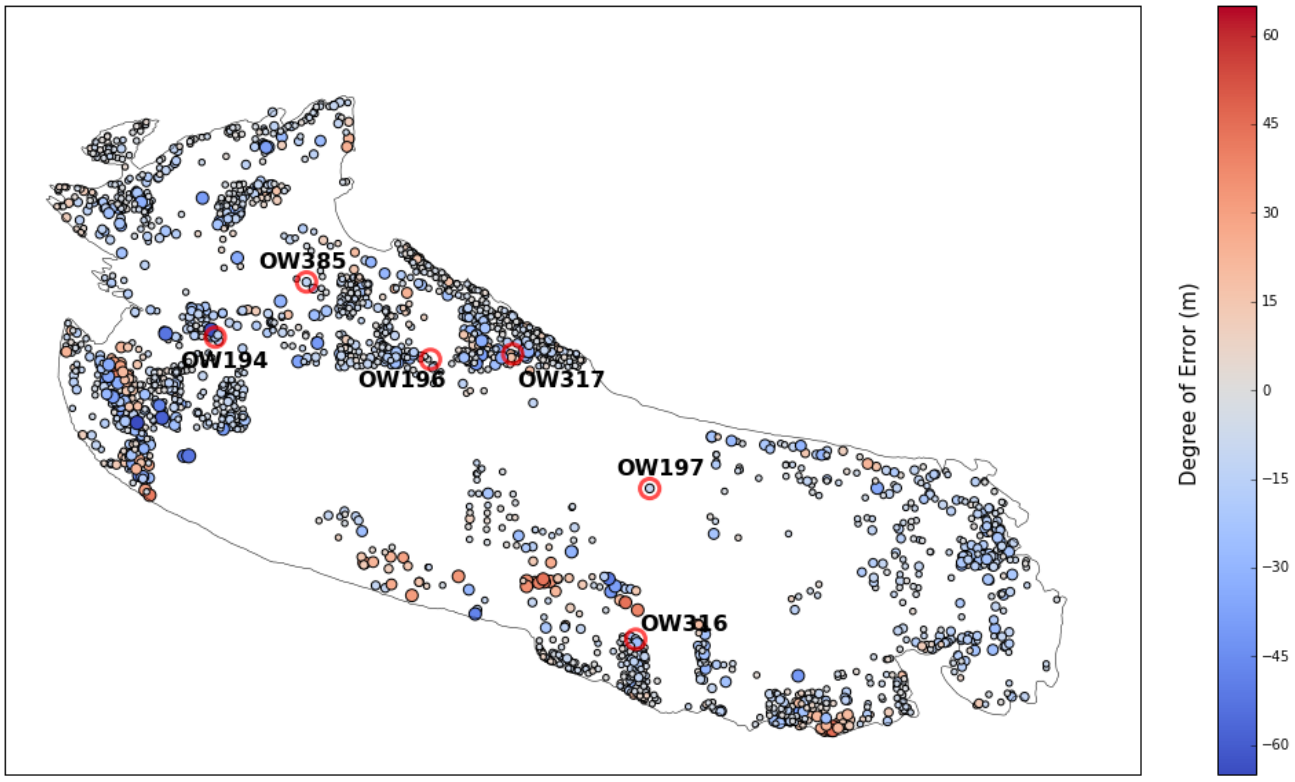

Figure 4.11 Spatial distribution of error. The colour of the solid circles indicates the magnitude and direction of the residual error (a red colour indicates an under estimation of groundwater level). The size of the solid circles has been scaled to represent the magnitude of the residual (larger circles indicate a higher degree of error). The red hollow circles represent the locations of the observation wells used for the transient calibration.

The locations of the observation wells used for the transient calibration are superimposed on the spatial distribution of the error of the WELLS dataset in Figure 4.11. This enables a comparison between the how the model performs against the two datasets. Assuming the datasets are comparable, the model error against the two datasets should match approximately. For comparison, Table 4.8 summarises the average model error for the transient observation well dataset and the approximate range of model error for the WELLS dataset. The average transient error is calculated from the calibration phase of the simulation (i.e. the same ME values as Table 4.6), except for OW385, which was calculated from the validation phase (i.e. the same ME value in Table 4.9, since the period of record of OW385 does not cover the calibration phase). The approximate error range for the WELLS dataset was estimated from error values proximal to each of the observation wells (Figure 4.11).

Table 4.8 Observation dataset error comparison.

	Mean Transient Error (m)	WELLS Dataset Error Range (m)
OW316	3.8	-10 to -20
OW196	-1.4	-10 to -20
OW197	-4.4	-10 to -20
OW194	-18.1	-10 to -20
OW317	-1.3	10 to 20
OW385	-13.1	-10 to -20

Of the five observation wells, only OW194 and OW385 match in both direction and magnitude between the two datasets. OW196 and OW197 match in direction but not magnitude, i.e. the model is over predicting the groundwater levels for both datasets (both values are negative), but the degree of over predication differs. At OW316 and OW317 direction of error does not match. Against the observation well dataset, the simulated groundwater level at OW316 is under predicted, while it is over predicted against the WELLs dataset. The opposite is true for OW317.

Overall, while there are some discrepancies between the residual error values calculated against the different observation datasets, the model is generally over estimating groundwater level by an amount that varies spatially, but is roughly -4.4 m (the ME).

Model Validation

The validation period is used to display the ability of the calibrated model to reproduce real world observations to an acceptable degree. As previously mentioned, the validation period followed the calibration period from October 1st 2005 to September 30th 2015, a ten-year period. The transient groundwater levels of the validation period are compared to the observation wells in Figure 4.12. The error statistics are summarised in Table 4.9.The validation period shows that the model is similarly unable to predict the depth to groundwater at a regional scale. The N-S coefficient values indicate at moderate fit at OW316 and OW196 (-4.9 and -3.6, respectively) and much poorer fit at OW197 and OW385 (-27.8 and -199.0, respectively); these values are similar to the calibration period. Again, the lack of fit is attributed to heterogeneities in the hydraulic properties of the fractured bedrock at the local scale.

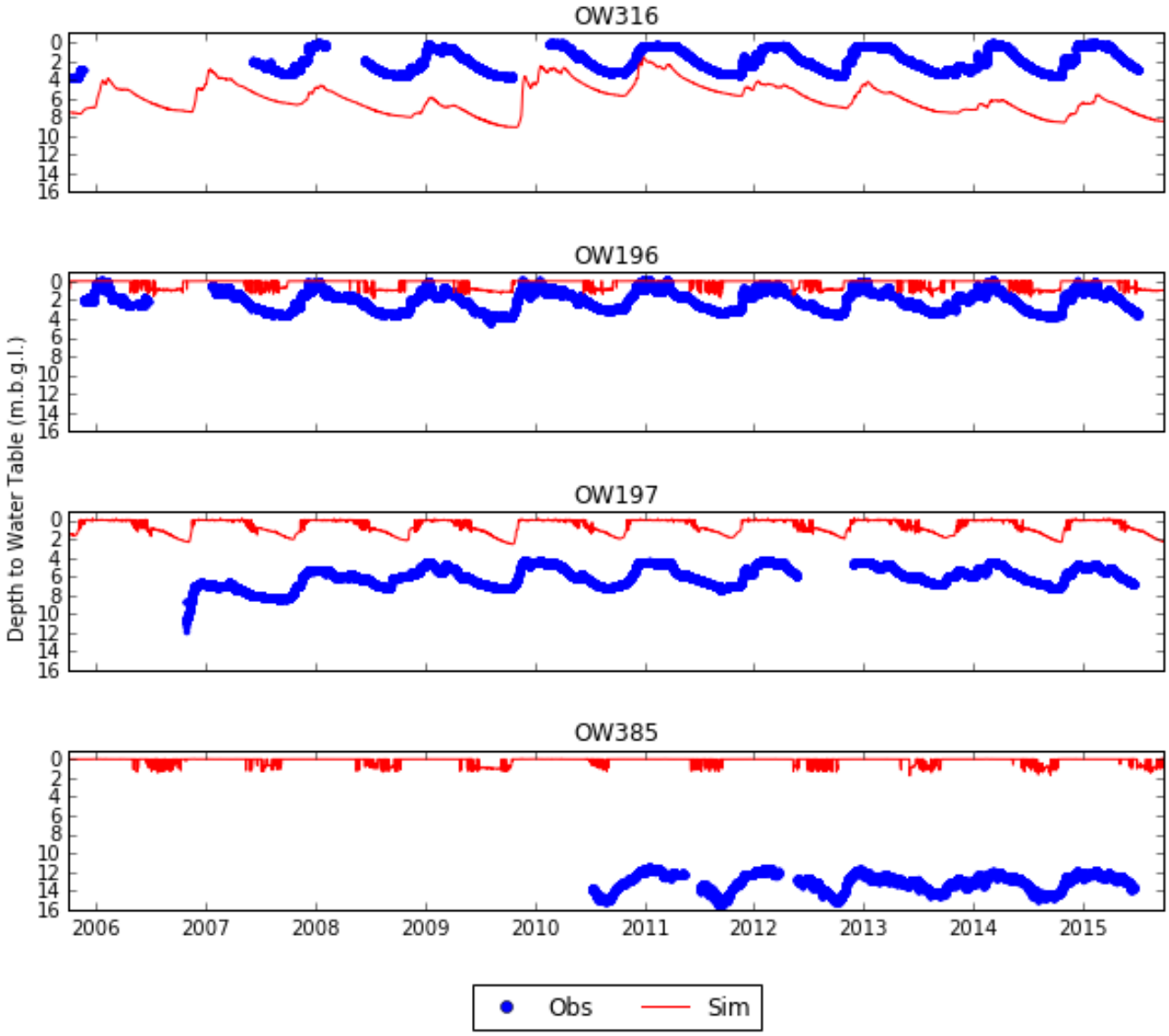

Figure 4.12 Simulated to observed fit of transient groundwater levels

Table 4.9 Validation observation well error statistics.

Error Statistic	OW316	OW196	OW197	OW385
ME (m)	2.5	-2.0	-5.7	-13.1
RMSE (m)	2.6	2.3	5.8	13.2
P_{cor}	0.59	0.20	0.62	0.43
N-S	-4.9	-3.6	-27.8	-199.0

Sensitivity Analysis

A sensitivity analysis was conducted to assess the individual parameter sensitivity. This helps assess the uniqueness of the model. Given that a large number of parameters used to construct this model were selected from literature values, determining parameter sensitivity aids in identifying parameters that would benefit the most from obtaining field observations, and subsequent parameter value constraint.

The sensitivity analysis was carried out by varying, both increasing and decreasing, one selected parameter and holding constant all others. The sensitivity of the selected parameter is qualitatively determined by comparison of the error statistics between the calibrated model result and the varied parameter result. Due to the length of model runs (>5 hrs) and number of parameters investigated, only one value either side of the calibrated parameter value (e.g. one increased and one decreased parameter value) was used. RMSE of the average groundwater levels, from 1992 to 2005, was selected to identify parameter sensitivities.

Five parameters were varied: LAI, Manning's M, soil UZ thickness, SZ lower level (depth) and the bedrock hydraulic conductivity. LAI was varied between 7.1 and 10.3, the range of published values for Douglas fir (refer to Section 4.2.4). Manning's M was varied from a low of 1 to a high of 7 $m^{1/3}/s$ to represent short grass prairie and forest with dense underbrush land cover types, respectively. The soil UZ thickness range tested was 0.5 and 2 m. This represents the likely range of soil thickness on Gabriola Island (refer to Section 2.6). To assess the sensitivity of the seepage face on the model, the level of the base of the SZ was tested (SZ Lower Level). The values chosen were 25 and 75 mbgl. The lower value represents the approximate thickness of the seepage face used in other studies (e.g. Foster, 2014; Larocque, 2014), while the higher value was selected arbitrarily to assess the influence a thicker seepage face would have on the model. The results of the sensitivity analysis are tabulated and displayed in Table 4.10 and Figure 4.13, respectively.

Table 4.10 Sensitivity analysis results. Average head difference is the difference between the calibated and tested average head over the entire model domain. The error statictic changes (ME and RMSE) are the differences between the error statistics calculated (against the WELLS database) for the calibrated and tested model.

Parameter Varied	Calibrated Value	Value Simulated	Resulting Changes		
			Average Head Difference (m)	ME (m) Change	RMSE (m) Change
Leaf Area Index	7.5	10.3	-0.04	-0.04	-0.01
		7.1	-0.05	+0.04	-0.01
Manning's M ($m^{1/3}/s$)	2.5	7	-0.06	-0.06	-0.02
		1	-0.03	+0.02	+0.01
Soil UZ Thickness (m)	2	2	-0.05	+0.05	+0.01
		0.5	-0.01	-0.01	-0.03
SZ Lower Level (m.b.g.l)	50	75	-1.43	-1.43	+0.01
		25	+1.82	+1.83	+0.52
Bedrock Hydraulic Conductivity (ms^{-1})	4.7×10^{-7}	1×10^{-6}	-5.1	+4.50	+7.89
		1×10^{-7}	+3.73	+3.37	+2.29

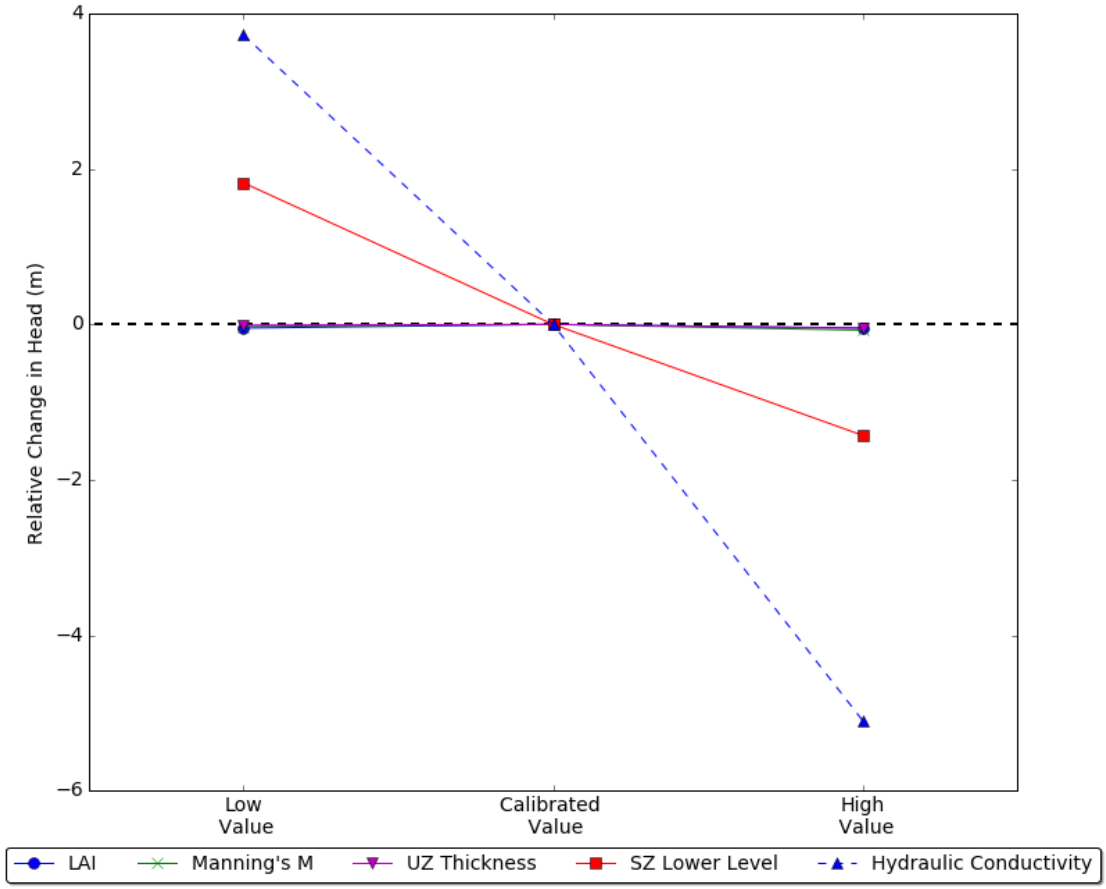

Figure 4.13 Sensitivity analysis results.

The most sensitive parameters tested were the 'SZ lower level', which is the elevation of the base of the SZ (which directly influences the thickness of the seepage face near the coast), and the hydraulic conductivity of the bedrock, with the latter being the most sensitive parameter. All other parameters resulted in average head changes of less than 0.1 m. For these two most sensitive parameters, the lower values increased the average head in the model, while the higher values decreased it. During the later stages of the model calibration, the aim was to lower overall model head, since the model was over predicting groundwater levels. On the face of it, increasing the lower level and/or hydraulic conductivity would have lowered the overall groundwater level in the model, theoretically achieving a more satisfactory calibration. However, lowering the overall head did not improve the model calibration. Rather, these changes increased the error at the observations wells (WELLS database), thus increasing the overall error statistics. For example, increasing the hydraulic conductivity to 1.0×10^{-6} m/s decreased the average groundwater levels by ~5 m, roughly the amount the model was over predicting the groundwater levels by compared to the WELLS database. But, analysis of the error statistics shows that this change

increased the model error, with increases to the ME and RMSE of 4.50 and 7.89 m, respectively.

The results of the sensitivity analysis imply that that the hydraulic conductivity and the thickness of the seepage zone have the largest control on the regional groundwater flow system; land surface and unsaturated hydrologic processes are not influential at the regional scale.

Water Balance

The water balance of the model simulation was extracted using the water balance tool in MIKE SHE. This tool extracts the average incremental water height equivalent (in mm) of components of the water balance (e.g. evapotranspiration and recharge) for the entire model domain at each time step. This extracted daily water balance dataset was then grouped into water years (WY) instead of calendar years. A water year is used to ensure that precipitation from wet seasons is grouped together, and not split between two different wet seasons. A water year runs from October 1st (e.g. 1995-10-01) to September 30th of the next year (e.g. 1996-09-30). The daily water balance was summed for each water year. The summed water balance components of interest (precipitation, actual evapotranspiration, runoff, recharge, and the water balance error) of each water year in the post spin-up period of the calibration phase of the simulation are tabulated in Table 4.11.

Table 4.11 Annual (WY) water balance. All values have units of mm.

	Precip	AET	Runoff	Recharge	Error
WY 95-96	1000	435	332	189	-22
WY 96-97	1253	431	476	209	-23
WY 97-98	790	381	335	203	-41
WY 98-99	1166	399	471	209	-36
WY 99-00	965	379	356	200	-24
WY 00-01	801	403	235	188	-6
WY 01-02	883	368	326	194	-33
WY 02-03	876	359	305	192	-25
WY 03-04	964	397	281	193	0
WY 04-05	1145	431	451	215	-38
WY Avg.	984	398	357	199	-25
WB %	100	40	36	20	-2.5

The average water year water balance matches relatively closely the water balance estimates in the conceptual model (Section 2.9, Table 2.6). For ease of comparison, the estimated range and the initial estimate of the water balance components are repeated in Table 4.12. All of the simulated water balance components are within the estimated ranges and are within five percentage points of the initial estimates. For the simulation, AET had the widest range (between 35 and 55 % of MAP), while recharge displayed the least amount of variability (17 to 26 % of MAP). The mean annual simulated recharge to Gabriola Island is 20% of precipitation (or 191 mm/year).

Table 4.12 Water balance comparison.

Water Balance Component	Estimated Range (% of MAP)	Initial Estimate (% of MAP)	Range of Simulation (% of MAP)	Average of Simulation (% of MAP)
Evapotranspiration	32 to 60	45	35 to 55	40
Runoff	32 to 50	40	29 to 42	36
Recharge	1 to 62.7	15	17 to 26	20

The average error within the simulation is relatively small (-2.5% of MAP). The negative error represents an overall retention of water in the model system. In other words, on average, slightly more water is entering the model than leaving it. This indicates that one, or any combination of, the following may be resulting in a slight accumulation of water in the model over the simulation period.

1. bedrock hydraulic conductivity is too low – groundwater is not able to move quickly enough through the model,

2. SZ discharge outlet is too thin – groundwater is not able to exit the model

Overall, however, the good agreement between the estimated and simulated water balance, and the relatively low error, indicate that the model is sufficiently calibrated.

Particle Tracking

The simulated 50-year well capture zones of all the groundwater wells sampled for tritium are relatively small (Figure 4.14). The simulated capture zones range in extent between approximately 120 and 330 m for the wells CC3 and CC4, respectively.

The relatively small, simulated capture zones suggest that the majority of the groundwater at the sample points is sourced a short distance from the wells. This suggests that the groundwater is highly mixed, with very little old, tritium depleted, groundwater contributing to the groundwater mixture. This conclusion is in agreement with the analysis of the groundwater tritium concentration in Section 3.2, i.e., all the groundwater samples had a measurable concentration of tritium.

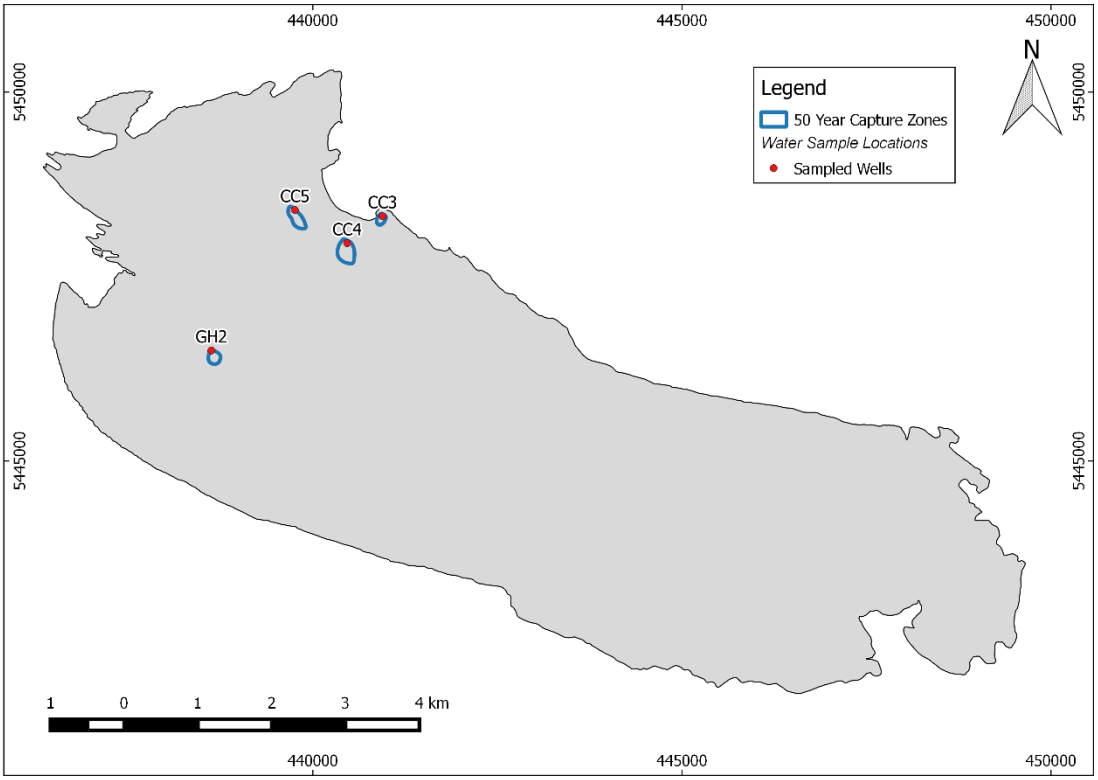

Figure 4.14 Simulated 50-year well capture zones.

However, there are a few limitations as to the accuracy of the capture zones presented. Firstly, the discretization of the model domain, both laterally and vertically, is not ideal in accurately calculating capture zones via particle tracking. The longitudinal extent of the largest capture zone (CC5) is ~ 350 m and the cell size is 150 m, meaning that the longest particle travel path was only calculated from the hydraulic head between two cells. Additionally, the single layer approach to the SZ means that vertical groundwater flow is not simulated. Thus, only horizontal particle travel paths are calculated. If vertical flow paths of water were present, the effect would be to decrease the size of the 50-year capture zones. Secondly, the use of the EPM approach to simulate groundwater flow in fractured bedrock does not account for local scale fracture heterogeneity and discrete fracture flow (i.e. the EPM approach

assumes a bulk effective porosity). For example, if a highly conductive discrete fracture was present, the capture zone would propagate out much further in the direction of the fracture compared with the estimated capture zones presented.

4.3. Model Limitations

An integrated numerical GW-SW model is ideally suited to understanding and estimating recharge at a regional scale. However, there are important limitations these regional scale models:

- The availability and uncertainty in input parameters. Integrated GW-SW models are highly parameterized and require data that may not available everywhere, or at all, in the model domain (e.g. van Genuchten parameters of fractured bedrock are not available from field and laboratory studies and these were estimated from previous modeling studies). Thus, assumptions regarding many parameters had to be made.
- Some processes occurring at a smaller scale, such as localised rapid recharge in areas of intensely fractured bedrock, are not represented in the model. The degree to which local processes influence groundwater levels is unknown. Additionally, due to the limitation of spatial discretization (coarser grid size), small scale variations in topography, and thus localized seepage, were not able to be simulated by the model.

Nevertheless, numerical models are invaluable as they have the ability to investigate the broader scale processes, such as controls on recharge dynamics, and how sensitive the hydrologic system is to future climate variability. These two topics are explored in more detail in the following chapter.

Chapter 5. Investigating Recharge on Gabriola Island

5.1. Introduction

This chapter contains the analysis and discussion of the modeling results with respect to the objectives of this thesis: (1) characterize the physical parameters which influence the spatial distribution of recharge and discharge; (2) determine the rainfall-runoff-recharge relationships controlling seasonal groundwater level variation; (3) investigate how climate change may influence recharge in a temperate setting. In detail, this chapter examines the spatial-temporal distribution of the recharge and seepage, the rainfall-runoff-recharge dynamics, and finally, how future projected climate change might influence these processes.

5.2. Spatial-Temporal Recharge and Seepage

Recharge and seepage vary spatially across the island. The average annual simulated rates of recharge and seepage are presented in Figure 5.1. Recharge and seepage are recorded in MIKE SHE as water transfer items, water transfer from the UZ to the SZ (positive) and SZ to the land surface (negative), respectively. The mean water transfer across the validation simulation period (October 1st, 2000 to September 30th, 2010) was calculated for each active grid cell; the mean transfer rates were then converted from day to year time units. In Figure 5.1, positive values (in blue) represent areas where recharge occurs on an average annual basis, while negative values (in red) represent seepage areas. Zero values represent areas where neither recharge nor seepage dominate on average, i.e. recharge is approximately equal to seepage. Recharge generally occurs in areas of higher elevation, while seepage occurs in areas of lower, and steeper, topography. It should be noted that both recharge and seepage occur in some cells over the simulation period, due to the rising of the water table as it intercepts the ground surface. For example, some areas of high recharge could have seepage occurring at some time in the year, however, much more recharge occurs an annual basis than seepage. This seasonal variation in recharge and seepage is discussed further below. Overall, more cells display a positive transfer direction (recharge); 1647 cells (70% of the model domain) compared to 694 cells (30%) for seepage. Thus, recharge occurs over more of the island than seepage areas, which

are more localised. However, the discharge flux of seepage is high, approximately 53% of recharge to the SZ is returned to the surface from seepage. In comparison, the SZ discharge to the coast and via pumping is 44% and 5% of recharge, respectively.

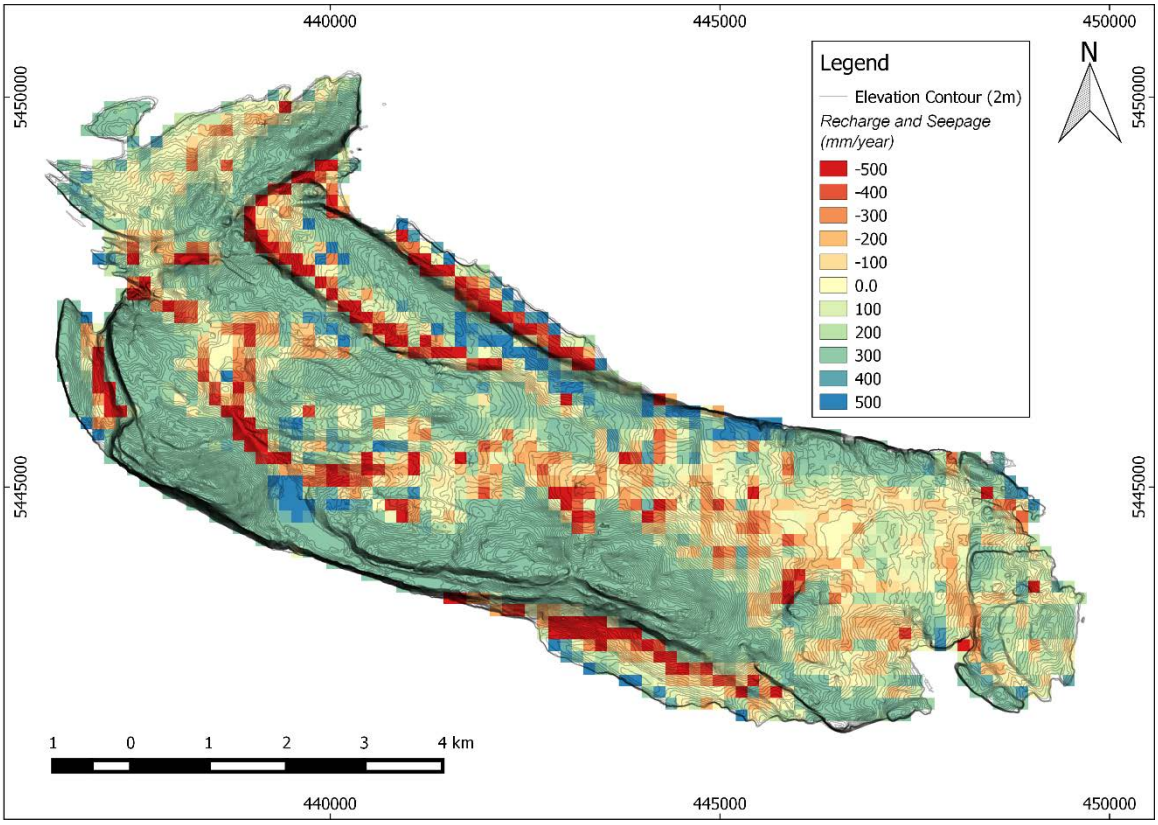

Figure 5.1 Average annual recharge and seepage (mm/year). The scale shows positive and negative numbers. Positive numbers represent recharge areas on an average annual basis, while negative numbers represent discharge zones on an average annual basis. Values close to zero are neither recharge nor discharge areas on an average annual basis.

The recharge and discharge patterns vary slightly on a seasonal basis as shown in Figure 5.2 - Figure 5.5 (fall (SON), winter (DJF), spring (MAM) and summer (JJA), respectively). The overall pattern is consistent with the mean annual recharge and seepage map shown in Figure 5.1, which suggests that recharge and seepage areas are generally seasonally persistent in most areas. The overall magnitude of recharge is much less during the summer as indicated by the near zero values over a larger portion of the island. Seepage during the summer is also somewhat lower. The distribution of seasonally persistent seepage and recharge areas are presented in

Figure 5.6. Only some of the cells (30%) simulate solely recharge at all time steps, with the majority of cells (66%) simulating both recharge and seepage variably throughout the year; very few cells simulate seepage all the time (4%).

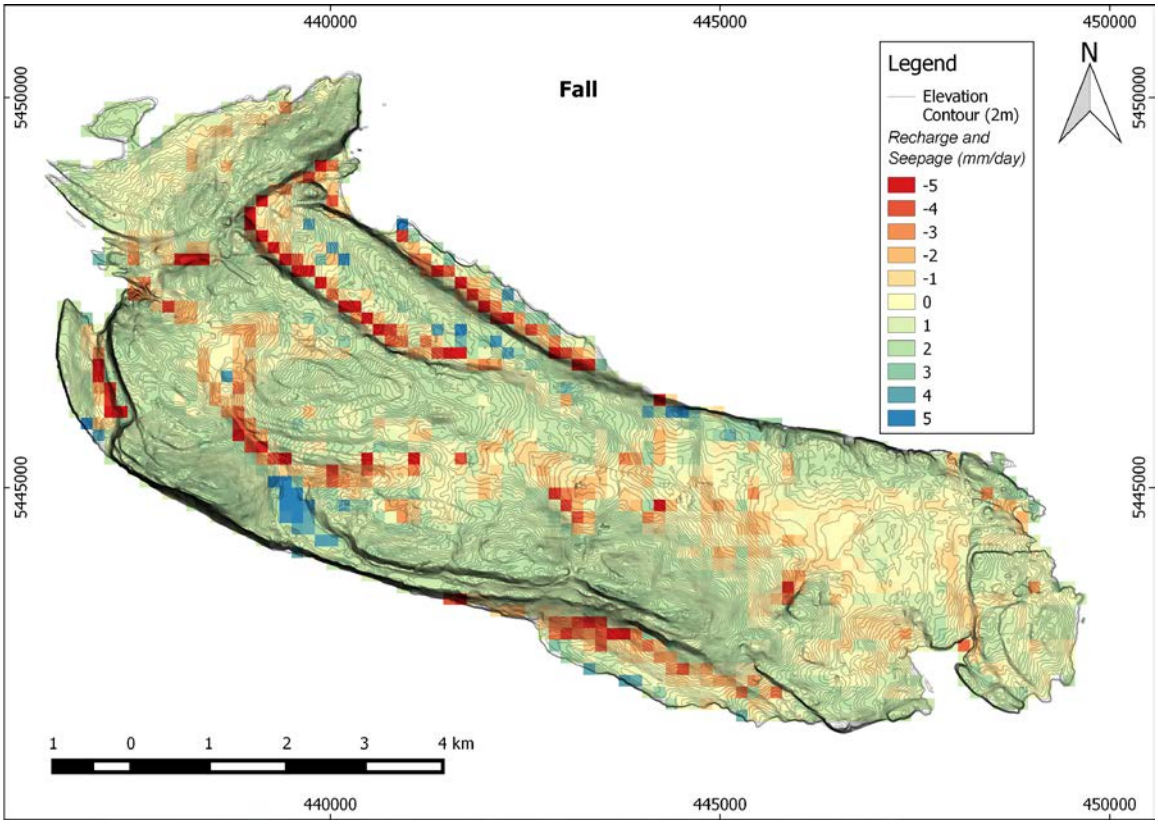

Figure 5.2 Average fall recharge and discharge (mm/day). The scale shows positive and negative numbers. Positive numbers represent recharge areas during the fall, while negative numbers represent discharge zones during the fall. Values close to zero are neither recharge nor discharge areas during fall.

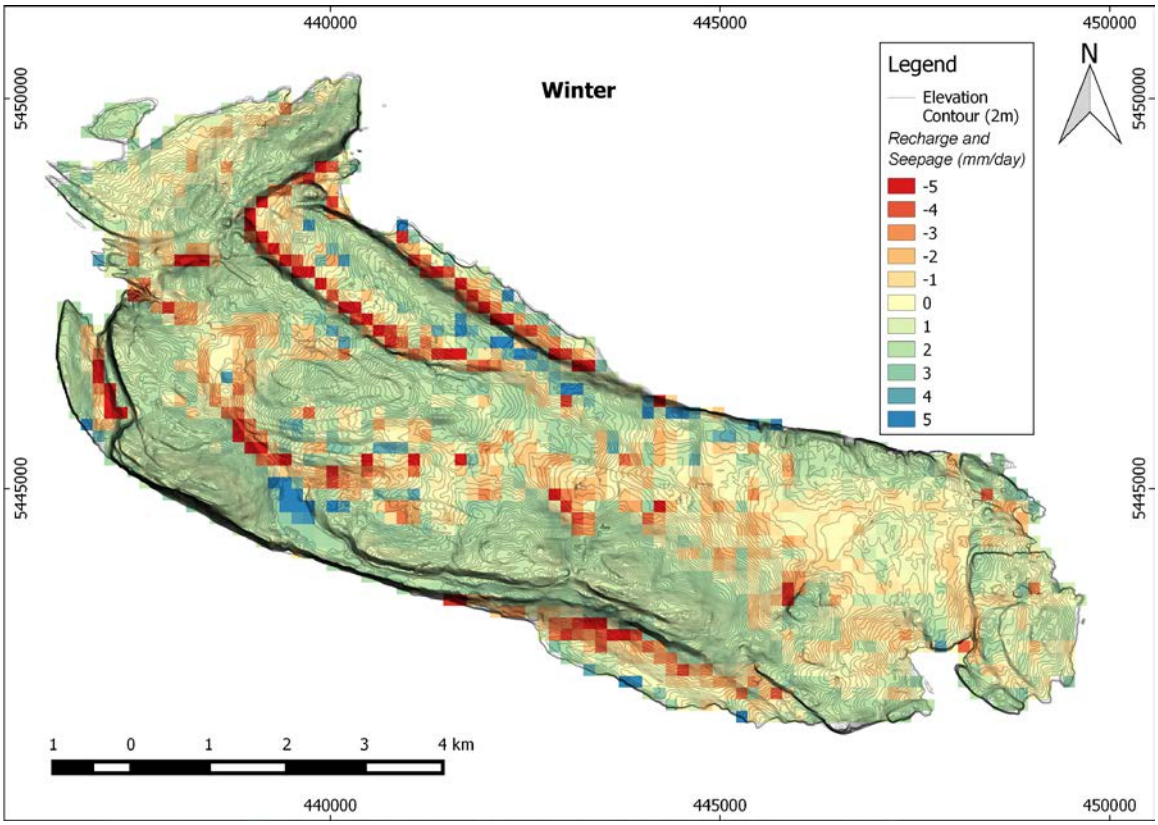

Figure 5.3 Average winter recharge and discharge (mm/day). The scale shows positive and negative numbers. Positive numbers represent recharge areas during the winter, while negative numbers represent discharge zones during the winter. Values close to zero are neither recharge nor discharge areas during winter.

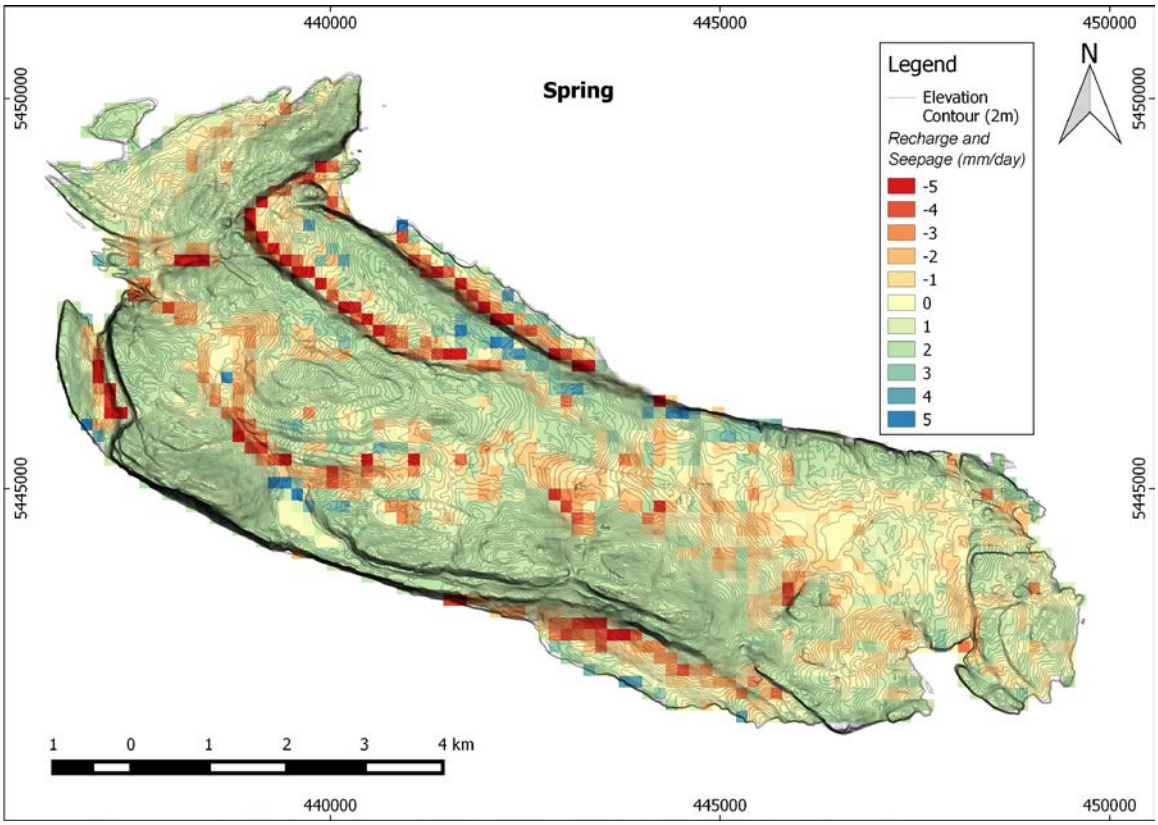

Figure 5.4 Average spring recharge and discharge (mm/day). The scale shows positive and negative numbers. Positive numbers represent recharge areas during the spring, while negative numbers represent discharge zones during the spring. Values close to zero are neither recharge nor discharge areas during spring.

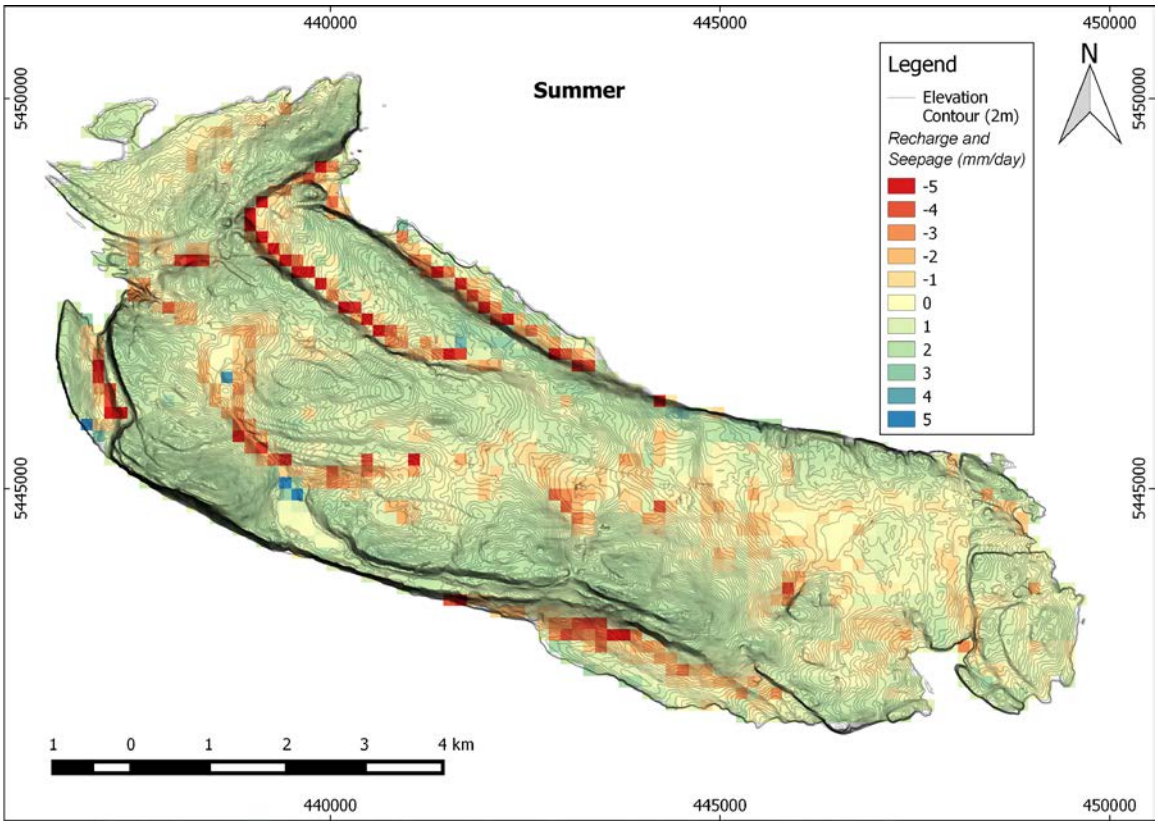

Figure 5.5 Average summer recharge and discharge (mm/day). The scale shows positive and negative numbers. Positive numbers represent recharge areas during the summer, while negative numbers represent discharge zones during the summer. Values close to zero are neither recharge nor discharge areas during summer.

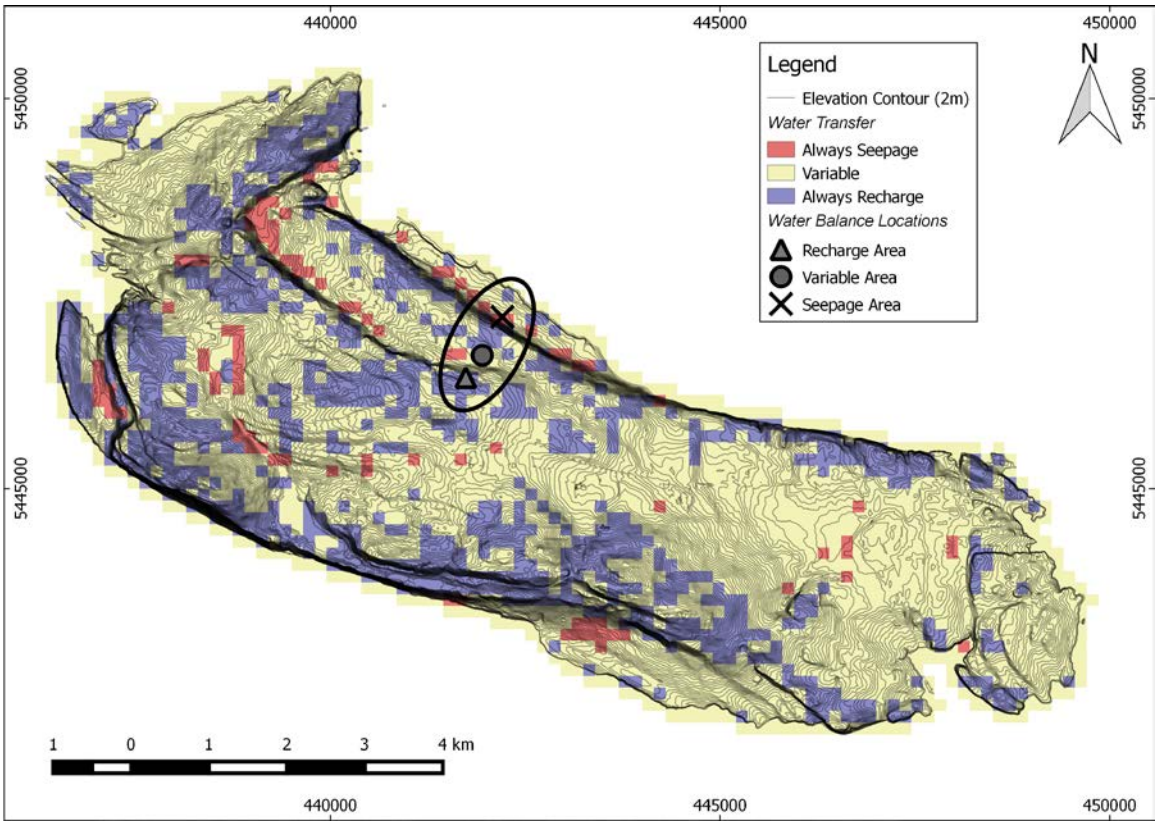

Figure 5.6 Water transfer direction. The direction of water transfer is with respect to the SZ for every time step of the simulation. Cells displayed as 'always recharge' only have recharge occurring (UZ to SZ water transfer), while the opposite is true of cells displayed as 'always seepage'. Cells designated 'variable' simulate both discharge and seepage at different time steps. The 'Water Balance Locations' correspond to the locations of the water balance plots in Figure 5.7 and Figure 5.8.

To get a more detailed understanding of the seasonal variability in recharge and seepage zones, as well as the role the depth of the water table plays where recharge and seepage are not persistent, three areas were investigated (a Seepage Area, Variable Area, and Recharge Area). The locations of these areas in the model and their positions on a conceptual slope are shown in Figure 5.6 and Figure 5.7, respectively. The recharge, seepage, and depth to water table time series data were extracted from the model at these locations for period representing an 'average water year' (WY). An average WY is defined here as a WY period (October to September) when the total precipitation was close to the longer-term average (~960 mm/WY). Conceptually, the areas represent different regimes of the typical seasonal water table fluctuations over the course of a year (Figure 5.7). In a seepage area, the water table

is constantly above the ground surface (even during the summer period), thus seepage is seasonally persistent. Conversely, in a recharge area the water table remains below the ground surface (even during the winter period). In this area, recharge is the dominant process. A variable area experiences both recharge and seepage. During the summer, the water table is lower than ground surface and only recharge occurs. Then when the water table is higher in winter, seepage then occurs.

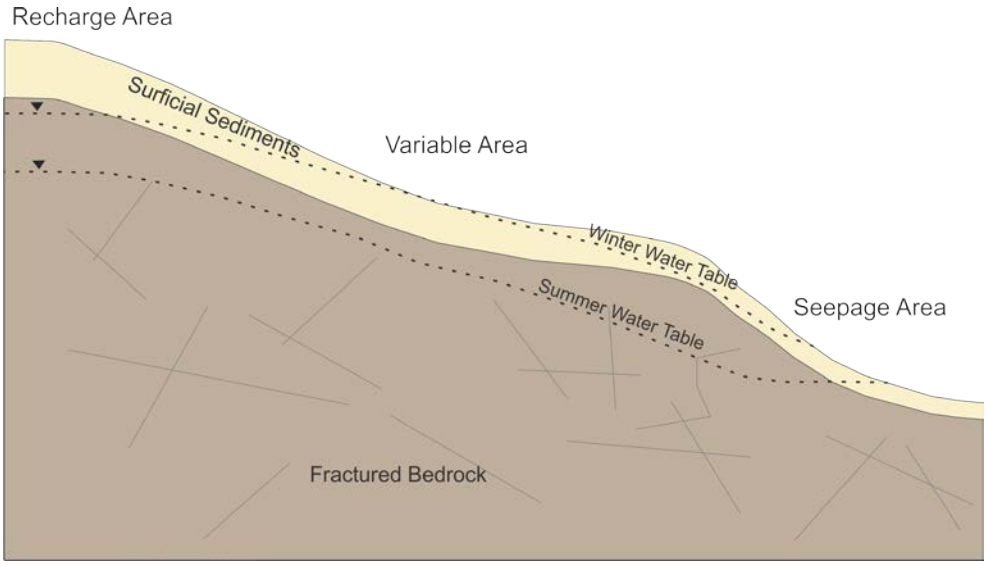

Figure 5.7 Conceptual location of water balance points. The seepage and recharge areas are located where only seepage or recharge, respectively, occur during the year (e.g. seepage never occurs in the recharge area). In the variable area, both recharge and seepage occur due to seasonal fluctuations in the water table. The location of these zones is shown on Figure 5.6.

Figure 5.8 presents the recharge, seepage, and depth to water table in each area for an average WY. During the average WY presented (2001/2002), precipitation was ~915 mm. In the seepage area, the water table remained above the ground surface with very little variation (shown by the negative depth below ground level value on the secondary y axis in Figure 5.8). Seepage occurred throughout the year, with very little variation (the blip towards the end of August 2002 notwithstanding). No recharge was registered at this location. In the recharge area, recharge was seasonally persistent, with no seepage registered. Recharge occurred at a fairly consistent rate, except in late December 2001 and early January 2002 when it was slightly more

variable. Unlike in the seepage area, the water table level was not constant, but rather fluctuated seasonally. Despite this, the water table remained well below the ground surface (>14 mbgl). In the variable area, both seepage and recharge occurred as a result of the seasonal fluctuation in the water table. Seepage occurred when the water table reached the ground surface (December 2001 to May 2002), and ceased when the water table dropped (June 2002 onwards). Recharge essentially occurred a constant rate throughout the WY, except during a brief period in mid-November 2001. In the variable area, recharge was also more seasonally variable than in the recharge area. As well, recharge was low at the beginning of the WY (October to November), before increasing rapidly to a fairly stable rate (despite some variability) from December 2001 to May 2002 (when the water table was at the ground surface during winter). Following this period, the recharge, and the water table, dropped slowly. While recharge was seasonally variable, it was much less variable than the seepage.

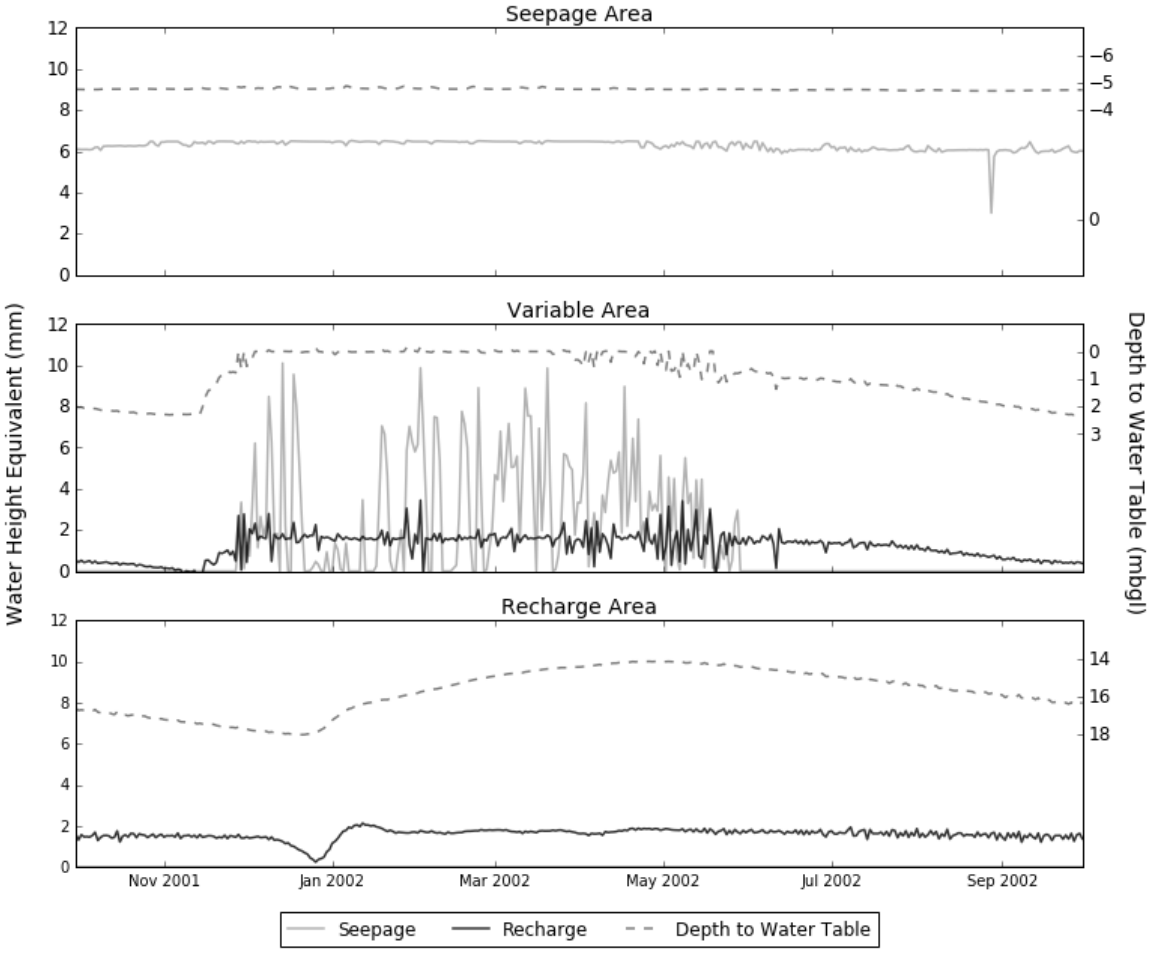

Figure 5.8 Recharge and seepage for the average water year at different locations along a slope. The recharge, seepage and depth to water table in metres below ground level (mbgl) are plotted at a daily frequency for an average water year (WY). An average WY is defined here as a WY period (October to September)) when the total precipitation was close to the longer-term average (~919 mm/WY). For this WY (2001/2002), precipitation was ~915 mm. The Seepage and Recharge areas are located where only seepage or recharge occur, respectively. At the Variable Area locations, both occur. The locations of these areas are shown on Figure 5.6.

The model did not include spatially varying vegetation cover, geology, or soil cover. Thus, the model cannot be used to assess how these physical parameters control recharge and seepage directly. However, a sensitivity analysis was undertaken during the calibration process to assess how sensitive the model is to changes in input parameters and model design (Section 4.2.12). The findings of the sensitivity analysis suggest that the parameters that have greatest influence of the groundwater level, and thus recharge, are the hydraulic conductivity of the bedrock and the thickness of the

seepage face at the external boundary of the model. The model was not sensitive to changes in the unsaturated zone (soil cover) and land surface (vegetation cover) parameters tested. Nevertheless, differences in these parameters can be expected to influence the groundwater levels to some degree at a local scale.

A recent complimentary study identified zones of seepage via field observation. Rathay (2016) characterised areas of seepage based on topography and seepage regime. The seepage areas were observed at different times in the year. Seepage area discharge was characterised as either perennial (seepage identifiable during all visits), seasonal (seepage only observed during winter), or none (no observed flow during any of the field visits). The seepage locations and discharge regime are superimposed over the water transfer direction in Figure 5.9 to compare the observed seepage locations to the model results of this thesis. The comparison indicates that the model's ability to reproduce seepage at the field sites was mixed. For example, at the seasonal locations on the northeastern coast of the island (BW1 and BW2), the model simulated variable cells (both seepage and recharge), which is consistent with the field site observations. However, the seasonal sites on the northwestern side of the island (EH1 and EH2) were simulated as recharge only (no seepage at any time). The perennial seepage area (MG) was also simulated as recharge only. Finally, the dry sites on the northeastern side of the island (SP1 and SP2) were simulated as recharge (consistent with the dry observation), while the EH3 was simulated as variable. Overall, the model was not able to reproduce the field seepage observations particularly well. The cause of this is most likely the coarse discretization of the model. Specifically, the localised sharp changes in topography, which are typical of the seepage locations, could not be represented in the model.

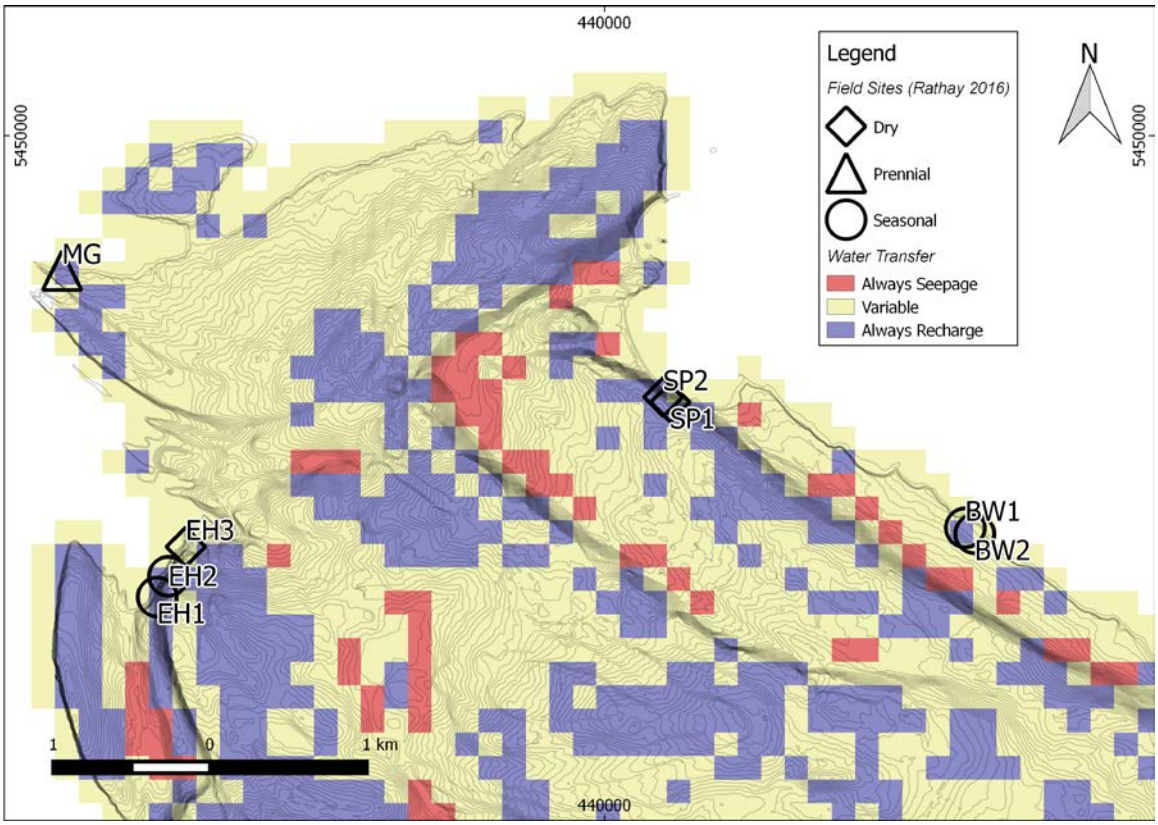

Figure 5.9 Comparison between water transfer direction and seepage locations identified in Rathay (2016). The direction of water transfer is with respect to the SZ for every time step of the simulation (as per Figure 5.6). Cells displayed as 'always recharge' only have recharge occurring (UZ to SZ water transfer), while the opposite is true of cells displayed as 'always seepage'. Cells designated 'variable' simulate both discharge and seepage at different time steps. The field sites are categorized into dry (never seeping), seasonal (dry in summer, seepage in winter), and perennial (always seeping).

As described in Section 3.2, tritium is a tracer that can be used to infer groundwater residence time. The presence of tritium in all of these samples suggests a mean residence time of less than 50 years (see Section 3.2.2). In Figure 5.10 the tritium content from the water samples collected as part of the field investigation (Section 3.2) are superimposed upon the average summer recharge and seepage model results. The comparison is summarized in Table 5.1.

The sample collected in the swamp (HS1) has high tritium and the model situates recharge at this location. Thus, this swamp is not a discharge location for groundwater, or the proportion of groundwater is very low. This agrees with the low

TDS (see Section 3.2.2) for this sample. All of the groundwater sample sites (GH2, CC3, CC4, and CC5) have tritium, and at all sites, the model simulates net recharge. This suggests that in recharge areas, the groundwater is relatively young as might be expected, and if there is mixing with older groundwater, the proportion of older groundwater must be quite small. The short residence time also agrees with the small capture zones simulated for these well locations (Figure 4.14). Finally, samples collected in creeks have higher tritium concentrations (although generally not as high as the swamp). At two of the three creek water sample sites (CC1 and CC2) the model simulated net seepage over summer, while at the other creek water sample site (GH1), the model simulated a mixed transfer (recharge and seepage approximately equal). Because the tritium content is relatively high, it can be inferred that either there is a large proportion of surface runoff in these samples that is mixed with deep groundwater discharge, or that the groundwater discharging in creeks is relatively young. Given that it was a particularly dry summer, it would seem that the latter is a more reasonable explanation. Overall, the combined tritium and model results suggest a rather rapid groundwater flow system on Gabriola Island.

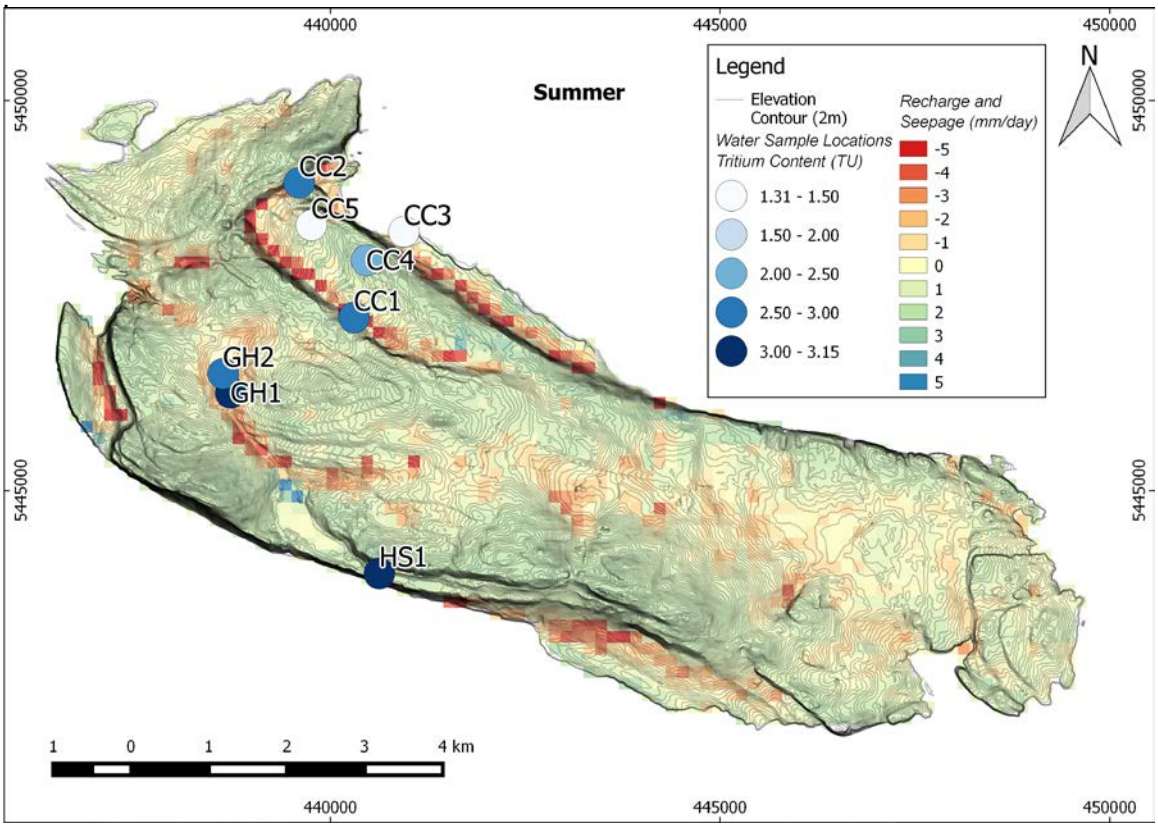

Figure 5.10 Comparison between average summer recharge and discharge and water sample tritium content. The scale shows positive and negative numbers (mm/day). Positive numbers represent recharge areas during the summer (as per Figure 5.5), while negative numbers represent discharge zones during the summer. Values close to zero are neither recharge nor discharge areas during summer. The tritium content (TU) is shown in colour scale, with light to dark shades representing low to high tritium content.

Table 5.1 Tritium content and recharge/seepage regime comparison.

Sample Site	Water Type	Tritium Content (TU)	Recharge/Seepage
HS1	Swamp	3.09	Recharge
CC1	Creek	2.9	Seepage
CC2	Creek	2.88	Seepage
GH1	Creek	3.15	Equal
GH2	Groundwater	2.74	Recharge
CC3	Groundwater	1.31	Recharge
CC4	Groundwater	2.07	Recharge
CC5	Groundwater	1.45	Recharge

5.3. Rainfall-Runoff-Recharge Dynamics

The rainfall-runoff-recharge dynamics are investigated using the MIKE SHE water balance tool to extract water balance items from the model. Water balance items are generally grouped by the module within MIKE SHE, i.e. OL, UZ, and SZ modules each have individual water balances. However, some of the water balance items overlap the individual modules. These overlapping items are generally water transfers between modules, e.g. infiltration is recorded as an output of the OL water balance, and an input into the UZ water balance. The individual water balance items are described in the subsequent sections.

Three characteristics of the rainfall-runoff-recharge dynamics were investigated to achieve the second research objective of this thesis (Section 1.3). The specific characteristics were: 1) the seasonal dynamics on an average annual basis, 2) the relationship between heavy rainfall events and groundwater level dynamics, and 3) the impact of inter-annual precipitation variability on the dynamics.

5.3.1. Seasonal Rainfall-Runoff-Recharge Dynamics

This section investigates how runoff and recharge vary on a seasonal basis in this temperate climate area. Specifically, it addresses the questions of: when, on average, recharge occurs, and, how runoff is generated at different times of the year.

As anticipated, there is seasonal variability in the rainfall-runoff-recharge dynamics. To investigate these dynamics, the individual module water balances were used rather than the 'total' model water balance, as the total water balance only reports water entering and exiting the whole model domain (all modules). The total water balance does not include the water exchange items between the modules that describe the rain-fall-runoff dynamics. Thus, the OL and UZ water balances are utilised here.

The seasonal global OL water balance is presented in Figure 5.11. The water balance items of the OL module are: 1) Precipitation, the canopy precipitation throughfall that reaches the ground surface; 2) Seepage, the transfer of water from the SZ to the ground surface; 3) Infiltration, the water transfer from OL to UZ; 4) OL Evaporation, the amount of water evaporated from ponded water (does not include soil

ET); and 5) Runoff, the amount of water exiting the model domain boundary (coast) via surface runoff.

During the wettest time of year (November to March), the excess precipitation that does not infiltrate the UZ contributes to runoff; this is most noticeable in December and January. The greatest difference between precipitation and infiltration coincides with the period of seasonally high water table (November to March). Not only is more runoff generated during this period, but seepage is also higher. Seepage is generated by the saturated overland flow process, where the water table reaches the ground surface. In fact, seepage begins to increase in November and remains somewhat higher and stable until April, before it reduces. As suggested by the spatial recharge and seepage results in the previous section, seepage does not normally take place in recharge areas – the two are generally separate. Therefore, seepage is taking place elsewhere on the island in response to the general rise in water table caused by greater precipitation during late fall and winter leads to more seepage. In Figure 5.9, the total water balance components for January suggest that seepage must also contribute to runoff because the difference between precipitation and infiltration is less than the runoff amount that month. What percentage of the runoff derives from seepage and from saturated overland flow is uncertain. Likely, this is highly variable at a local scale depending on water table depth.

Conversely, during the summer months (April to October), infiltration matches precipitation, and runoff is thus low. The majority of the precipitation that falls during late spring and summer infiltrates the ground surface. During these drier months, seepage to the ground surface, from perennial seepage areas, is dominant source of runoff.

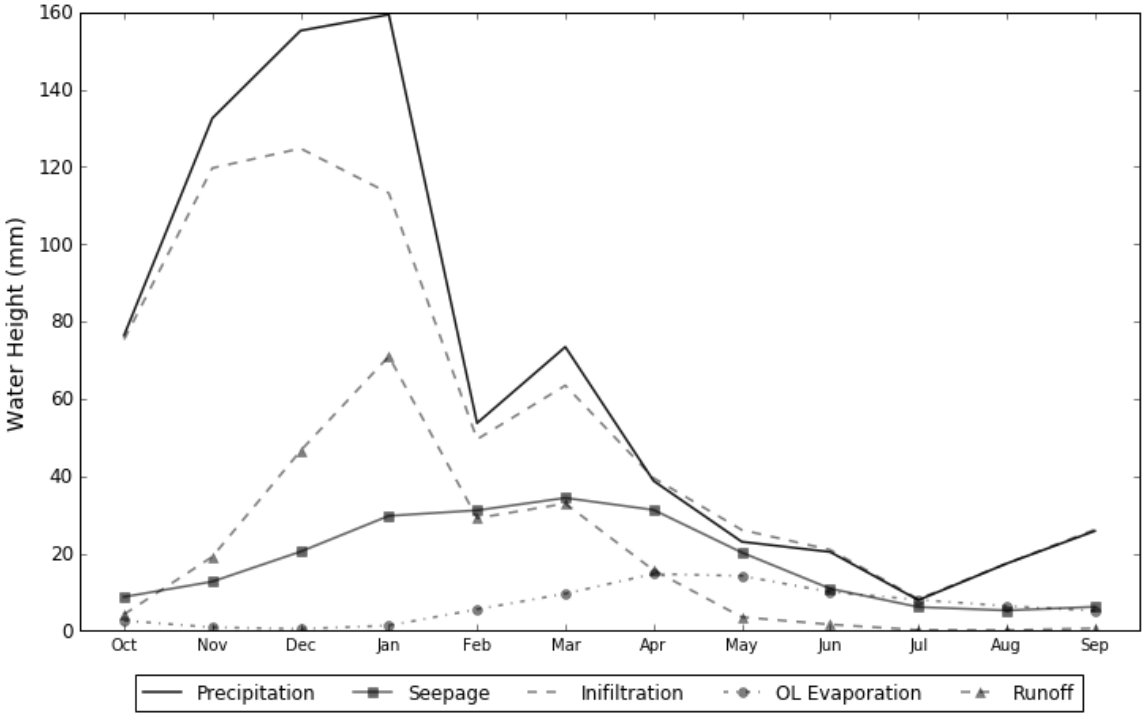

Figure 5.11 Global OL water balance. Water balance items are average monthly totals. Results from the validation period were used to calculate averages. OL Evaporation represents the water evaporated from surface ponding. Note, only the first 9 years of the simulation were used (e.g. 2000-2009) due to the winter precipitation in 2010 being extremely heavy (~ twice as much precipitation fell), thus skewing the average results.

The UZ water balance is presented in Figure 5.12. The water balance items of the UZ module are: 1) Infiltration, water transfer from OL to UZ (identical to OL water balance); 2) UZ Evapotranspiration, the amount of water evapotranspired from the UZ (includes root transpiration and evaporation from soil); 3) Recharge, water transfer from UZ to SZ (output of water from the base of the UZ column); and 4) UZ Storage Change, cumulative change in UZ storage. The UZ storage change is not a direct measure of the moisture content (e.g. proportion of pore space filled). Rather, it is a record of the relative change in UZ storage. For example, a decreasing UZ storage value indicates a drying of the UZ (a decrease in soil moisture). Thus, residual moisture of the UZ contributing to recharge year-round, while possible, remains uncertain.

As shown in Figure 5.10, recharge occurs year round, but increases from October to January, when it reaches a pseudo-stable rate, before declining from April

through to September. This trend matches closely with the seepage dynamics in Figure 5.11. The increase in infiltration starts in July, but UZ evapotranspiration is still high, so the UZ storage change continues to decline and recharge remains low. There appears to be a 2-month lag time between the increase in infiltration and the increase in recharge and UZ storage change. The lag-time represents the time it takes for the infiltration to travel vertically through the UZ and reach the water table as recharge (SZ), gradually filling up the spaces / fractures. This time lag is caused by the thicker UZ following summer (water table is lowest). Recharge still occurs after periods where UZ evapotranspiration is equal to or exceeds infiltration (May and August). In addition, UZ storage gradually decreases over this timeframe reflecting the gradual loss of soil moisture, below the evaporation and root zone. The continuation of recharge during these months of UZ moisture deficit (UZ ET is higher than infiltration) can be explained by residual water in the UZ below the depth of active UZ ET continuing to travel downward to reach the water table. However, due to the limitation of UZ storage reporting by MIKE SHE, this process is unable to be confirmed.

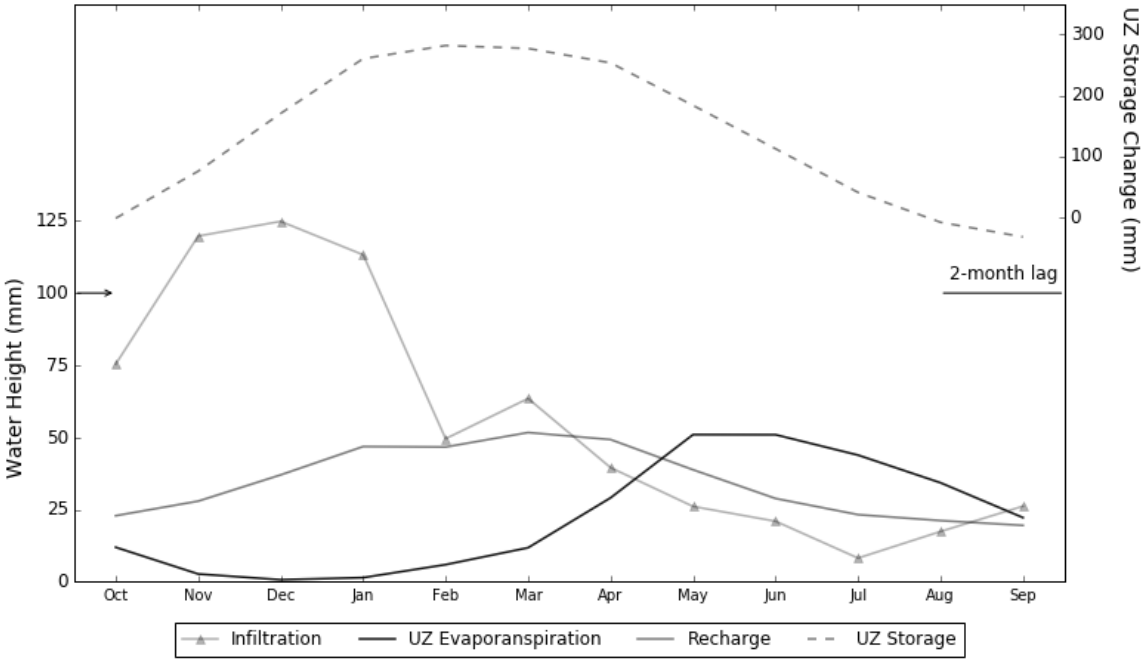

Figure 5.12 Global UZ water balance. Water balance items are average monthly totals. Results from the validation period were used to calculate averages. Note, only the first 9 years of the simulation were used (e.g. 2000-2009) due to the winter precipitation in 2010 being extremely heavy (~ twice as much precipitation fell), thus skewing the average results. UZ storage is a relative measure of the cumulative change in moisture content of the UZ. When UZ storage increases, the moisture content increases.

5.3.2. Heavy Rainfall Events

Heavy rainfall events, defined here as single events of high precipitation (>20 mm per day), are expected in increase in frequency and magnitude in the future. These high intensity rainfall events may exceed the infiltration capacity of the soil/bedrock, resulting in infiltration excess overland flow. Thus, heavy rainfall events may limit the amount of precipitation that infiltrates the ground surface and reaches the water table as recharge.

Figure 5.13 shows the response of the water table to heavy rainfall events at the variable area location. Two time periods are presented, winter and summer, representing periods of a high and low water table, respectively. The winter time period was chosen as it included several daily precipitation amounts greater than 20 mm per day. During the winter period, the water rises in smooth pulses that appear to mimic

the cumulative rainfall amount, for example, in early December 2002. The multiple heavy rainfall events in mid-December, cause a significant rise in the water table that persists into January, until another period of rain including a heavy rain event cause the water level to rise abruptly again. The record shows that successive periods of rain, most of which include heavy rain events, result in fairly abrupt rises in the water table. During winter, the effect of a single heavy rain event is difficult to determine because heavy rain events tend to occur during periods of rainfall rather than as single events. Cumulative rainfall definitely influences the water table rise as evidenced by the early December water table rise, but effect of single heavy rain events on water table rise is less clear.

During the summer period (Figure 5.13), small variations in the water table are apparent, but there are no strong water table responses to any rain event, particularly the heavy rainfall event in August 2003. The water table simply declines gradually through the summer.

Clearly, the depth of the water table is a factor in controlling the response of the water table to heavy rainfall events. When the water table is near surface (as in winter), the water table is more responsive to rainfall, but there appears to be more of an influence of cumulative rainfall than simply heavy rain events. Infiltration also closely matches precipitation during these rainfall events during this and other time periods investigated (precipitation up to 65 mm/day). This finding suggests that the infiltration capacity was not exceeded at this location.

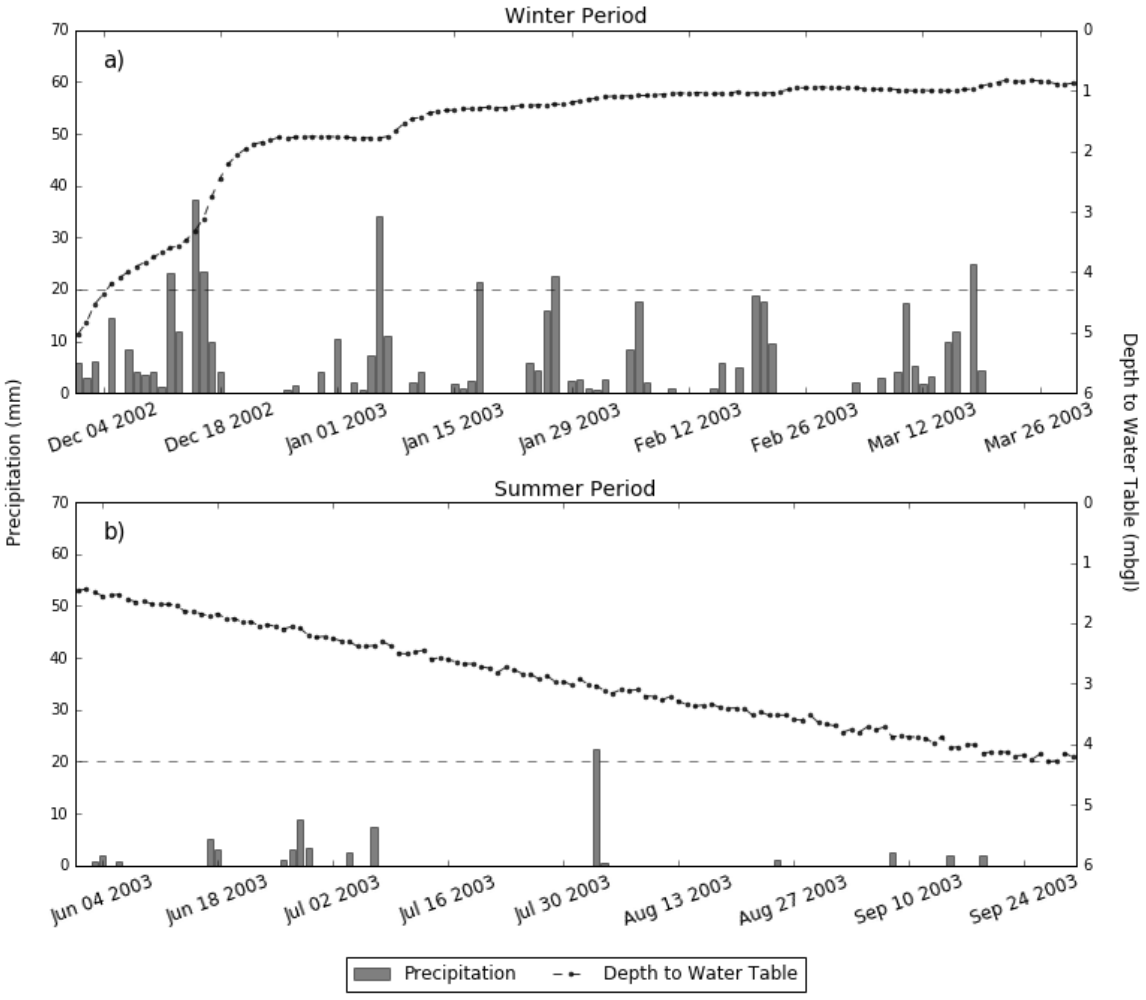

Figure 5.13 Water table response to heavy rainfall in a) winter and b) summer at the variable area. Precipitation events are daily totals. The dashed horizontal line represents the heavy rainfall event threshold (>20 mm/day).

5.3.3. Comparing Wet and Dry Years

Inter-annual variation in precipitation can affect the sustainability of groundwater resources. Years with less precipitation generally result in less recharge to an aquifer, thus lowering the amount of water stored in the aquifer. Fractured rock aquifers are particularly susceptible changes in annual precipitation due to the inherently low storage of the aquifer. Thus, investigating the effect that wet and dry years have on fractured rock aquifers is important for groundwater management.

Figure 5.14 shows the response of a variable area to varying amounts of total precipitation during each of three WYs. WY 2006/2007 represents a high precipitation WY (1267 mm), WY 2001/2002 an average WY (919 mm), and WY 2000/2001 a low precipitation WY (778 mm). The total precipitation clearly influences the position of the water table and whether or not seepage occurs. As precipitation decreases from year to year, e.g. from WYs 2006/2007 to 2001/2002 to 2000/2001, the minimum and maximum of the seasonal variations in the water table also decrease; overall the water table decreases. However, even after a low precipitation WY (2000/2001), the occurrence of an average precipitation WY (2001/2002) returns the water table back to average conditions, suggesting that the system has some built in resilience to low precipitation years.

The amount of precipitation in the high precipitation WY (2006/2007) causes the water table to reach the ground surface, resulting in seepage (February to March). The high degree of variability of seepage and recharge during this period is caused by the very thin UZ when the water table nears the ground surface. When this occurs, precipitation is transmitted quickly to the SZ due to the thin UZ. In contrast, seepage does not occur in the average and lower precipitation WYs. Recharge areas show a similar response (higher WT in wet WYs and lower WT in drier WYs), but only a variable area is included here as it demonstrates the occurrence of seepage during the higher precipitation WY.

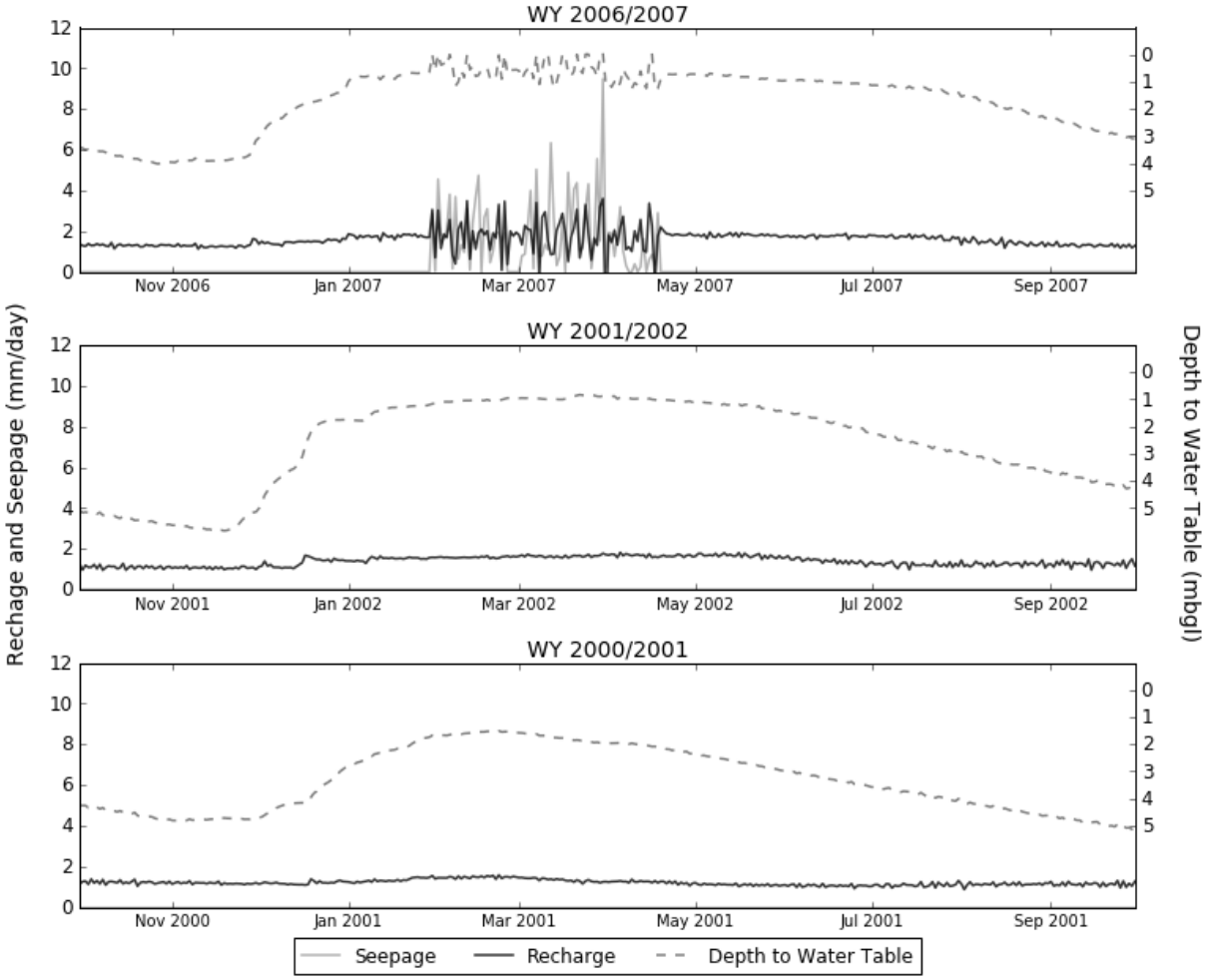

Figure 5.14 System response to different total WY precipitation. The response of a variable area to different amounts of annual precipitation that falls in a WY. WY 2006/2007 represents a high precipitation WY (1267 mm), WY 2001/2002 an average WY (919 mm), and WY 2000/2001 a low precipitation WY (778 mm).

5.4. Future Recharge

Under future climate conditions, simulated recharge and other components of the water balance experience variable changes compared to the historical climate conditions. A comparison between select water balance components under historical and future climate conditions is presented in Figure 5.15; the changes in seasonal and annual water balance items are tabulated in Table 5.2, and presented visually in Figure 5.16.

Table 5.2 Change in global water balance components seasonally and annually (mm)

		Fall	Winter	Spring	Summer	Annual
Precip.						
	2050s	30	33	25	-4	85
	2080s	40	44	31	-2	113
ET						
	2050s	7	2	4	-3	9
	2080s	8	4	11	1	23
Runoff						
	2050s	18	47	15	2	81
	2080s	20	54	17	1	91
Infiltration						
	2050s	14	3	15	-5	28
	2080s	22	8	17	-5	42
Recharge						
	2050s	8	17	12	-2	35
	2080s	8	21	14	-3	40
Seepage						
	2050s	8	18	14	4	44
	2080s	8	21	15	3	47

In general, all components of the water balance are slightly higher under future climate conditions on an annual basis. The fall and winter months have the greatest increase in precipitation (between 30 and 44 mm), while there is less of an increase in spring (between 25 and 31 mm). In summer, there is a slight reduction in precipitation (between -4 and -2 mm). Future ET is relatively consistent with historical conditions, with only slight increases in fall, winter, and spring (between 2 and 11 mm), and very little change to a slight reduction in summer (between -3 and 1 mm). For runoff, the largest changes are observed during winter (between 47 and 54 mm). Fall and spring runoff changes less than winter (between 15 and 20 mm). There is a marginal increase in runoff over summer (between 1 and 3 mm). Infiltration increases moderately in fall and spring (between 14 and 22 mm), increases slightly in winter (between 3 and 8 mm), and decreases in summer (-5 mm). Recharge and seepage show similar seasonal changes. The greatest changes are in winter and spring (between 12 and 21 mm), while in fall there is a minor increase (8 mm). The only substantial seasonal

difference between recharge and seepage is during summer. The summer seepage increases marginally (between 3 and 4 mm), while recharge decreases marginally (between -2 and -3 mm). Annually, runoff increases the most (81 and 91 mm for the 2050s and 2080s, respectively). Infiltration, recharge, and seepage all increase moderately (between 28 and 47 mm). Evapotranspiration increases the least annually (9 and 23 mm for the 2050s and 2080s, respectively). Overall, the 2080s water balance components are higher than the 2050s components.

The cause of the overall increase in the water balance components is the increase in the precipitation; the only input into the system. As Figure 5.15 and Figure 5.16 clearly show, the increase in runoff is the most significant response in the system (particularly in winter). The increase in infiltration occurs during the fall and later spring months. Whereas in winter, when the precipitation increase is still high, there is no substantial increase in infiltration. The increases occur when the water table is generally below the ground surface, while in winter, the water table is generally at or near the ground surface. Thus, the excess precipitation that cannot infiltrate the ground surface occurs as saturated overland flow. The increase in seepage is directly linked to the increase in recharge. As more recharge occurs, the water table will intercept the ground surface more often. Thus, more seepage will occur.

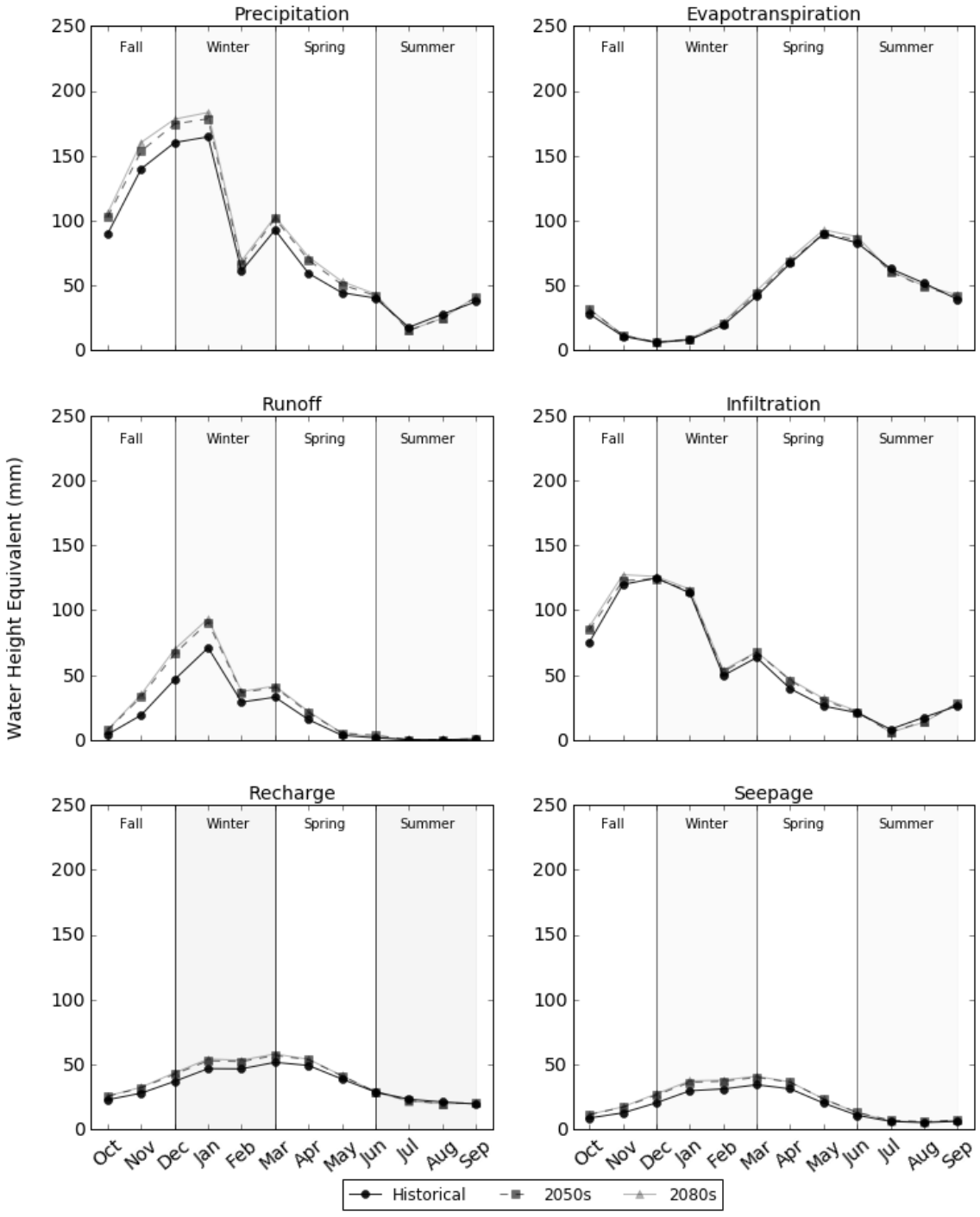

Figure 5.15 Global model water balance components under historical (2000-2009) and future (2050-2059 and 2080-2089) projected climate conditions.

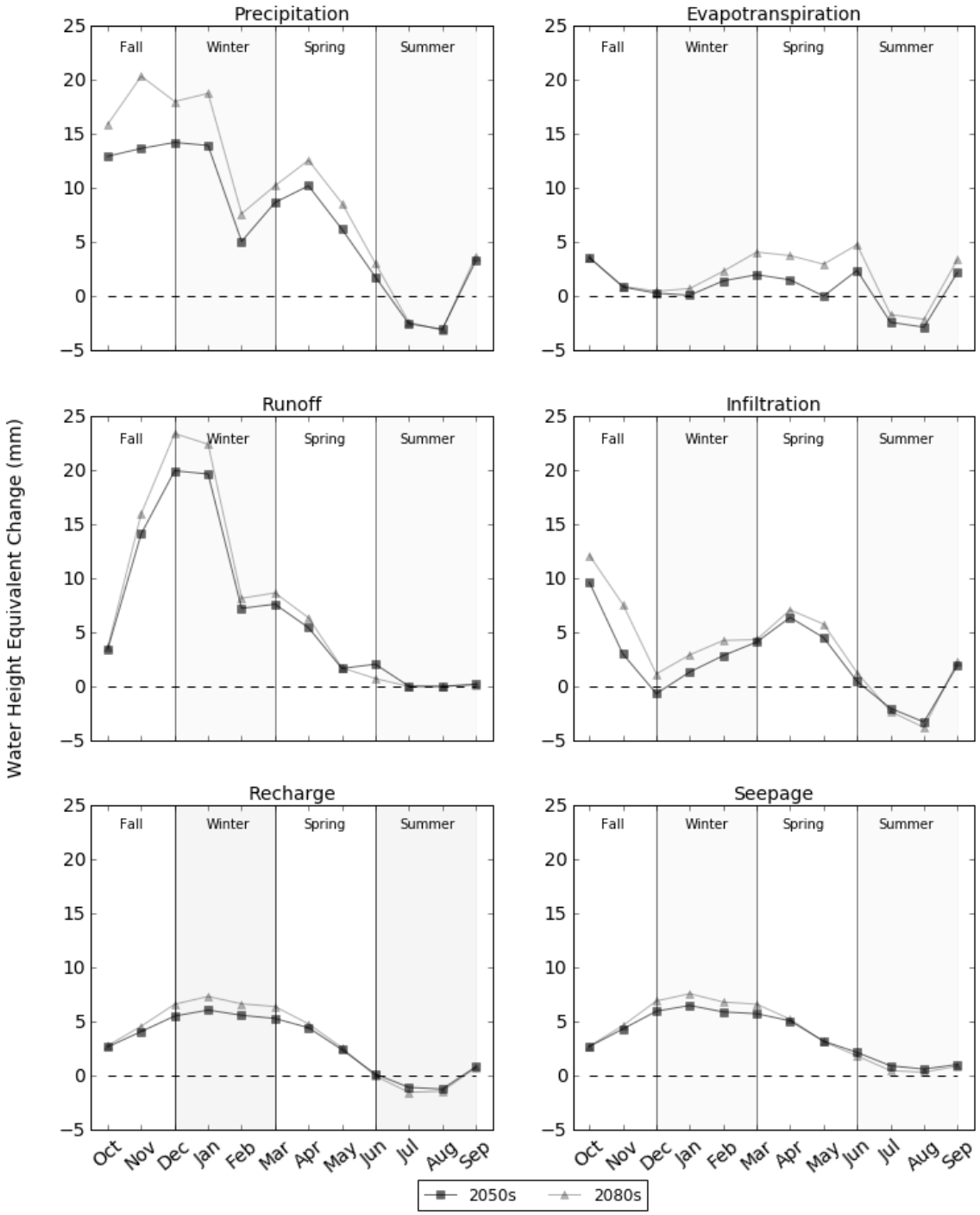

Figure 5.16 Global model water balance component monthly change from historical to future climate conditions.

The projected increase in future precipitation appears to result principally in an increase of runoff, and to a lesser extent recharge. The model results suggest the total average annual recharge will increase under future climate conditions. On an annual

basis, recharge during the 2050s will increase by 8%, and during the 2080s by 10%. The increase is primarily realised during winter to early spring. At other times of the year, the future monthly recharge is similar to the historical rates.

Projected future climate conditions affect the inter-annual variability of the rainfall-runoff-recharge dynamics. Figure 5.17 and Figure 5.18 display the same example WYs (a wet WY, an average WY, and a dry WY) as in Figure 5.14, but are shifted to show the future climate results. During wet WYs (2006/2007, 2056/2057, 2086/2087), the depth to the water table is approximately the same elevation, if only slightly higher in later time periods. However, since the water table is so close to the ground surface during historical climate conditions (Figure 5.14, WY 2006/2007), the slight increase in the position of the water table causes it to intercept the ground surface earlier in the year and also continue to intersect ground surface for longer. As a result, seepage occurs earlier and the amount of WY seepage increases.

During the average and dry WYs, the depth to the water table is between 1 to 2 m lower under future conditions. This results in the water table reaching the ground surface from approximately February to April, while under historical conditions the water table did not reach ground surface. There is still no seepage during the dry WY under future climate conditions. In addition to the water table rising, the peak is sustained for a longer period due to increased precipitation under the future climate conditions. Overall, under projected future climate conditions, the model results suggest the increase in precipitation will cause the water table to rise. This rise in water table will be most notable during the average and drier WYs when the there is more room for an increase in the water table positon. During wetter WYs, there is less of a noticeable increase in the water table positon. However, seepage will occur earlier in the year, and for a longer period.

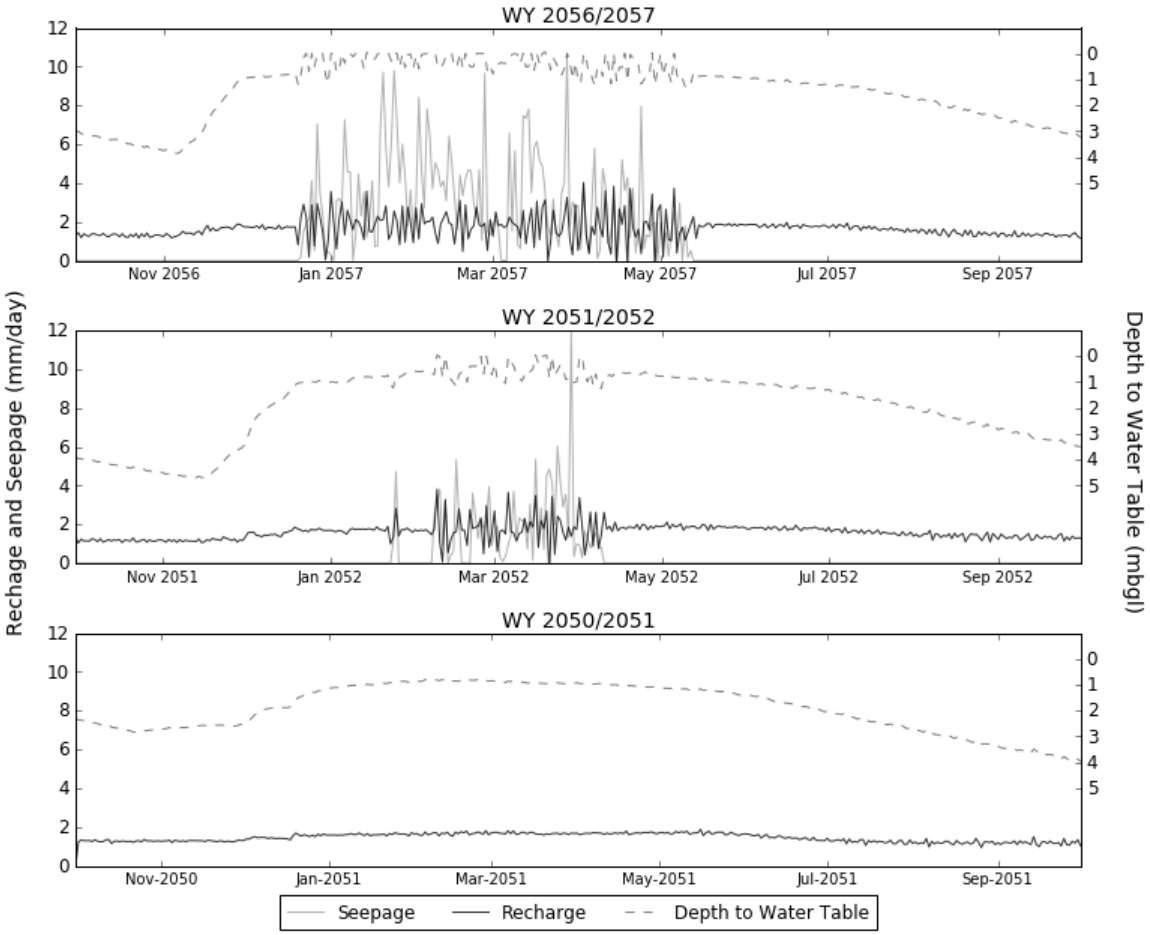

Figure 5.17 System response to 2050s climate in different total WY precipitation. The response of a variable area to different amounts of annual precipitation that falls in a WY. WY 2056/2057 represents a high precipitation WY (1280 mm), WY 2051/2052 an average WY (1001 mm), and WY 2050/2051 a low precipitation WY (841 mm).

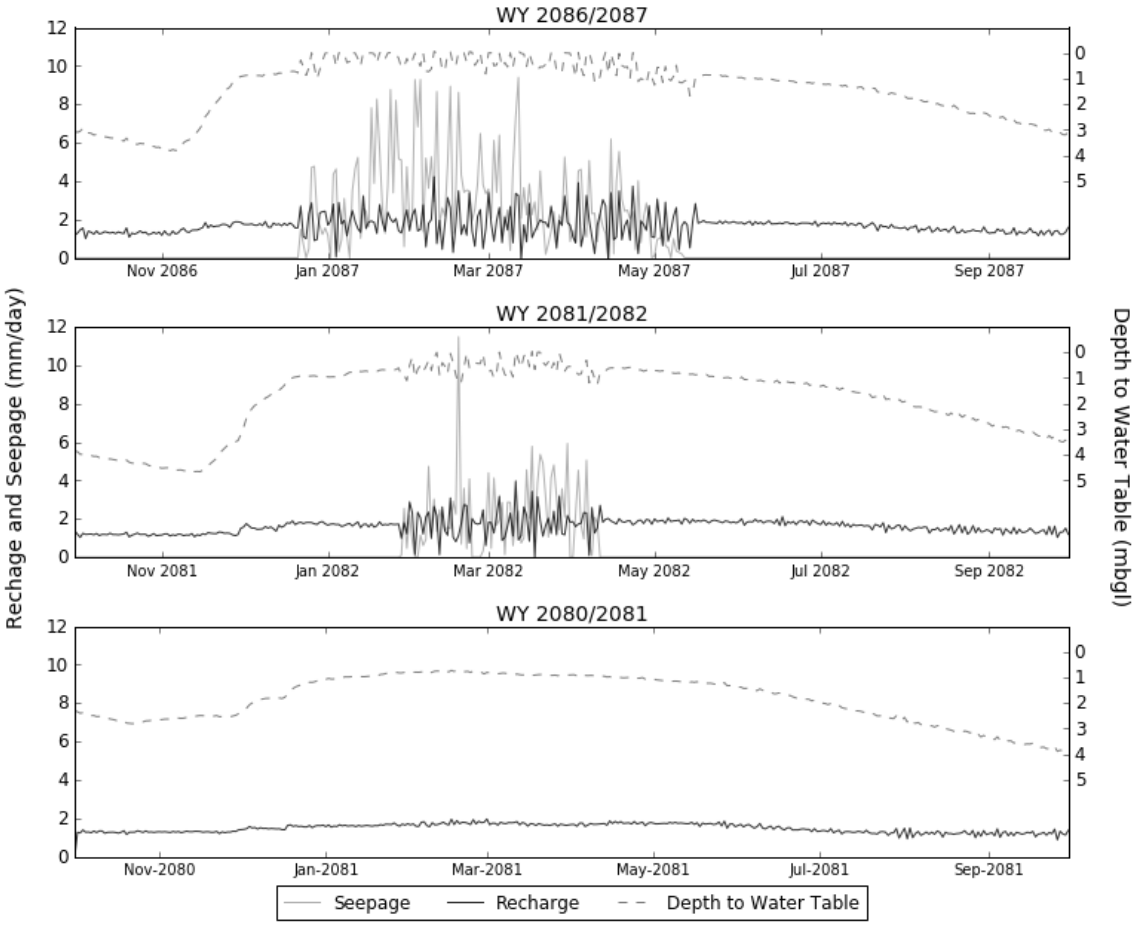

Figure 5.18 System response to 2080s climate in different total WY precipitation. The response of a variable area to different amounts of annual precipitation that falls in a WY. WY 2086/2087 represents a high precipitation WY (1316 mm), WY 2081/2082 an average WY (1029 mm), and WY 2080/2081 a low precipitation WY (865 mm).

The location of perennial seepage and recharge areas change little under future climate conditions. Figure 5.19 and Figure 5.20 present the spatial distribution of these areas on the island. Visually, the distribution of the areas is very similar that of historical conditions (Figure 5.6). The percentage of the island where perennial recharge occurs decreases slightly from 30% to 28%, while the perennial seepage areas increase from 4% to 5%. The percentage of the island that exhibits both recharge and seepage also increases, from 64 to 67%.

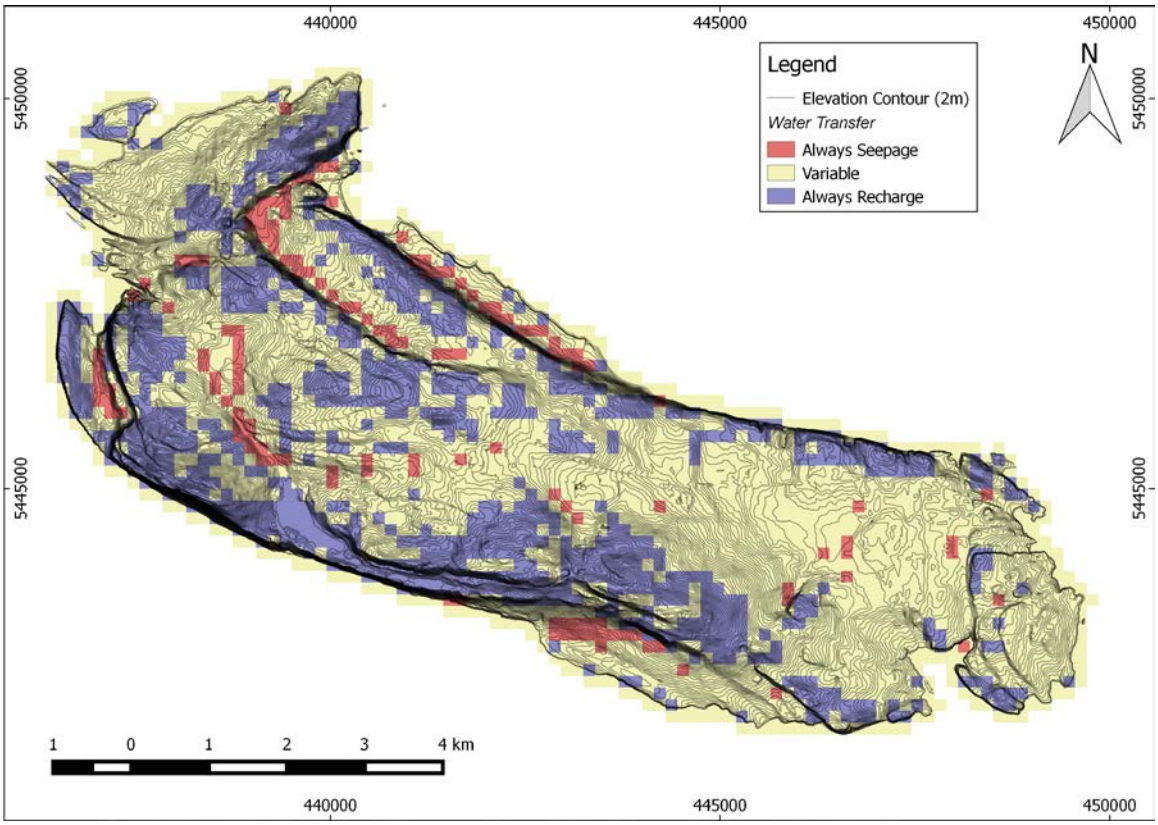

Figure 5.19 Water transfer direction during the 2050s simulation. The direction of water transfer is with respect to the SZ for every time step of the simulation. Cells displayed as 'always recharge' only have recharge occurring (UZ to SZ water transfer), while the opposite is true of cells displayed as 'always seepage'. Cells designated 'Variable' simulate both discharge and seepage at different time steps.

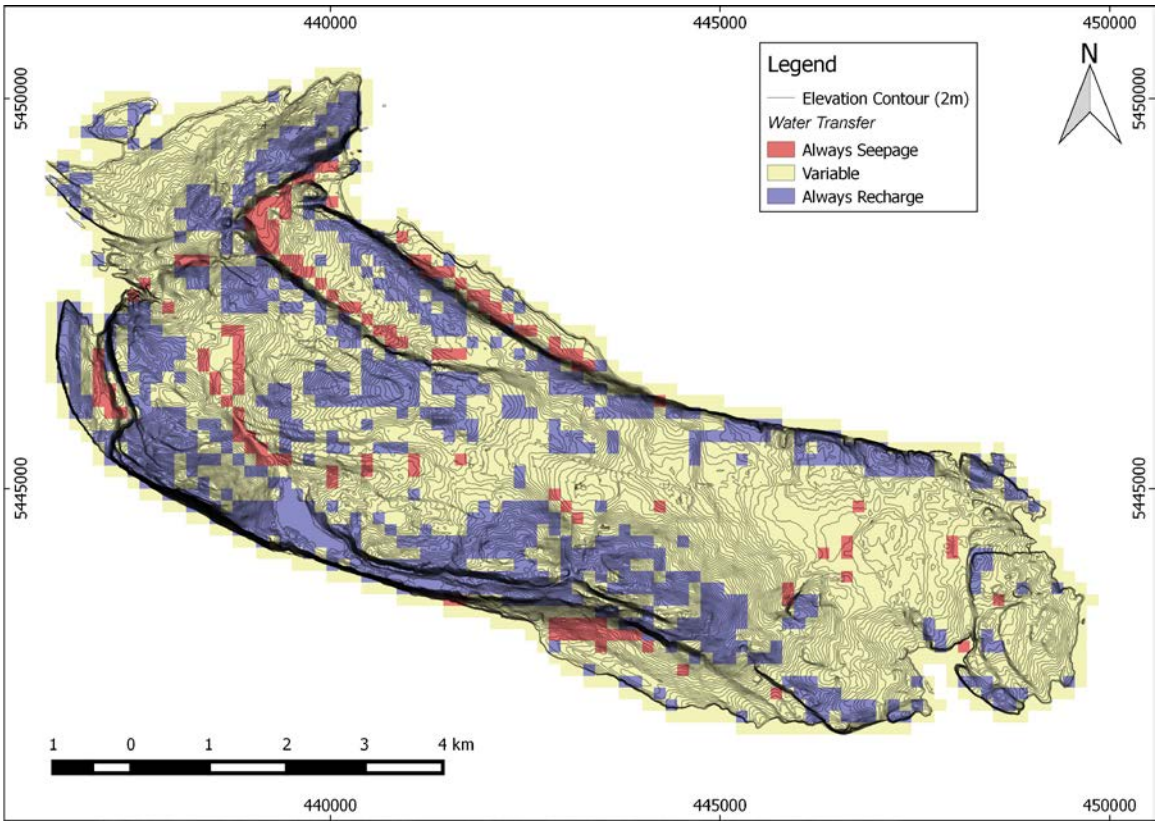

Figure 5.20 Water transfer direction during the 2080s simulation. The direction of water transfer is with respect to the SZ for every time step of the simulation. Cells displayed as 'always recharge' only have recharge occurring (UZ to SZ water transfer), while the opposite is true of cells displayed as 'always seepage'. Cells designated 'variable' simulate both discharge and seepage at different time steps.

5.5. Uncertainties and Limitations

While the integrated land surface - subsurface model was adequate to address the thesis research objectives, there are some uncertainties.

- Firstly, while input flux to the model is relatively well constrained (assuming spatially uniform precipitation), the output fluxes are not; in particular, the runoff and subsurface outflow to the coast. A lack of stream gauging causes uncertainty in the runoff flux, while the uncertain thickness of the coastal boundary zone leads to the poorly constrained coastal outflow flux.

- The coarse discretization of the model domain may not be ideally suited to the accurate development of seepage faces due to topographical variation not being represented adequately.

- Although generally extensive, the water balance of the UZ does not include a soil moisture term or differentiate between runoff generation types. This made it difficult to definitively identify the runoff generation mechanism.

- The future climate data set was obtained by apply shift factors to historic precipitation data. This does not account for the predicted increase in precipitation intensity in the future.

Chapter 6. Conclusions and Recommendations

6.1. Introduction

The main research objectives of this study were to: 1) characterize the physical parameters that control the spatial distribution of recharge to the fractured bedrock aquifer on Gabriola Island (BC); 2) determine the rainfall-runoff-recharge relationship that influences the seasonality of groundwater levels; and 3) estimate how climate change may influence recharge in a temperate climate setting. To meet these objectives, two tasks were completed. Firstly, evapotranspiration and relative groundwater age data were collected during a field investigation and used to calibrate the numerical model. Secondly, a coupled land surface - subsurface numerical model of Gabriola Island was developed and calibrated using the MIKE SHE code. Historical and predicted future climate conditions were simulated.

6.2. Characterizing Recharge

Recharge and seepage vary spatially across the island. Recharge generally occurs in areas of higher elevation, while seepage occurs in areas of both lower and steeper topography. The overall magnitude of recharge is much less during the summer compared to the other seasons as indicated by the near zero values over a larger portion of the island. Seepage during the summer is also somewhat lower compared to the other seasons. Seasonally persistent (perennial) recharge and seepage areas are also evident. The perennial seepage locations cover a minimal proportion of the island (4%), while areas of perennial recharge are more common (30%). However, the majority of the island exhibits both recharge and seepage flux (66%). On an average annual basis, the recharge is the dominant net flux (more recharge than seepage), with seepage flux dominated areas making up the remainder. In perennial seepage areas, the water table is consistently above the ground surface with the seepage flux relatively constant throughout an average water year (WY). In perennial recharge areas, the water table does not reach the ground surface, thus no seepage can occur. A seasonal response of the water table is exhibited in recharge areas. Over the majority of the island, where both seepage and recharge flux occur, the seasonal fluctuations and relatively shallow position of the water table cause seepage to occur in the wetter winter months as the rising water table intercepts the

ground surface. A sensitivity analysis of the model suggested that the hydraulic conductivity of the fractured bedrock and the thickness of the coastal discharge boundary were the dominant parameters that influence recharge and discharge.

6.3. Rainfall-Runoff-Recharge Dynamics

During the wettest season precipitation exceeds infiltration and a substantial increase in runoff is simulated. This increase in runoff is generated by the saturated overland flow process, where the water table has risen to the ground surface. As a result, excess precipitation occurs as runoff. The model results suggest both groundwater seepage and this excess precipitation combine to produce the seasonal increase in runoff. What proportion each of the runoff sources contributes is uncertain. Further, it is likely to be spatially variable. During summer, discharge from perennial seepage areas is the dominant source of runoff as the majority of precipitation can infiltrate the ground surface (due to the generally lower water table). There appears to be a lag time between the increase in infiltration and the increase in recharge. The increase in infiltration starts in August, while the recharge rate does not begin to increase until October, representing an approximate 2-month lag time. The lag time represents the time it takes to for the infiltration to travel vertically and reach the water table in the saturated zone (SZ). This is controlled by the presence of a thicker unsaturated zone (UZ) following summer, increasing the travel time of water infiltrating the ground surface to reach the water table. Recharge still occurs after periods where evapotranspiration from the (UZ) is equal to or exceeds infiltration (May and August), even considering the 2-month lag time. Limitations within UZ module of MIKE SHE precludes the elucidation of this process.

The model results suggest that the depth to the water table is the factor controlling the response of the water table to heavy rainfall events. During winter, when the water table is shallow, the water table is responsive to these events. However, the water table response appears to be influenced more by the cumulative rainfall than individual daily events. When the water table is deeper, as in summer, no response is observed. Infiltration closely matches the rainfall event amount during these periods of deeper water table depth, suggesting that the infiltration capacity of the soil is not exceeded in certain locations.

Inter-annual variability in precipitation can alter the recharge-seepage regime and the seasonal water table dynamics. The water table in an area that, under a normal WY is close, but not intercepting the ground surface, will, during a wetter WY, develop seepage during the high point of the seasonal water table. Conversely, during a drier WY, the same area will display a much shorter lived seasonal high water table before recession starts. Even after a low precipitation WY, the occurrence of an average precipitation WY returns the water table back to average conditions, suggesting some resilience to drought. However, the study did not consider the potential cumulative impact from successive dry WYs.

6.4. Future Recharge

Under future climate conditions, recharge and other components of the water balance experience variable changes compared to the historical climate conditions. Precipitation, evapotranspiration, runoff, infiltration, recharge, and seepage are all slightly higher on an average annual basis. However, the timing of these increases varies between individual water balance components. The fall, winter, and spring months are projected to experience the greatest increase in precipitation. An increase in runoff is the most significant response of this increase in precipitation (particularly in winter). This increase in runoff is due to a general rise in the average position of the water table at all times in the year. The water table will intercept the ground surface more often. Therefore, increasing the occurrence and amount of saturated overland flow. The higher water table, caused by recharge increasing, also increases groundwater seepage. During summer, all the water balance components experience either a reduction, or very little change.

Model results suggest that the increase in average position of the water table will extend the period of the seasonal high water table, i.e. the seasonal high will be sustained for longer, increasing seepage where the ground surface is intercepted. The location of perennial seepage and recharge areas change little under future climate conditions however. The percentage of the island where perennial recharge occurs decreases slightly, whereas perennial seepage increases slightly. The areas exhibiting both recharge and seepage also increase slightly in proportion.

Overall, the increase in precipitation under future projected climate will principally result in increased runoff, and to a lesser extent increased recharge. The model results suggest that recharge will increase by 8% in the 2050s and by 10% in the 2080s. The increase is primarily realised during winter to early spring. At other times of the year, the projected monthly recharge is similar to the historical rates. In general, there is little difference between the 2050s and 2080s model results.

6.5. Recommendations

The MIKE SHE model developed for Gabriola Island is a highly parametrized one. It was necessary to estimate numerous properties for data which were lacking. Specifically, the van Genuchten parameters of the fractured bedrock were not available from the literature, thus were highly uncertain. Further work could focus on attempting to estimate these from empirical experiments. The depth of the coastal groundwater discharge zone was also not well constrained. The model sensitivity analysis suggested that this part of the system had a significant influence on the model results. For example, decreasing the thickness of this boundary condition caused an increase in the general position of the water table, and vice versa. The hydraulic conductivity of the fractured bedrock was altered to maintain an acceptable model calibration as a consequence. Further investigation into this coastal zone would help alleviate some of the model uncertainty. Additionally, extra discharge observation data for model calibration would aid in reducing the uniqueness of the model. For example, winter stream flow gauging and estimates of coastal groundwater discharge would help in the calibration of the land surface and saturated zone modules, respectively.

While the study investigated inter-annual variability of precipitation on the groundwater level dynamics, it did not consider prolonged climate extremes (e.g. drought). For example, the cumulative effect of consecutive dry WYs could change the way system recovers.

Finally, this study did not consider the increase in rainfall intensity predicted by global climate models (GCMs). While the modelling results suggest that heavy rainfall events do not exceed the infiltration capacity of the soil, increases in precipitation intensity may change this. Thus, the rainfall-runoff-recharge dynamics may be altered as a result.

References

Abbott, M. D., Lini, A. and Bierman P. R., 2000. d18O, dD and 3H measurements constrain groundwater recharge patterns in an upland fractured bedrock aquifer, Vermont, USA, *J. Hydrol*., 228, 101–112.

Abbott, M. B., Bathurst, J. C., Cunge, J. A., O'Connell, P. E., and Rasmussen, J., 1986. An introduction to the European hydrological system — systeme hydrologique europeen, “SHE”, 2: Structure of a physically-based, distributed modelling system. Journal of Hydrology, 87(1–2), 61-77.

Ali, M., Abustan, I., Rahman, M., Haque, A., 2012. Sustainability of groundwater resources in the North-Eastern Region of Bangladesh. *Water Resources Management* 26 (3), 623–641.

Allen, S.L., 1990. Measurement and estimation of evaporation from soil under sparse barley crops in northern Syria. *Agricultural and Forest Meteorology*, 49 291-309

Allen, D.M. and Kirste, D., 2012. Results of the July 2011 Groundwater Chemistry Sampling Study on Mayne Island, British Columbia. Report prepared for the Mayne Island Integrated Water Systems Society. Simon Fraser University, Burnaby, BC, 39 pp.

Allen, D.M., Liteanu, E., Bishop, T.W., and Mackie, D.C., 2002. Determining the hydraulic properties of fractured bedrock aquifers of the Gulf Islands, B.C. Final report. Department of Earth Sciences, Simon Fraser University. Submitted to Al Kohut, BC Ministry Water, Land and Air Protection.

Allen, D.M. and Matsuo, G.P., 2001. Results of the Groundwater Geochemistry Study on Hornby Island, British Columbia. Report prepared for the Islands Trust, Victoria, B.C., 119 pp.

Allen, D.M. and Suchy, M. 2001. Results of the groundwater geochemistry study on Saturna Island, British Columbia. Report submitted to the Island Trust, Victoria, B.C., 127 pp.

Allen, D.M., Whitfield, P.H., and Werner, A. 2010. Groundwater level responses in temperate mountainous terrain: regime classification, and linkages to climate and streamflow. *Hydrological Processes, 24*, 3392-2412.

Allison, G.B., 1987, A review of some of the physical, chemical, and isotopic techniques available for estimating groundwater recharge, in Simmers, I. ed., Estimation of Natural Groundwater Recharge: Proceedings of the NATO Advanced Research Workshop on Estimation of Natural Recharge of Groundwater (with special reference to Arid and Semi-Arid Regions), Antalya, Side, Turkey, March 8-15, 1987, Springer, p. 49–72.

Appaih-Adjei, E.K. 2006. *Climate change impacts on groundwater recharge in Gulf Islands, Canada* (Master dissertation). Lund University, Lund, Sweden.

Anderson, P., Woessner, W. W., Hunt, R. 2015. *Applied Groundwater Modeling: Simulation of Flow and Advective Transport.* San Diego, CA: Academic Press

Barlow, P. M., and Reichard E. G., 2010. Saltwater intrusion in coastal regions of North America, *Hydrogeol. J.*, 18, 247–260

Bates, B., Kundzewicz, Z.W., Wu, S., Palutikof, J.P., 2008. Climate Change and Water. Technical Paper VI of the Intergovernmental Panel on Climate Change. Intergovernmental Panel on Climate Change Secretariat, Geneva, 210 pp.

Beigi, E. and Tsai, F.T.C, 2015. Comparative study of climate-change scenarios on groundwater recharge, southwestern Mississippi and southeastern Louisiana, USA. *Hydrogeology Journal*. 23 (4). 789-806.

Black, T.A., 1979. Evapotranspiration from Douglas Fir stands exposed to soil water deficits. *Water Resources Research.* 15 (1)

B.C. Ministry of Energy and Mines 2005, Geofile 2005-3, by N.W.D. Massey, D.G. MacIntyre, P.J. Desjardins and R.T. Cooney.

Burbey T.J., Hisz D., Murdoch L.C., Zhang M., 2012. Quantifying fractured crystalline-rock properties using well tests, earth tides and barometric effects. *J Hydrol* 414–415:317–32

Cannon, A. J., 2008. Probabilistic multi-site precipitation downscaling by an expanded Bernoulli-gamma density network, *J. Hydrometerol*, 9(6), 1284–1300.

Carlsson H., Carlsson L., Jamtlid A., Nordlander H., Olsson O., Olsson T., 1983. Cross-hole techniques in a deep seated rock mass. Bull Int Assoc Eng Geol 26, pp. 377–384.

Carter, T.R., E.L. La Rovere, R.N. Jones, R. Leemans, L.O. Mearns, N. Nakićenović, A.B. Pittock, S.M. Semenov, and J. Skea. 2001: Developing and applying scenarios. In: Climate Change 2001: Impacts, Adaptation, and Vulnerability. Contribution of Working Group II to the Third Assessment Report of the Intergovernmental Panel on Climate Change [McCarthy, J.J., O.F. Canziani, N.A. Leary, D.J. Dokken, and K.S. White (eds)]. Cambridge University Press, Cambridge and New York, pp. 145-190

Cartwright I. and Morgenstern U., 2012. Constraining groundwater recharge and the rate of geochemical processes using tritium and major ion geochemistry: Ovens Catchment, southeast Australia. *Journal of Hydrology*, 275, 137-149.

Chesnaux, R., Allen, D.M., and Jenni, S., 2009. Regional fracture network permeability using outcrop scale measurements. *Engineering Geology*, 108, 259-271.

Chesnaux, R., 2013. Regional recharge assessment in the crystalline bedrock aquifer of the Kenogami Uplands, Canada. *Hydrological Sciences*. 58 (2), 421-436

Chiew, F. H. S., and McMahon, T. A. 1991. The appiciability of Morton's and Penman's evapotranspiration estimates in rainfall-runoff modeling. *Water Resources Bulletin, AWRA, August 2001.* 27, No. 4.

Clague, J.J.1983. Glacio-isostatic effects of the Cordilleran ice sheet, British Columbia. In: Shorelines and Isostacy, eds. D.E Smith and A.G. Dawson. London: Academic Press.

Clark, I., Fritz, P., 1997. Environmental Isotopes in Hydrogeology. Lewis Publishers, Florida. 328 pp.

Cook, P.G., Solomon, D.K., Sanford, W.E., Busenberg, E., Plummer, L.N. and Poreda, R.J., 1996. Inferring shallow groundwater flow in saprolite and fractured rock using environmental tracers. *Water Resour. Res*., 32: 1501-1509.

Cranfield University Silsoe, 2002 . AWSET (Version 3.0)

Crosbie, R.S., Jolly, I.D., Leaney, F.W., Petheram, C., 2010. Can the dataset of field based recharge estimates in Australia be used to predict recharge in data-poor areas? *Hydrol Earth Syst Sci* 14. 2023–2038

Currell, M., Carwright, I., Bradley, D. and Han, D., 2010. Recharge history and controls on groundwater quality in the Yuncheng Basin, north China. *Journal of Hydrology*. 385, 216-229.

Daamen, C.C., Simmonds, L.P., Wallace, J.J., Laryea, K.B., and Sivakumar, M.V.K, 1993. Use of microlysmeters to measure evaporation from sandy soils. *Agricultural and Forest Meteorology*, 65 159-173

Dakin, R.A., Farvolden, R.N., Cherry, J.A., and Fritz, P., 1983, Origin of dissolved solids in groundwaters of Mayne Island, British Columbia, Canada: *Journal of Hydrology*, v. 63, p. 233–270,

DHI. (2007). MIKE SHE User Manual, Volume 2: Reference Guide, Danish Hydraulic Institute: Denmark.

Denny, S., Allen, D.M. and Journeay, M. 2007. Drastic-Fm: a modified vulnerability mapping method for structurally controlled aquifers in the southern Gulf Islands, British Columbia, Canada. *Hydrogeology Journal, 15*, 483-493.

Earle S. and E. Krogh. 2004. Geochemistry of Gabriola's groundwater, Shale: Journal of the Gabriola, Historical & Museum Society, No. 7, Jan 2004

EBA. 2011. Geohazard Report and Mapping, Gabriola Island, BC. Report to Islands Trust.

England T.D.J. 1989. Late Cretaceous to Paleogene evolution of the Georgia Basin, Southwestern British Columbia, Ph.D. thesis, Memorial University of Newfoundland.

Environment Canada. 2015. *Station Results – 1981-2010 Climate Normals and Averages on Gabriola Island*. Retrieved from http://climate.weather.gc.ca/climate_normals/results_1981_2010_e.html?stnID=172&lang=e&StationName=gabriola&SearchType=Contains&stnNameSubmit=go&dCode=4&dispBack=1 (March, 2015)

Ferguson, G., and Gleeson, T. 2012. Vulnerability of coastal aquifers to groundwater use and climate change. *Nature Climate Change, 2(5)*, 342-345.

Fernandes, R., Korolevych, V., and Wang, S. 2007. Trends in Land Evapotranspiration over Canada for the Period 1960–2000 Based on In Situ Climate Observations and a Land Surface Model. *J. of Hydrometeorology*. 18.

Fitzsimons V.P. and Misstear B.D.R., 2006. Estimating groundwater recharge through tills: a sensitivity analysis of soil moisture budgets and till properties in Ireland. *Hydrogeology Journal* 14: 548-561.

FLNRO, 2011. Baseline Thematic Mapping Present Land Use Version 1 Spatial Layer. Published by Ministry of Forests, Lands and Natural Resource Operations (FLNRO).

Foweraker, J.C. (1974). Groundwater investigations on Mayne Island. Report no.1. Evaluation, development and management of the groundwater resource on Mayne Island. Department of Lands, Forests, and Water Resources. File 02329013.

Foster S., 2014. *Characterizing groundwater – surface water interactions within a mountain to ocean watershed, Lake Cowichan, British Columbia.* M.Sc. Thesis. (Masters Thesis). Simon Fraser University, BC, Canada

Freeze, R.A., Cherry, J.A., 1979. Groundwater. Prentice-Hall Inc., Eaglewood Cliffs, NJ. 604 pp.

Freeze, A. R. and Harlan L. R., 1969. Blueprint for a physically-based, digitally-simulated hydrologic response model. *J. Hyrology*, 9 , 237-258.

Gao, G., Xu, C., Chen, D., and Singh, V.P., 2012. Spatial and temporal characteristics of actual evapotranspiration over Haihe River basin in China. *Stoch Environ Res Risk Assess* 26:655-669

Gay, C.B. and Edmunds, W.M., 1996. Groundwater recharge estimation using chloride, stable isotopes and tritium profiles in the sands of northwest Senegal. *Environemtnal Geology*, 27, 246-251.

Gee, G.W. Wierenga, P.J., Andraski, B.J., Young, M.H., Fayer, M.J., and Rockhold, M.L., 1994. Variations in water balance and recharge potential at three western desert sites. *Soil Sci. Soc. Am. J*., 58: 63-71.

Gleeson, T., Novakowski, K., and Kyser, K.T., 2009. Extremely rapid and localized recharge to fractured rock aquifer. *Journal of Hydrology*, *376*, 496-509.

Gleeson, T., Smith, L., Moosdorf, N., Hartmann, J., Dürr, H.H., Manning, A.H., van Beek, L.P.H., Jellinek, A.M., 2011. Mapping permeability over the surface of the Earth. Geophys. Res. Lett. 38

Green, T. M. Taniguchi, H. Kooi, J. Gurdak, K. Hiscock, D. Allen, H. Treidel, A. Aureli. 2011. Beneath the surface of global change: Impacts of climate change on groundwater. *Journal of Hydrology*, *405*: 532-560.

Harte, P.T., Winter, T.C., 1996. Factors affecting recharge to crystalline rock in the Mirror Lake Area, Grafton County, New Hampshire. In: U.S.G.S. Toxic Substances Hydrology Program – Proceedings of the Technical Meeting, Colorado Springs, Colorado, September 20–24, 1993, Water-Resources Investigations Report 94- 4015.

Healy, R., and Scanlon, B.R. 2010. Estimating Groundwater Recharge: Cambridge University Press, New York, NY.

Heppner, C. S., Nimmo, J. R., Folmar, G. J., Gburek, W. J. and Risser, D. W., 2007. Multiple-methods investigation of recharge at a humid-regionfractured rock site, Pennsylvania, USA, *Hydrogeol. J.,* 15, 915–927.

Hodge, W.S. 1977. A preliminary geohydrological study of Saltspring Island. Groundwater Section, Hydrology Division, Water Investigations Branch, BC Ministry of Environment.

Hodge, W.S. 1995. Groundwater conditions on Saltspring Island. Groundwater Section, Hydrology Branch, Water Management Division, Ministry of Environment, Land and Parks

Holding, S., Allen, D.M., Foster, S., Hsieh, A., Larocque, I., Klassen, J., Van Pelt, S.C., 2016. Groundwater vulnerability on small islands. *Natrue Climate Change*, 6. 1100-1103

Jaber, F. H. and S. Shukla 2012. MIKE SHE: model use, calibration, and validation. ASABE Transactions 55 (4): 1479-188.

Jasechko, S., Birks, S. J., Gleeson, T., Wada, Y., Fawcett, P. J., Sharp, Z. D., McDonnell, J. J. and Welker J. M. 2014. The pronounced seasonality of global groundwater recharge. *Water Resour. Res*., 50, 8845–8867

Jiang, X.W., Wang, X.S., and Wan, L., 2010. Semi-empirical equations for the systematic decrease in permeability with depth in porous and fractured media. *Hydrogeology Journal.* 18(4): p. 839-850.

Journeay, J.M. and Morrison, J. 1999. Field investigation of Cenozoic structures in the northern Cascadia forearc, southwestern British Columbia. *In* Current Research 1999-A, Geological Survey of Canada, Ottawa, ON, pp.239-250.

IAEA/WMO, 2015. Global Network of Isotopes in Precipitation. The GNIP Database. Accessible at: http://www.iaea.org/water

Kazemi, G. A., Lehr, J. H., and Perrochet, P. 2006. *Groundwater age*. Wiley-Interscience.

Kenney, A.E. and van Vliet, L.J.P. 1986. “Gabriola Island (Interim) Soil Inventory. BC Ministry of Environment, Land Resource Unit.

Kinama, J.M.; Stigter, C.J.; Ong, C.K.; Ng'ang'a, J.K.; and Gichuki, F.N., 2005. Evaporation from soils below sparse crops in contour hedgerow agroforestry in semi-arid Kenya. *Agricultural and Forest Meteorology* 130:149-162.

Larocque, I. 2014. *Hydrogeology of Salt Spring Island, British Columbia* (Master thesis). Simon Fraser University, Canada.

Leij, F. J. 1996. The UNSODA unsaturated soil hydraulic database: User's manual. Cincinnati, Ohio: National Risk Management Research Laboratory, Office of Research and Development, U.S. Environmental Protection Agency. Retrieved from http://hdl.handle.net/2027/mdp.39015050283400

Ligget, J.E. and Allen, D.A.. 2010. Comparing approaches for modeling spatially distributed direct recharge in a semi-arid region (Okanagan Basin, Canada). *Hydrogeology Journal, 18*, 339-357.

Liteanu, E. 2003. *The role of aquifer heterogeneity in saltwater intrusion modeling, Saturna Island, BC, Canada* (Masters dissertation). Simon Fraser University, Vancouver, Canada.

Liu, J., Chen, J. M., Cihlar, J., 2003. Mapping evapotranspiration based on remote sensing: An application to Canada’s landmass. *Water Resources Research*. Vol. 39, No. 7.

Lu, N. and Godt, J., 2013. *Hillslope Hydrology and Stability*. Cambridge university press

Luoma, S., Okkonen, J., 2014. Impacts of future climate change and Baltic Sea level rise on groundwater recharge, groundwater levels, and surface leakage in the Hanko Aquifer in southern Finland. *Water* 6:3671–3700

Mackie, D.C. 2002. *An integrated structural and hydrogeologic investigation of the fracture system in the upper Cretaceous Nanaimo Group, southern Gulf Islands, British Columbia* (Masters thesis). Simon Fraser University, Vancouver, Canada.

Mays, G., 2013. Groundwater resources sustainability: past, present, and future. *Water Resources Management, 27*(13), 4409-4424.

Meidinger, D. V., and Pojar, J. (1991). Ecosystems of British Columbia. Special report series, B.C. Ministry of Forests.

Metcalf, M. and Robbins, G., 2014. Evaluating groundwater sustainability for fractured crystalline bedrock. *Water Science and Technology: Water Supply*, 14, 127-134.

Meixner T., Manning A.H., Stonestrom D.A., Allen D.M., Ajami H., Blasch K.W., Brookfield A.E., Castro C.L., Clark J.F., Gochis D.J., Flint A.L., Neff K.L., Niraula R., Rodell M., Scanlon B.R., Singha K., Walvoord M.A., 2016. Implications of projected climate change for groundwater recharge in the western United States. *J Hydrol* 534, 124–138

MoE, 2015a. Ministry of Environment (MoE), province of British Columbia, British Columbia Soil Mapping Spatial Data (a compilation of digital soil mapping datasets). Data available from the British Columbia Ministry of Environment, Ecosystem Information Section at: http://www.env.gov.bc.ca/esd/distdata/ecosystems/Soil_Data/SOIL_DATA_FGDB/ [Accessed September 14th, 2015]

MoE, 2015b. Ministry of Environment (MoE), province of British Columbia, British Columbia WELLS Database. Water Stewardship Division, BC. Retrieved from http://www.env.gov.bc.ca/wsd/data_searches/wells/ (August, 2015)

Monteith, J. L. 1965. Evaporation and environment" *Symposia of the Society for Experimental Biology* 19: 205–224

Mustard, P.S. 1994. The upper Cretaceous Nanaimo Group, Georgia Basin. *Geology and geological hazard of the Vancouver region, southwestern British Columbia*, bulletin 481, 27-95.

Niazi, A,, Bentley, L.R., and Hayashi, M., 2017. Estimation of spatial distribution of groundwater recharge from stream baseflow and groundwater chloride. *J. Hydrol.*. 546. 380-392.

Nuszdorfer, F.C., Klinka, K., Demarachi, D.A. (1991). Ecosystems of British Columbia. Special report series, Chapter 5, B.C. Ministry of Forests.

Oda, M., 1986. An equivalent continuum model for coupled stress and fluid flow analysis in jointed rock masses. *Water Res* 22, pp. 1845–1856.

Pacific Climate Impacts Consortium (PCIC). (2016). *Regional analysis tool*. Retrieved from http://www.pacificclimate.org/analysis-tools/regional-analysis-tool, January, 2016.

Penman, H. L. (1948). Natural evaporation from open water, bare soil and grass. Proceedings of the Royal Society of London. Series A, Mathematical and Physical Sciences, 193(1032), 120-145.

Plauborg, F., 1995. Evaporation from bare soil in a temperate humid climate - measurement using micro-lysimeters and time domain reflectometry. *Agricultural and Forest Meteorology* 76 1-17

Praamsma, T., Novakowski, K., Kyser, K., and Hall K., 2009. Using stable isotopes and hydraulic head data to investigate groundwater recharge and discharge in a fractured rock aquifer, *J. Hydrol*., 366, 35–45.

Prych, E. A., 1998. Using chloride and chlorine-36 as soil-water tracers to estimate deep percolation at selected locations on the U.S. Department of Energy Hanford Site, Washington, *U.S. Geol. Surv. Water Supply Pap*., 2481, 67 pp.

Rathay S., 2016. *Response of a fractured bedrock aquifer to recharge from heavy rainfall events.* M.Sc. Thesis. (Masters Thesis). Simon Fraser University, BC, Canada.

Rohde, M.M., Edmunds, W.M., Freyberg, D., Sharma, O.P., Sharma, A., 2015. Estimating aquifer recharge in fractured hard rock: analysis of the methodological challenges and application to obtain a water balance (Jaisamand Lake Basin, India). *Hydrogeol J*. 23, 1573

Rivard, C., Paniconi, C., Vigneault, H. and Chaumont, D. 2014. A watershed-scale study of climate change impacts on groundwater recharge (Annapolis Valley, Nova Scotia, Canada). *Hydrological Sciences Journal*, 59 (8), 1437-1456.

Rutqvist, J., Tsang, C.-F. and Stephansson O., 1998. Determination of fracture storativity in hard rocks using high pressure testing. *Water Resources Research* 34: 2551–2560.

Rwasoka, D.T., Gumindoga, W., and Gwenzi, J., 2011. Estimation of actual evapotranspiration using the Surface Energy Balance System (SEBS) algorithm in the Upper Manyame catchment in Zimbabwe. *Physics and Chemistry of the Earth*, Parts A/B/C 36:736-746.

Salve, R., Ghezzehei, T.A., Jones, R., 2008. Infiltration into fractured bedrock. *Water Resources Research* 44, W01434.

Sanford, W. 2011. Calibration of models using groundwater age. *Hydrogeology Journal*, *19*(1), 13-16.

Scanlon, B., Healy, R., Cook, P., 2002. Choosing appropriate techniques for quantifying groundwater recharge. *Hydrogeology Journal* 10 (1), 18–39.

Scibek, J., Mackie, D., Sivak, T., and Petersmeyer, C.W., 2013. Regional district of Nanaimo Water Budget Project, Gabriola, DeCourcy, and Mudge Islands - Phase 1: Hydrogeological conceptual model and water budget. SRK consulting & Thurber Engineering Ltd. Submitted to Regional District of Nanaimo.

Shamir, E., Megdal, S.B., Carrillo, C., Castro, C.L., Chang, H.-I., Chief, K., Corkhill, F.E., Eden, S., Georgakakos, K.P., Nelson, K.M., Prietto, J., 2015. Climate change and water resources management in the upper Santa Cruz River, Arizona. *J. Hydrol*., 521. 18–33.

Singh, A., 2011.Estimating long-term regional groundwater recharge for the evaluation of potential solution alternatives to waterlogging and salinization. *J. Hydrol.*, 406. 245–255

Smerdon, B.D., Allen, D.M., Grasby, S.E. and Berg, M.A. 2009. An approach for predicting groundwater recharge in mountainous watersheds. *Journal of Hydrology, 365*, 156-172.

Snow, D. T., 1968. Rock fracture spacings, openings, and porosities. *J Soil Mech found Div* ASCE. 96.

Solomon, D.K., Cook, P.G., 2000. 3H and 3He. Environmental Tracers in Subsurface Hydrology. Kluwer Academic Publishers, 397-424 pp.

Sophocleous, M, 2002. Interactions between groundwater and surface water: the state of the science, *Hydrogeol. J.*, 10, 52–67

Sophocleous, M., 2004. Climate change: why should water professionals care? *Ground Water* 42 (5), 637.

Spittlehouse, D. L. and Black, T. A. 1979. Determination of Forest Evapotranspiration Using Bowen Ratio and Eddy Correlation Measurements, *J of Applied Meteorology and Climatology*. 18.

Statistics Canada. (2015). *Population and dwelling counts for Canada, provinces and territories, and designated places, 2011 and 2006 censuses*. Retrieved from http://www12.statcan.gc.ca/census-recensement/2011/dp-pd/hlt-fst/pd-pl/TableTableau.cfm?LANG=Eng&T=1302&SR=1&S=51&O=A&RPP=9999&PR=59&CMA=0 (March, 2015)

Surrette, M., Allen, D.M. and Journeay, M. 2008. Regional evaluation of hydraulic properties in variably fractured rock using a hydrostructural domain approach. *Hydrogeology Journal, 16(1)*, 11-30.

Taylor, R.G., Scanlon, B., Doll, P., Rodell, M., van Beek, R., Wada, Y., Longuevergen, L., Leblanc, M., Famiglietti, J.S., Edmunds, M., Konikow, L., Green, T.R., Chen, J., Taniguchi, M., Bierkens, M.F.P., MacDonald, A., Fan, Y., Maxwell, R.M., Yechieli, Y., Gurdak, J.J., Allen, D.M., Shamsudduha, M., Hiscock, K., Yeh, P.J.F., Holman, I., and Treidel, H. 2012. Ground water and climate change. *Nature Clim. Change*. 3. Pp 322 – 329.

Thomas, S.C. and Winner, W.E. 2000. Leaf area index of an old-growth Douglas-fir forest estimated from direct structural measurements in the canopy. Can. J. For. Res. 30: 1922–1930

Todd, RW; Klocke, N.L.; Hergert, G.W., and Parkhurst, A.M., 1991. Evaporation from soil influenced by crop shading, crop residue, and wetting regime. *Transactions of the ASAE* 34: 461-466.

Toews, M.W. and Allen, D.M., 2009. Evaluating Different GCMs for Predicting Spatial Recharge in an Irrigated Arid Region. *Journal of Hydrology*, 374: 265-281

Tóth, J., 1963. A theoretical analysis of groundwater flow in small drainage basins. *J. Geophys. Res*., 68, 16, 4795-4812.

Trapp, A. 2011. *Constraining a density-dependent groundwater flow model using multiple calibration time periods* (Masters dissertation). Universität Stuttgart, Stuttgart, Germany.

Tribble, G., 2008. Ground water on tropical Pacific Islands--understanding a vital resource: U.S. Geological Survey Circular 1312, 35 p. [http://pubs.usgs.gov/circ/1312/] (Accessed May 2015).

Trofymow, J. A., Porter, G. L., Blackwell, B. A., Arksey, R., Marshall, V., & Pollard, D. (1997). Chronosequences for research into the effects of converting coastal British Columbia old-growth forests to managed forests: an establishment report (Inf. Rep. BC-X-374). Victoria, B.C., Canada: Natural Resources Canada, Canadian Forest Service, Pacific Forest Centre

United States Department of Agriculture (USDA) (1986). Urban hydrology for small watersheds. Technical release 55 (TR-55). June, 1986. Table 3-1.

Voeckler, H. M., Allen, D. M., and Alila, Y., 2014. Modeling coupled surface water – groundwater processes in a small mountainous headwater catchment. *Journal of Hydrology*, 517(0), 1089-1106.

Wada, Y., Wisser, D., and Bierkens M.F.P., 2014, Global modeling of withdrawal, allocation and consumptive use of surface water and groundwater resources, *Earth Syst. Dyn*., 5(1), 15–40

Warner, S.D., 2007. Climate change, sustainability, and ground water remediation:the connection. *Ground Water Monit. Remed*. 27 (4), 50–52.

Wei, Z. Q., Egger, P., Descoeudres, F., 1995. Permeability predictions for jointed rock masses. *Int J Rock Mech Min Sci Geomech* 3,. pp.251–261.

Welch, L.A. and Allen, D.M., 2012. Consistency of Groundwater Flow Patterns in Mountainous Topography: Implications for Valley-Bottom Water Replenishment and for Defining Hydrogeological Boundaries. *Water Resources Research,* 48.

Welyk T.J. and Baldwyn J., 1994. Gabriola, Valdez, Thetis and Kuper Islands, Well Allocation Plan, March 1994, Regional Water Management, Vancouver Island Region, Nanaimo BC

Werner, A.D., Bakker, M., Post, V.E.A., Vandenbohede, A., Lu, C., Ataie-Ashtiani, B., Simmons, C.T., Barry, D.A., 2013. Seawater intrusion processes, investigation and management: recent advances and future challenges. *Adv Water Res.* 51. 3–26

Xu, C. and Singh, V.P., 2005. Evaluation of three complementary relationship evapotranspiration models by water balance approach to estimate actual regional evapotranspiration in different climatic regions. *Journal of Hydrology* 308:105-121.

Zhang, L., Hickel, K., Dawes, W.R., Chiew, F. H. F., Wester, A. W., and Briggs, P. R., 2004. A rational function approach for estimating mean annual evapotranspiration. *Water Resources Research.* Vol 40, Issue 2.

Appendix: Water Sample Chemical Analysis Results[1]

Sample ID	Water Type	Easting[2]	Northing	Approx. Depth (mbgl)	Alkalinity as $CaCO_3$ (mg/L)	Tritium (TU)	Tritium Error (TU)	**Al[3]**	**As**	**B**	**Ba**	**Ca**	Fe
CC1	Creek	440303	5447220	N/A	166.7	2.9	0.12	0.009	0.006	0.075	0.008	13.435	0.206
CC2	Creek	439599	5448945	N/A	212.1	2.88	0.17	0.008	0.006	0.057	0.011	28.394	0.005
CC3	Groundwater	440942	5448319	60.96	344.2	1.31	0.05	33.328	0.001	2.248	0.032	4.207	0.326
CC4	Groundwater	440462	5449714	83.82	338.3	2.07	0.08	7.377	0.002	2.855	0.010	11.631	0.050
CC5	Groundwater	439755	5448403	60.96	355.8	1.45	0.08	4.323	0.002	2.449	0.142	22.678	0.050
CM1	Swamp	440872	5444583	N/A	73.8	N/A	N/A	0.045	0.005	0.027	0.000	5.975	0.238
DB1	Creek	448136	5444896	N/A	291.7	N/A	N/A	0.017	0.007	0.213	0.004	14.398	0.027
GH1	Creek	438720	5446255	N/A	162.9	3.15	0.16	0.191	0.005	0.064	0.009	15.688	3.213
GH2	Groundwater	438624	5446499	42.672	222.1	2.74	0.11	0.085	0.003	0.117	0.001	7.845	0.174
HS1	Swamp	440614	5443949	N/A	149.6	3.09	0.1	0.013	0.003	0.032	0.006	14.685	0.222

[1] Table continues onto next page.

[2] Coordinate projection is UTM 10.

[3] The units of the results are mg/L unless otherwise stated.

Sample ID	K	Li	Mg	Mn	Mo	Na	S	Si	Sr	Zn	F	Cl	Br	NO3	PO43	SO4
CC1	1.999	0.003	3.003	0.000	0.000	26.135	7.778	9.288	0.056	0.005	0.110	11.229	0.089	1.170	N/A	6.104
CC2	1.965	0.002	9.271	0.000	0.000	18.533	11.450	5.834	0.139	0.003	0.127	21.492	0.219	3.969	N/A	8.777
CC3	0.547	0.012	0.508	0.079	0.000	88.974	9.917	11.026	0.053	0.017	0.223	20.346	0.042	0.256	N/A	14.980
CC4	0.711	0.009	5.389	0.019	0.001	81.190	15.054	8.964	0.085	0.032	0.497	31.433	0.167	0.879	N/A	20.537
CC5	0.629	0.010	5.906	0.113	0.001	61.837	10.056	11.832	0.219	0.008	0.295	22.192	0.109	1.776	N/A	12.408
CM1	0.284	0.001	2.248	0.001	0.000	5.130	1.916	0.178	0.043	0.006	0.048	5.128	0.002	0.030	N/A	1.187
DB1	1.205	0.003	3.170	0.000	0.001	57.399	16.316	8.530	0.061	0.013	0.215	16.020	0.052	0.870	0.226	15.274
GH1	2.212	0.003	5.209	0.008	0.000	28.777	15.815	9.363	0.065	0.005	0.099	19.607	0.203	3.757	N/A	10.206
GH2	0.589	0.007	2.732	0.027	0.001	60.859	29.408	10.641	0.049	0.138	0.088	21.023	0.232	0.141	N/A	31.454
HS1	0.257	0.001	4.608	0.001	0.001	9.653	4.613	2.579	0.085	0.009	0.102	4.271	0.004	0.150	N/A	3.212